SANDIA REPORT
SAND2017-2103
Unlimited Release
Printed mm 2017

Geomechanical Simulation of Bayou Choctaw Strategic Petroleum Reserve - Model Calibration

Byoung Yoon Park

Prepared by
Sandia National Laboratories
Albuquerque, New Mexico 87185 and Livermore, California 94550

Sandia National Laboratories is a multi-mission laboratory managed and operated by Sandia Corporation, a wholly owned subsidiary of Lockheed Martin Corporation, for the U.S. Department of Energy's National Nuclear Security Administration under contract DE-AC04-94AL85000.

Issued by Sandia National Laboratories, operated for the United States Department of Energy by Sandia Corporation.

Available to DOE and DOE contractors from
U.S. Department of Energy
Office of Scientific and Technical Information
P.O. Box 62
Oak Ridge, TN 37831

Telephone: (865) 576-8401
Facsimile: (865) 576-5728
E-Mail: reports@adonis.osti.gov
Online ordering: http://www.osti.gov/bridge

Available to the public from
U.S. Department of Commerce
National Technical Information Service
5285 Port Royal Rd.
Springfield, VA 22161

Telephone: (800) 553-6847
Facsimile: (703) 605-6900
E-Mail: orders@ntis.fedworld.gov
Online order: http://www.ntis.gov/help/ordermethods.asp?loc=7-4-0#online

SAND2017-2103
Unlimited Release
Printed mm 2017

Geomechanical Simulation of Bayou Choctaw Strategic Petroleum Reserve I: Model Calibration

Byoung Yoon Park

Geotechnology & Engineering (Org. 6912)
Sandia National Laboratories
P.O. Box 5800
Albuquerque, NM 87185-MS0751

Abstract

A finite element numerical analysis model has been constructed that consists of a realistic mesh capturing the geometries of Bayou Choctaw (BC) Strategic Petroleum Reserve (SPR) site and multi-mechanism deformation (M-D) salt constitutive model using the daily data of actual wellhead pressure and oil-brine interface. The salt creep rate is not uniform in the salt dome, and the creep test data for BC salt is limited. Therefore, the model calibration is necessary to simulate the geomechanical behavior of the salt dome. The cavern volumetric closures of SPR caverns calculated from CAVEMAN are used for the field baseline measurement. The structure factor, A_2, and transient strain limit factor, K_0, in the M-D constitutive model are used for the calibration. The A_2 value obtained experimentally from the BC salt and K_0 value of Waste Isolation Pilot Plant (WIPP) salt are used for the baseline values. To adjust the magnitude of A_2 and K_0, multiplication factors *A2F* and *K0F* are defined, respectively. The *A2F* and *K0F* values of the salt dome and salt drawdown skins surrounding each SPR cavern have been determined through a number of back fitting analyses. The cavern volumetric closures calculated from this model correspond to the predictions from CAVEMAN for six SPR caverns. Therefore, this model is able to predict past and future geomechanical behaviors of the salt dome, caverns, caprock, and interbed layers. The geological concerns issued in the BC site will be explained from this model in a follow-up report.

ACKNOWLEDGMENTS

This research is funded by SPR programs administered by the Office of Fossil Energy of the U.S. Department of Energy.

The author would like to thank Courtney G. Herrick and Steven R. Sobolik of Sandia provided technical reviews. Leigh Cunningham of Sandia manager and Anna C. Snider Lord of Sandia project manager who supported this work. As always, the support of Diane Willard and Wayne Elias of DOE is greatly appreciated. Paul Malphurs of DOE also is greatly appreciated, as is his comprehensive review of this report. This report has been improved by these individuals.

CONTENTS

FIGURES

TABLES

Intentionally Blank

NOMENCLATURE

3D	Three-Dimensional
BC	Bayou Choctaw
CGZ	Clay and Gypsum Zone
DOE	U.S. Department of Energy
EFF	Extended File Format
E-W	East-West
FE	Finite Element
GAZ	Gypsum-Anhydrite Zone
ID	Identification
M-D	Multi-Mechanism Deformation
MIT	Mechanical Integrity Test
MMB	Million Barrels
MVS	Mining Visualization System
N-S	North-South
OBI	Oil-Brine Interface
ONI	Oil-Nitrogen Interface
PLC	Power Law Creep
Sandia	Sandia National Laboratories
SPR	Strategic Petroleum Reserve
UTP	Union Texas Petroleum
WH	West Hackberry
WIPP	Waste Isolation Pilot Plant

Intentionally Blank

1. INTRODUCTION

1.1. Background

The U.S. Strategic Petroleum Reserve (SPR) stores crude oil in 60 caverns located at four sites located along the Gulf Coast. The reserve contains approximately 695 MMbbls (110 Mm^3) of crude oil. Most of the caverns were solution mined by the U.S. Department of Energy (DOE) and are typified as cylindrical in shape. In reality, the geometry, spacing, and depths of the caverns are irregular. Sandia National Laboratories (hereafter 'Sandia'), on behalf of DOE, is evaluating the mechanical integrity of the salt surrounding existing petroleum storage caverns in the Bayou Choctaw (BC) Salt Dome in Louisiana.

Geotechnical concerns arise due to the close proximity of the some of the caverns to each other (e.g., Caverns 15 and 17) or to the edge of salt (e.g., Cavern 20) [Park, et al. 2006]. In addition to the SPR caverns at BC, eight other caverns exist, which store various hydrocarbons and are operated by private industry. Also, there are nine abandoned caverns, one of which collapsed (Cavern 7) in 1954 and another (Cavern 4) which is believed to be in a quasi-stable condition. The integrity of wellbores at the interbed between the caprock and salt is another concern because oil leaks occurred at the interbed in the Big Hill site [Park, 2014]. When oil is withdrawn from a cavern in salt using freshwater, the cavern enlarges. As a result, the pillar separating caverns in the SPR fields is reduced over time due to usage of the reserve. The enlarged cavern diameters and smaller pillars reduce underground stability [Park and Ehgartner, 2011]. It is necessary to establish a limit for the remaining pillar thickness between caverns without threatening the structural integrity of the caverns.

DOE may increase the size of the reserve. The BC site is the smallest SPR site. The site is limited in its expansion capability due to the small size of the salt dome and other commercial storage operations on the dome. The SPR may expand the site's capacity through the development of two new caverns on existing SPR property [Park and Ehgartner, 2012]. The impacts of the expansion by two caverns on underground creep closure, surface subsidence, infrastructure, and well integrity need to be investigated using a high resolution numerical model.

1.2. Objective

Sandia uses large-scale, three-dimensional (3D) computational models to model the geomechanical behavior of underground storage facilities consisting of solution-mined caverns in a salt dome. Recent advances in the state-of-art in geomechanics modeling have enabled 3D analyses to be performed. 3D analyses capture the actual geometry and layout of a cavern field and result in more realistic simulations. The complexities within the BC cavern field require such advanced simulations as the field has a long history of development resulting in 26 caverns of various shapes, depths, and states. This report attempts to model these conditions and addresses the resulting performance and stability issues.

This report describes a series of geomechanical simulations of BC SPR. As the first of the series, Park and Roberts [2016] developed a three-dimensional finite element mesh capturing realistic geometries of BC site has been constructed using the sonar and seismic survey data obtained from the field. The mesh consists of hexahedral elements because the salt constitutive model is coded using hexahedral elements. This report describes the model calibration to match the analysis results to the field observations as the second of the series. The next report will provide

solutions for the geotechnical concerns mentioned above as the third of the series and conclusions.

1.3. Previous Work

Since the SPR conceptual design started in 1978 [PB/KBB, 1978], several finite element (FE) analyses have been performed to assess the long-term performance and stability of the caverns, each with increasing levels of constitutive model development and technical complexity. Preece and Foley [1984] conducted two-dimensional axisymmetric idealizations and each cavern was simulated independently of the others. The failure function was based on accumulated strain as a function of pressure. While the analyses at that time predicted stability, cavern workover conditions were not simulated. Ehgartner and Sobolik [2002] used a 30-degree wedge to simulate a symmetric 19-cavern field geometry. The caverns in that simulation were modeled as true cylinders.

Park et al. [2006] constructed a 3D finite element model allowing control of each cavern individually because the location and depth of caverns and the date of excavation are irregular. The total cavern volume has practical interest, as this void space affects total creep closure in the BC salt mass. Operations including both cavern workover, where wellhead pressures are temporarily reduced to atmospheric, and cavern enlargement due to leaching during oil drawdowns[1] that use water to displace the oil from the caverns, were modeled to account for as many as the five future oil drawdowns in the six SPR caverns. The shapes of all caverns and salt dome were simplified by cylindrical and elliptical shapes, respectively, because of the limitations of computer capacity, mesh generation software, and so on.

The U.S. Department of Energy announced plans in 2006 to leach two new caverns and convert one of the existing caverns within the Bayou Choctaw salt dome to expand its petroleum reserve storage capacity. An existing finite element mesh [Park et al., 2006] was modified by adding two caverns and increasing the size of existing BC-102. The structural integrity of the three expansion caverns and the interaction between all the caverns in the dome were investigated. The impacts of the expansion on underground creep closure, surface subsidence, infrastructure, and well integrity were quantified. Potential shapes for the two new caverns included cylindrical and bifrustum, and so the effect of these was investigated. Two scenarios were used for the duration and timing of workover conditions where wellhead pressures were temporarily reduced to atmospheric pressure [Park and Ehgartner, 2008].

Lord et al. [2009] suggested alternative locations for two new caverns. Park and Ehgartner [2010] investigated the structural integrity of the three expansion caverns and their interaction with other caverns in the dome in a manner similar to the previous analyses [Park and Ehgartner, 2008]. The impacts of the expansion by three caverns on underground creep closure, surface subsidence, infrastructure, and well integrity were quantified as well. For these, the existing 3D FEM mesh [Park and Ehgartner, 2008] was modified by changing the locations of two new caverns.

1 “Drawdown” is when the crude oil is withdrawn from the cavern. Fresh water injection is used to withdraw the crude oil. Because the cavern enlarges due to salt dissolving from the cavern walls, it is called a “drawdown leach”.

JAS3D, a three dimensional iterative solid mechanics code, had been used for structural analyses for the Strategic Petroleum Reserve system since the 1990s. JAS3D was no longer supported by Sandia National Laboratories, and has been replaced by ADAGIO. To validate the transition from JAS3D to ADAGIO, the existing JAS3D input decks and user subroutines for Bayou Choctaw and Big Hill models were converted for use with ADAGIO. The calculation results from the ADAGIO runs were compared to the JAS3D. Since the Adagio results were very similar to the JAS3D results, ADAGIO was judged to be performing satisfactorily [Park, 2013].

1.4. Advancement

There are several important advances in this new computational simulation over the historical simulations described in Section 1.4:

1. This simulation uses a three-dimensional finite element mesh capturing realistic geometries of the salt dome and caverns at the BC site. The process of converting complex cavern and dome geometries obtained from seismic and sonar measurements, into a finite element mesh suitable for large-scale geomechanical calculation of site performance, has evolved substantially over the past 20 years. Recent advances by Park and Roberts [2016] to create highly-realistic mesh geometries has improved our capability to understand complex physical processes, for example the stability of caverns in close proximity of the caverns to each other or to the salt dome boundary. In the previous models in Section 1.3, the shapes of all caverns were simplified by cylindrical shapes and an elliptical shape was applied to the section of the dome as an approximation for the actual shape of the dome.
2. This simulation uses the multi-mechanism deformation (M-D) model as a salt constitutive model. The previous analyses were conducted using the Power Law Creep (PLC) model. The PLC, a subset of M-D, considers only the secondary creep rate (steady-state, long term), while M-D considers not only the secondary but also the primary (initial stage, short term) and tertiary (beyond steady-state) creep rates. The M-D will provide more accurate numerical predictions considering the short term salt behaviors due to the daily changes of internal pressure of the caverns.
3. This simulation considers the interbed between the caprock and salt top, and the interface between the salt dome and surrounding in situ rock stratigraphy. The interbed will be used to check the integrity of wellbores at the salt top. The interface will allow for evaluating various models of the deformation and integrity of the salt dome boundary with the surrounding host rock, which will have a direct effect on creep deformation in the salt between BC-20 and the salt dome edge.
4. This simulation uses the daily wellhead pressure histories of SPR caverns that were recorded at the field office. The real wellhead pressure plus the oil/brine pressure gradient was applied on the inside boundary of each SPR cavern as a function of depth. The cavern internal pressure acts against the lithostatic pressure to impede the inward movement of the wall, floor, and roof of the cavern due to salt creep. The previous simulation used the simplified wellhead pressure by an average pressure over a period

under normal operating conditions for each cavern. Zero wellhead pressure was used for workover[2] conditions.

5. This simulation considers the oil-brine interface (OBI) depth change over time. Previous existing analyses assumed that the SPR caverns were filled fully with oil. In reality however, the caverns were not always fully filled with oil. Brine filled the bottom portion of the cavern, and the brine volume changes with time. The difference between pressure gradients of oil (0.37 psi/ft of depth) and brine (0.52 psi/ft of depth) cannot be ignored. So, amount of oil and brine in a cavern over time were considered.
6. This simulation applies a reasonably calculated internal pressure on the boundary of each abandoned cavern. The abandoned caverns were all plugged with the exception of BC-4. The wellheads were cut off below the surface and buried. The abandoned caverns were filled fully with brine after plugging. The lithostatic pressure gradient with depth is larger than the brine pressure gradient. The gradient difference drives the cavern volumetric closure due to salt creep. The brine volume does not decrease over time because there are no brine leaks, while the cavern volume decreases due to creep until an equilibrium state is reached. The hydrostatic pressure in the cavern increases until pressure equilibrium, i.e. the pressure head increases for some time after the plugging. The pressure head, which is an additional hydrostatic pressure due to the cavern volumetric closure, is calculated at equilibrium. These calculated value are used over time as a wellhead pressure history for each cavern in the analysis. In the previous analyses, a pressure due to brine head and pressure gradient of 0.52 psi/ft is applied on the cavern boundaries.

1.5. Software

For many years, geomechanical analyses performed by Sandia utilized JAS3D, Version 2.0 [Blanford et al., 2001], a three-dimensional finite element program developed by Sandia, designed to solve large quasi-static nonlinear mechanics problems. JAS3D is no longer supported by Sandia, and has been replaced by ADAGIO [SIERRA Team, 2010, 2011; Arguello et al., 2012]. ADAGIO is written for parallel computing environments, and its solvers allow for scalable solutions of very large problems. The ADAGIO structure is different from JAS3D. ADAGIO uses the SIERRA Framework, which allows for coupling with other SIERRA mechanics codes. The existing JAS3D input decks and user subroutines for the Big Hill and Bayou Choctaw SPR works have been converted for use with ADAGIO [Park, 2013].

Create geometries and mesh generation:

Cubit 15.0b 64 bit Build 393458
Revised 2014-07-30
Copyright 2001 Sandia Corporation

Combine meshed blocks:

GJoin2 Version 1.32 (A GENESIS database combination program)
Revised 2009/12/02
Copyright 1988 Sandia Corporation

2 "Workover" is when the wellhead pressure of the cavern is dropped to atmospheric pressure for maintenance.

Solver:

SIERRA ADAGIO (A GENESIS database combination program)
Revised 2009/12/02
Copyright 1988 Sandia Corporation

Post-process:

ParaView 1.32 (A GENESIS database combination program)
Revised 2009/12/02
Copyright 1988 Sandia Corporation

Blot II-2 Version 3.12
Revised 2016/08/22
Copyright 2009 Sandia Corporation

Intentionally Blank

2. SITE DESCRIPTIONS

The BC salt dome, located in south-central Louisiana near Baton Rouge (Figure 1), was discovered in 1926. Since then over three hundred oil and gas wells have been drilled on and around the dome, as well as numerous shallow holes drilled into the caprock. Since 1937, Allied Chemical Corporation has drilled over twenty brine wells on the dome. In 1976, U.S. Department of Energy (DOE) purchased eleven of these leached caverns and was storing approximately twenty two million barrels of crude oil in three of the caverns (numbered 15, 18, and 19), forming part of the SPR Program [Hogan, 1980].

Since 1980, SPR caverns 18, 19, and 20 have been enlarged substantially; Union Texas Petroleum (UTP) Caverns 6 and 26 have been constructed, and Caverns 101 and 102 have been leached by DOE. Cavern 102 was traded to UTP in a swap for Cavern 17, now used for SPR oil storage. In 1992 UTP converted its brine Cavern 24 to natural gas storage. UTP had leached in 1993 along the northeast dome edge [Neal et al., 1993]. The UTP caverns have gone through several changes in ownership - first UTP, then Petrologistics, and now Boardwalk. The DOE re-purchased Cavern 102 from Boardwalk to use for SPR in 2012.

Data from the 300 oil and gas wells were used to construct contour maps and cross sections of the salt dome and the overlying caprock. Figure 2 shows a plan view of the BC site with salt contour lines defining the approximate location of the salt dome edge. The locations of the six SPR caverns, nine Boardwalk caverns, one inactive cavern, and seven abandoned caverns are included. A vertical cross section through Cavern 4 and Cavern 18 provides a geologic representation near the middle of the dome as shown Figure 3.

The surface and near-surface sediments overlying the BC dome are of Pleistocene through Holocene age. The oldest sediments consist of proglacial sands and gravels with some clay layers. These sediments are overlain by alternating sequences of sand, silts, and clays [Hogan, 1980].

Two distinct zones are found in the caprock at BC: an upper zone, termed the clay and gypsum zone (CGZ); and a lower zone, called the massive gypsum-anhydrite zone (GAZ). The CGZ is composed of layers of gypsum intercalated with clay. The proportion of clay to gypsum is highly variable, with generally more clay than gypsum. The GAZ is predominantly gypsum-anhydrite with minor amounts of clay, sand, and gypsum [Hogan, 1980].

The top of the BC salt dome lies between 600 and 700 ft below the surface. The east flank dips gently downward to 1,500 feet where the dip increases to approximately 80º between 2,000 and 6,000 ft. The west flank of the dome is overhung between 1,000 and 5,000 ft. Below 6,000 to 8,000 ft, the slope of the salt surface diminishes to about 60º [Hogan, 1980].

The lithology surrounding the salt dome contains up to 30,000 ft of silts, sands, shales, limestones, and evaporites. These sediments were deposited in a variety of sedimentary environments including desert basin, evaporating flat, ocean basin, and delta [Hogan, 1980].

The stratigraphy near the BC salt dome is shown in Figure 3. The top layer of overburden, which consists of sand, silts, and clays, has a thickness of 500 ft. The caprock, consisting of gypsum, anhydrite, and sand, is 160 ft thick. The bottom of the deepest cavern (Cavern 27) is at a depth of 6,280 ft. For the vertical direction constraint at the bottom of the model, sufficient thickness between the lowest cavern bottom and the model bottom is necessary to not affect the structural

reaction by the bottom boundary. Therefore, the depth of the salt dome is considered up to 6,400 ft below the surface. All SPR caverns are located below 2,000 ft.

The faults shown in Figures 2 and 3 will be ignored in the FE model because the faults do not extend to the salt thus are not expected to affect the structural behavior of the SPR caverns. And, by ignoring the shear zone, the model of overburden and the cap rock layers are able to be simplified.

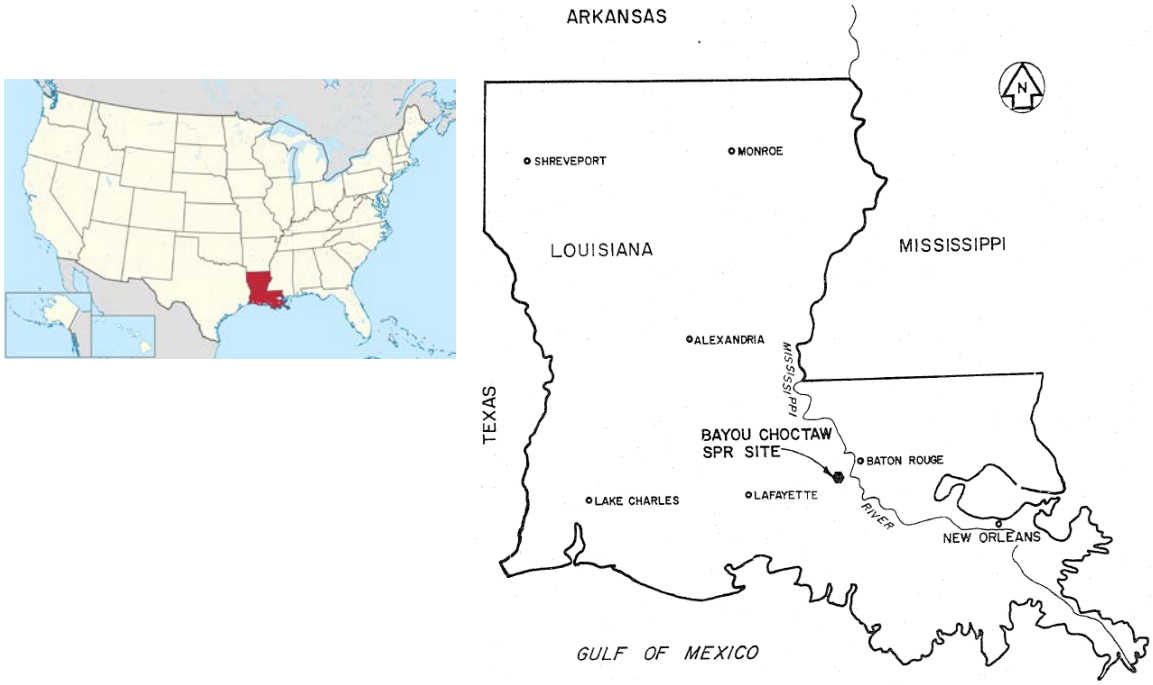

Figure 1 Bayou Choctaw SPR site location map

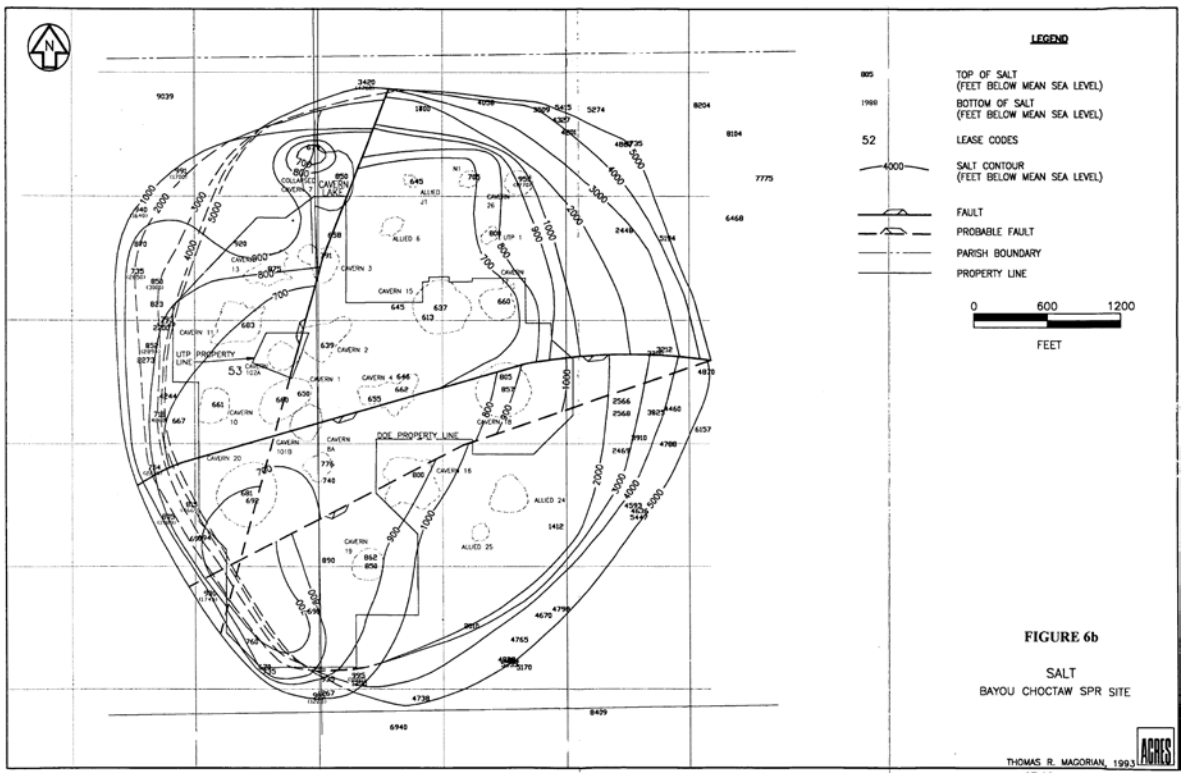

Figure 2 Bayou Choctaw site plan view [Neal et al., 1993]

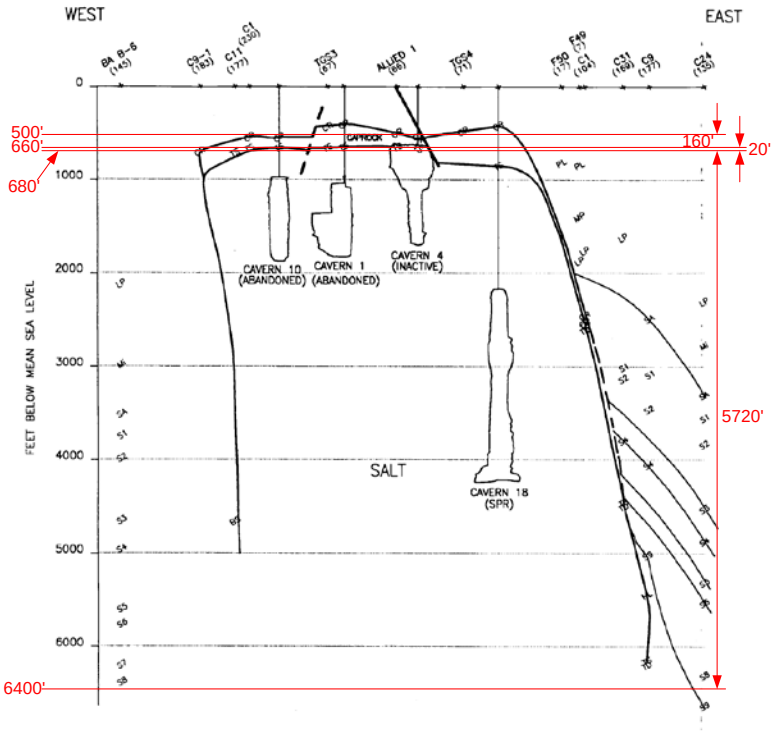

Figure 3 Stratigraphy near the Bayou Choctaw salt dome [Neal et al., 1993] and the thickness of each layer used for modeling.

Intentionally left blank

3. GOEMETRICAL CONDITIONS

3.1. Basic Rule

Finite element codes such as SIERRA/ADAGIO[3] are designed to conduct simulations with finite elements that are either tetrahedral or hexahedral. Two constitutive material models, i.e. the PLC model and the M-D model, are available in ADAGIO to represent salt behavior. These two material models are programmed in SIERRA/ADAGIO assuming eight-node hexahedral elements. Therefore, the mesh for the BC SPR site must be constructed with hexahedral elements. Hexahedral elements include six convex quadrilateral sides, or facets, with the eight corners where these facets intersect being the eight nodes for the element. The cavern boundaries such as the ceiling, wall, and floor are obtained from sonar measurements, and the irregular geometries of these boundaries ultimately require various shapes of facets. Similarly, the geometry of the flank of the salt dome, obtained from seismic measurements, also consists of complicated shapes of facets. To construct a mesh with convex hexahedral elements for a geological volume keeping the complicated geometry as much as possible, the following rules were established and followed:

1. Each perimeter (cavern and dome) consists of the same number of vertices at each depth interval
2. The reference distance between vertices on a perimeter is:
    a. about 20 ft for caverns
    b. about 80 ft for dome
3. The vertical thickness of an element level is kept constant at 20 ft
4. 15% cavern volume increase for each drawdown leach

Modeling of the leaching process of the caverns is performed by deleting a pre-meshed block of elements along the walls of the cavern so that the cavern volume is increased by 15 percent per drawdown. The 15% volume increase is typical for a standard freshwater drawdown, although salt quality can vary that amount. Also, typical leaching processes tend to increase cavern radius more at the bottom of the cavern than at the top, with very little change to the roof and floor of the cavern. For the purposes of this modeling effort for Bayou Choctaw, leaching is assumed to add 15% to the volume of the cavern, and is assumed to occur uniformly along the entire height of the cavern, with no leaching in the floor or roof of the caverns. Each leaching layer, or onion skin, is built around the perimeter of the meshed cavern volume using the same rules stated previously. The detailed steps and methodologies to construct the FE mesh were provided by Park and Roberts [2015].

3 ADAGIO is the most recently Sandia-developed 3D solid mechanics code. It is written for parallel computing environments, and its solvers allow for scalable solutions of very large problems. ADAGIO uses the SIERRA Framework, which allows for coupling with other SIERRA mechanics codes.

3.2. Salt Dome

The top of the dome lies between 600 and 700 ft below the surface. The salt surface on the top of the dome is relatively flat, sloping gently outward to a depth of approximately 1000 ft where the angle suddenly steepens sharply. The cross-sectional area within the 1000 ft contour is about 284 acres. The east flank dips gently downward to 1500 ft where the dip increases to approximately 80° between 2000 and 6000 ft. The west flank of the dome is overhung between 1000 and 5000 ft. Below 6000 to 8000 feet on both flanks, the slope of the salt surface begins to flatten toward 60°. The change in the dip of the salt mass is demonstrated by the sectional area of the dome at 5000 feet which is 371 acres. By 9000 ft, however, the area has increased to 742 acres. Calculations show an average dome growth rate between 2.8×10^{-4} to 3.5×10^{-4} in/year since the end of the Pliocene. The steepest dip is found on the west flank where there is the pronounced caprock and salt overhang. Other small overhangs are indicated on the east and north flanks [Hogan, 1980].

The three-dimensional seismic survey over the Bayou Choctaw salt dome used in this study was shot originally in 1994, and the objective of the original processing appears to have been deep petroleum targets along the flanks of the salt dome [Rautman et al., 2009]. Sandia has completed the interpretation and first-pass modeling of the Bayou Choctaw salt dome using 3-D seismic information. The seismic volume was licensed from Seitel Data, Ltd., and it comprises approximately 16 square miles of data centered directly on the Bayou Choctaw dome. After examining the as-received processed data, Sandia determined to reprocess the un-composited field data to improve resolution of the shallower portion of the stratigraphic section, including the upper portion of the salt stock. Geologic interpretation of the resulting custom-processed information has been on-going for some time. However, Sandia have completed a first-pass modeling effort of the interpreted data [Rautman et al., 2008].

Roberts [2015] generated the salt dome image using the seismic data and 4DIM[4] tool. Park and Roberts [2015] constructed the three-dimensional hexahedral FE mesh using the seismic data and the CUBIT mesh generation tool as shown Figure 4. The 3D-coordinates of vertices are resampled from the seismic image. The real salt dome top is not flat as shown in the seismic image in Figure 4. The uneven top surface should create poorly shaped elements. To avoid a poor shape, the vertex data above the elevation of -1320 ft are removed (a process called ‘trimming’). The salt dome leans to the west. The coordinates of vertices at every 20 ft element level from elevations -1300 ft through -680 ft are calculated considering the leaning. In similar, the vertex data below the elevation of -5880 ft are trimmed off. The vertex data for the lower salt blocks are translated vertically downward from the vertex data of the bottom of trimmed salt dome block (-5880 ft). The leaning slope of dome is not considered for the lower salt block. The dome mesh consists of 286 element levels each 20 ft thick. The bottom elevation is -6400 ft.

4 Four-Dimensional Interactive Model Player developed by C Tech.

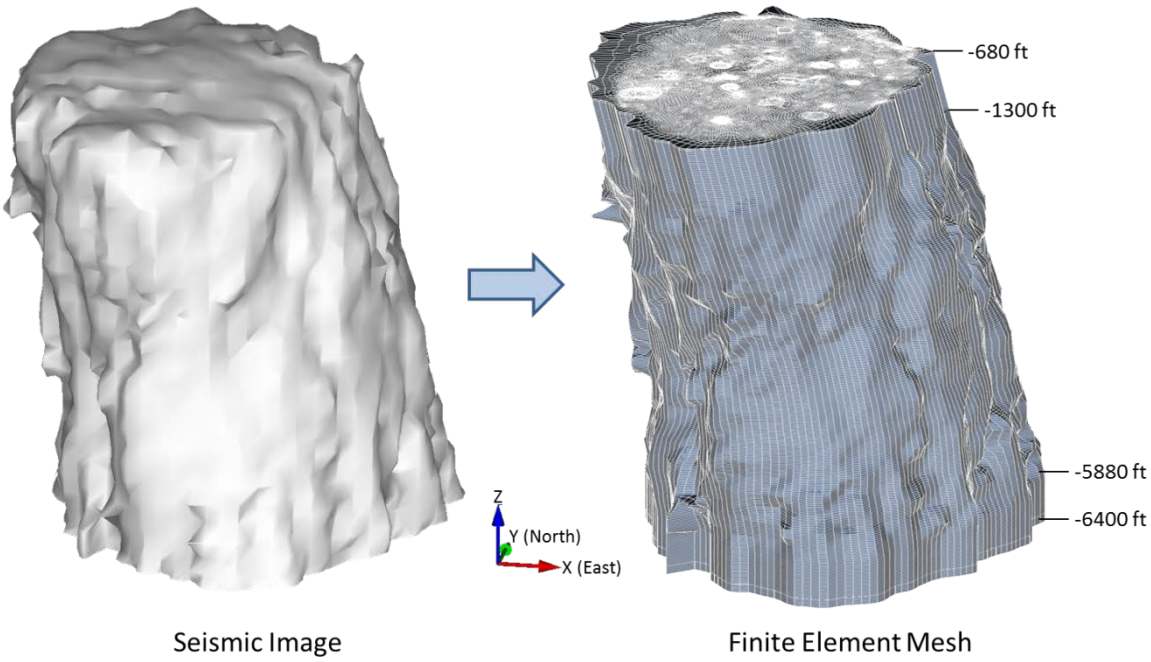

Figure 4 Images of Bayou Choctaw salt dome obtained from the seismic survey (left) and hexahedral finite element mesh using the seismic survey data

3.3. Lithologies Surrounding the Salt Dome

3.3.1. Overburden

The surface and near surface sediments overlying the Bayou Choctaw dome are of Pleistocene through Holocene age. The oldest sediments consist of proglacial sands and gravels with some clay layers. These sediments are overlain by an alternating sequence of sands, silts, and clays [Hogan, 1980]. The bottom of overburden layer (top of the dome) is not flat as shown in Figure 3. The bottom is simplified as a flat to avoid creating poor-shaped elements. Figure 5 shows the meshed overburden block that is 12,000 ft long, 11,000 ft wide, and 500 ft thick. The thickness of each element layer is 20 ft in this model, so the mesh has 25 element levels vertically. Each element is hexahedral.

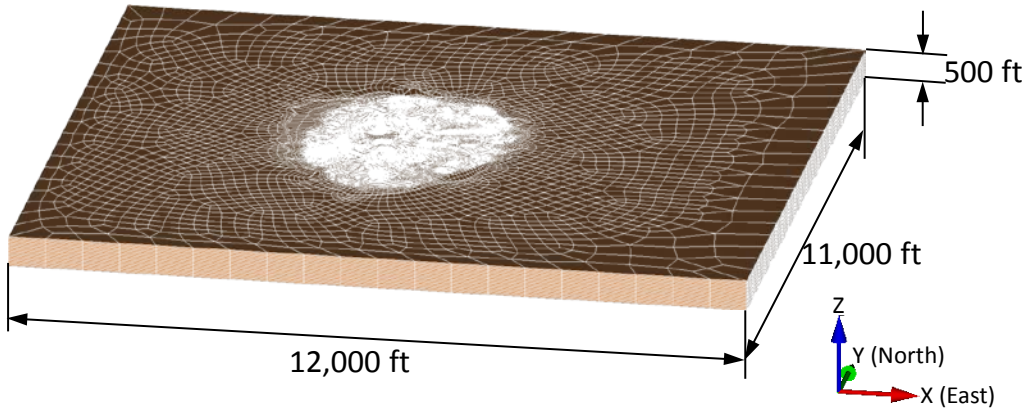

Figure 5 Overburden meshed block

3.3.2. Caprock

Two distinct zones are found in the caprock at Bayou Choctaw: an upper zone, termed the clay and gypsum zone; and the lower zone, called the massive gypsum-anhydrite zone. The clay and gypsum zone is composed of layers of gypsum intercalated with clay. This zone is up to 150 ft thick and lies within 400 to 433 ft of the surface. The massive gypsum-anhydrite zone is the lower unit and consists of gypsum-anhydrite with some clay and sand. A discontinuous massive layer of gypsum-anhydrite, 20 to 60 ft thick, marks the top of this zone which lies within 500 to 600 ft of the surface. Faults and fractures in the caprock, formed by salt dissolving and collapse at the salt/caprock contact, result in a highly permeable and discontinuous unit with little structural strength [Hogan, 1980].

Figure 6 shows the BC caprock image generated using the seismic data and 4DIM tool, and hexahedral FE mesh. Since this image was developed from contours which were hand-drawn, some of the surfaces appear a flat. The bottom of the caprock surface is based on the topography of the salt dome top. The actual caprock top and bottom are not flat. The uneven top and bottom may produce poorly shaped elements. To avoid a poor shape, the vertex data for the caprock are translated vertically upward from the vertex data of the flat surface of salt dome top as shown in Figure 4. The thickness of each element layer is 20 ft in this model, so the mesh has 8 element levels vertically because the caprock is simplified as a flat slice block 160 ft thick as shown in Figure 3.

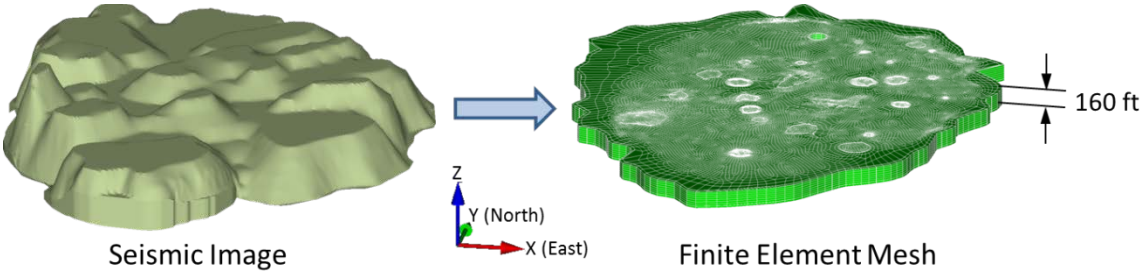

Figure 6 Image of Bayou Choctaw caprock obtained from the seismic survey (left) and hexahedral finite element mesh

3.3.3. Interbed

Oil leaks were found in wellbores of Caverns 105 and 109 at the Big Hill (BH) SPR site. According to the field observations, two instances of casing damage occurred at the depth of the interbed between the caprock bottom and salt top. A three dimensional finite element model was constructed to investigate horizontal and vertical displacements in each well as it crosses the various interbeds. The analysis results indicate that the casings of Caverns 105 and 109 failed, respectively, from shear stress that exceeded the casing shear strength due to the horizontal movement of the salt top relative to the caprock, and tensile stress due to the downward movement of the salt top from the caprock. The salt top subsides because the volumes of caverns in the salt dome decrease with time due to salt creep closure, while the caprock does not subside at the same rate as the salt top because the caprock is thick and stiff. This discrepancy causes deformation of well. ADAGIO has a contact surface algorithm for modeling contact and sliding behavior between two solid surfaces. However, this algorithm has a limitation on the number of

elements in the model. The number of elements in the BH model was over the limitation. In place of a contact surface, a thin soft layer of elements is used for the interface between lithologies. The thin soft element layer is assumed to behave mechanically like a contact surface from a perspective of relative displacement between two lithologies [Park, 2014].

A similar interbed layer is implemented in the BC model to represent the salt/caprock contact. The collapse zone at the BC salt/caprock contact, is a highly permeable and discontinuous unit with little structural strength [Hogan, 1980]. The contact zone is modeled by the thin soft element layer interbed block to evaluate the caverns' geomechanical effect on wellbore integrity. Figure 7 shows the BC interbed FE mesh. The real interbed between the salt dome and caprock is not flat. The uneven interbed could cause poorly shaped element to be generated. To avoid the poor shape, the vertex data for the interbed are translated vertically upward from the vertex data of the simplified flat surface of salt dome top. The thickness of interbed layer is assumed to be 20 ft, so it has one element level.

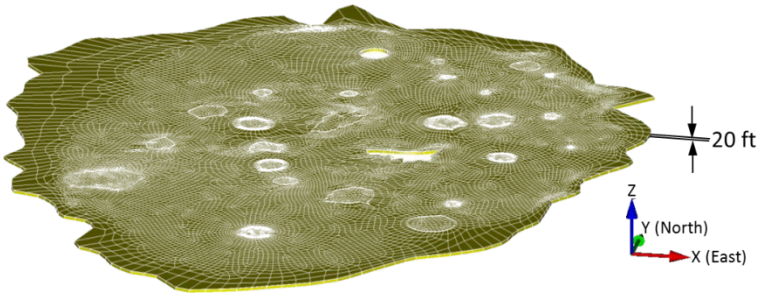

Figure 7 Finite element mesh of interbed between caprock and salt top

3.3.4. Interface between dome and far-field

The Bayou Choctaw salt dome is a piercement structure which has penetrated Mesozoic through Quaternary sediments. As in other types of intrusions, the salt dome must displace the overlying sediments as it pushes upward. Any sediment deposited above the dome must be either pushed aside and/or lifted up, increasing the chance of erosion occurring on the loosened material. The mechanical failure of the sediments surrounding the dome has caused faults to develop both radially from and tangentially to the dome in a series of graben-horst structures [Hogan, 1980].

To consider the faults surrounding the dome, the interface block is inserted between the dome and sediments surrounding the dome which consists of the caprock, interbed, and salt dome blocks. As with the interbed block in Section 3.3.3, a thin soft layer of elements is used for the interface between lithologies, i.e. this model contains an interface block between the dome and surrounding sediments (hereafter 'surrounding rock' or 'far-field') as shown Figure 8.

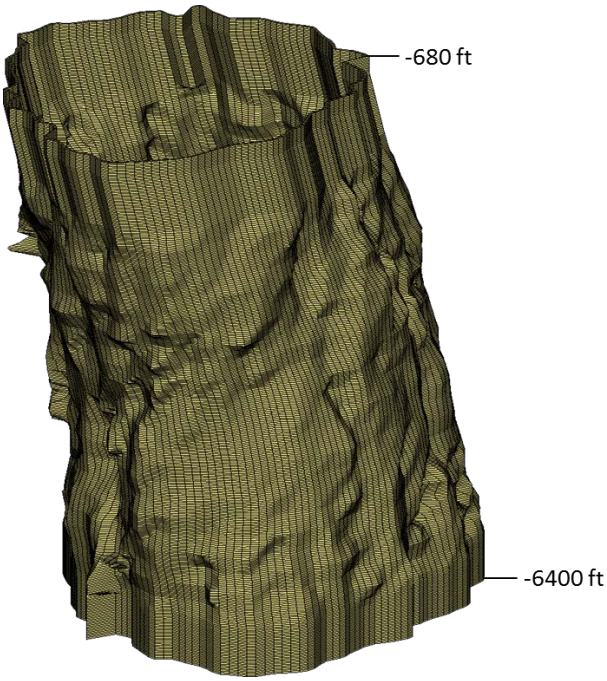

Figure 8 Finite element mesh of interface between dome and far-field

3.3.5. Far-field

The Bayou Choctaw salt dome lies within the Gulf Coast geosyncline, an area of sediment deposition from the Mesozoic era to the present. In the site area, the geosyncline contains up to 30,000 ft of silts, sands, shales, limestones, and evaporites. These sediments were deposited in a variety of sedimentary environments including desert basin, evaporating flat, ocean basin, and delta. Salt domes within the geosyncline occur in two regions: a northern belt through northern Louisiana and Mississippi, and a southern belt along the Gulf Coast and offshore. The Bayou Choctaw dome is on the northern edge of the southern coastal belt of salt domes. The largest tectonic feature near the site is the Baton Rouge fault system which lies approximately five miles to the north. The fault trends from Breton Sound, Louisiana, to Matagorda Bay, Texas, a distance of more than 500 miles. In Louisiana the Baton Rouge fault marks the northern limit of the southern Gulf Coast salt domes [Hogan, 1980].

For simplification, the rock surrounding the salt dome is assumed to be made of an isotropic, homogeneous, linear elastic material in this model. The surrounding rock block encircles the interface, caprock, interbed, and salt dome blocks. The lengths of the confining boundaries are 11,000 ft in the N-S direction and 12,000 ft in the E-W direction as shown Figure 9. The sizes of the caverns are much smaller than the dome size. The model boundary distances (surrounding rock dimensions) can be regarded as being an infinite distance away from the caverns (i.e. fixed boundaries can be applied).

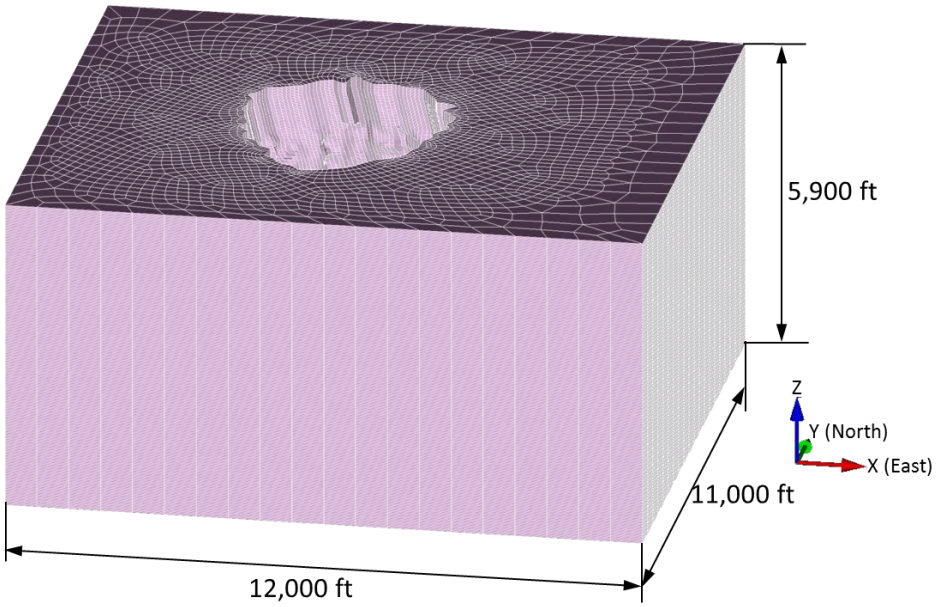

Figure 9 Finite element mesh of surrounding rock (far-field)

3.4. Caverns

3.4.1. Sonar Data Manipulation

Representations of the BC caverns based on sonar data were incorporated into the geomechanical model to provide a more realistic depiction of the caverns. To facilitate this, the cavern sonar data were resampled to a nodal spacing more appropriate for the geomechanical model. The actual sonar data is delivered from the sonar contactors. An additional processing code SONAR7[5] was used to turn these contractor files into a format compatible with the MVS[6] geologic modeling software suite. This is a mature process which has been used for many years at Sandia. This step is necessary to provide a full three-dimensional surface model of the sonar data. The assigned vertices in the FE mesh created in CUBIT need to be at specific depth intervals which may not correspond to the actual sonar sampling locations. Continuous three-dimensional surface models of the survey data are created, which allows sampling at any depth needed. This resampling step is performed through an algorithm coded using Python. Then, the resampled node coordinates data sets for the caverns are generated as the output in this step. The resampled nodal data are converted into CUBIT vertex data through Microsoft Excel manipulation. The mesh is constructed using cavern slice blocks of 20-ft thick layers generated using the coordinates of vertices.

Table 1 lists the elevations of cavern top and bottom, cavern volumes, and the dates when the sonar data were obtained. The cavern volumes calculated from SONAR7 and CUBIT are different. The SONAR7 volumes are calculated from the full three-dimensional surface model of

5 A data conversion program developed by Sandia. SONAR7 converts sonar data sets with various formats provided by different vendors into the extended file format (EFF) and other MVS compatible formats.

6 MVS (Mining Visualization System) is C Tech's flagship product for state-of-the art analysis and visualization. MVS was designed from the ground up to meet the demanding requirements of underground and surface mining analysis. Its tools are also used by civil engineers and advanced environmental modelers.

the sonar data, while the CUBIT volumes are calculated from the FE discretized mesh. Typically, the CUBIT-generated volumes are slightly less than those from SONAR7 because the curved surfaces are converted into flat facets with four nodes. The volume differences are usually less than 5% except for BC-3, 10, 11, 13, 18, and N1. BC-3, 10, 11, and 13 are abandoned, so and their volume discrepancies are not expected to significantly affect the global salt behavior because they were all plugged with their wellheads cut off below ground surface and buried. The BC-N1 has a very irregular shape. It is far from the SPR caverns, so it is also not expected to influence the behaviors of the SPR cavern. The bottom part of BC-18 is much larger than the upper, and the resulting distortion of the geometry to create the FE mesh for this cavern accounts for the volume discrepancy. The 3D hexahedral element meshes for 26 caverns constructed using various functions in CUBIT are shown in Figure 10.

Table 1 Elevations of cavern tops and bottoms, cavern volumes, and sonar survey dates. Blue, green, and gray fonts indicate the SPR, Boardwalk, and abandoned caverns, respectively.

Cavern ID	Sonar Survey Date for Mesh Data	Top Elevation (ft)	Bottom Elevation (ft)	Volume (bbl)		Difference (B-A)/A
				Sonar7 (A)	Cubit (B)	
BC-1	5/30/1980	-1040	-1780	8,321,703	7,979,595	-4.1%
BC-2	7/28/1983	-780	-1520	9,168,111	9,413,900	2.7%
BC-3	7/13/1977	-1020	-1840	5,016,299	4,176,331	-16.7%
BC-4	7/30/2013	-640	-1680	6,254,862	6,125,965	-2.1%
BC-6	11/1/2006	-1240	-1560	865,285	845,144	-2.3%
BC-7	Collapsed in 1954	0	-1960	2,900,000	2,872,777	-0.9%
BC-8	5/31/1980	-1300	-1960	3,022,481	2,927,863	-3.1%
BC-10	9/13/1973	-1000	-1980	6,357,213	5,574,316	-12.3%
BC-11	3/10/1978	-1080	-1740	8,907,671	7,400,907	-16.9%
BC-13	8/13/1977	-1120	-1860	4,042,210	3,325,433	-17.7%
BC-15	4/15/2009	-2600	-3260	16,493,972	16,141,623	-2.1%
BC-16	6/28/2004	-2620	-3220	11,427,940	11,231,618	-1.7%
BC-17	4/16/2009	-2600	-3960	11,395,042	11,120,677	-2.4%
BC-18	1/6/2009	-2140	-4160	18,323,973	16,776,640	-8.4%
BC-19	4/14/2009	-2980	-4200	11,994,283	11,823,169	-1.4%
BC-20	12/13/2013	-3820	-4180	9,418,726	9,392,715	-0.3%
BC-24	4/17/1992	-3100	-4320	5,954,764	5,914,635	-0.7%
BC-25	10/30/2007	-2580	-5660	17,153,669	16,601,697	-3.2%
BC-26	10/11/1996	-2300	-3320	2,395,796	2,395,466	0.0%
BC-27	10/28/2007	-5940	-6280	1,370,853	1,313,614	-4.2%
BC-28	10/29/2007	-4700	-6240	2,222,859	2,218,799	-0.2%
BC-J1	7/27/2006	-2860	-3900	1,243,321	1,186,069	-4.6%
BC-N1	12/5/2003	-1920	-3480	1,880,690	1,753,729	-6.8%
BC-UTP	10/14/2006	-2380	-3480	1,567,808	1,500,687	-4.3%
BC-101	2/1/2005	-2580	-4780	12,454,068	12,188,119	-2.1%
BC-102	2/22/2012	-2640	-5220	9,678,299	9,602,558	-0.8%

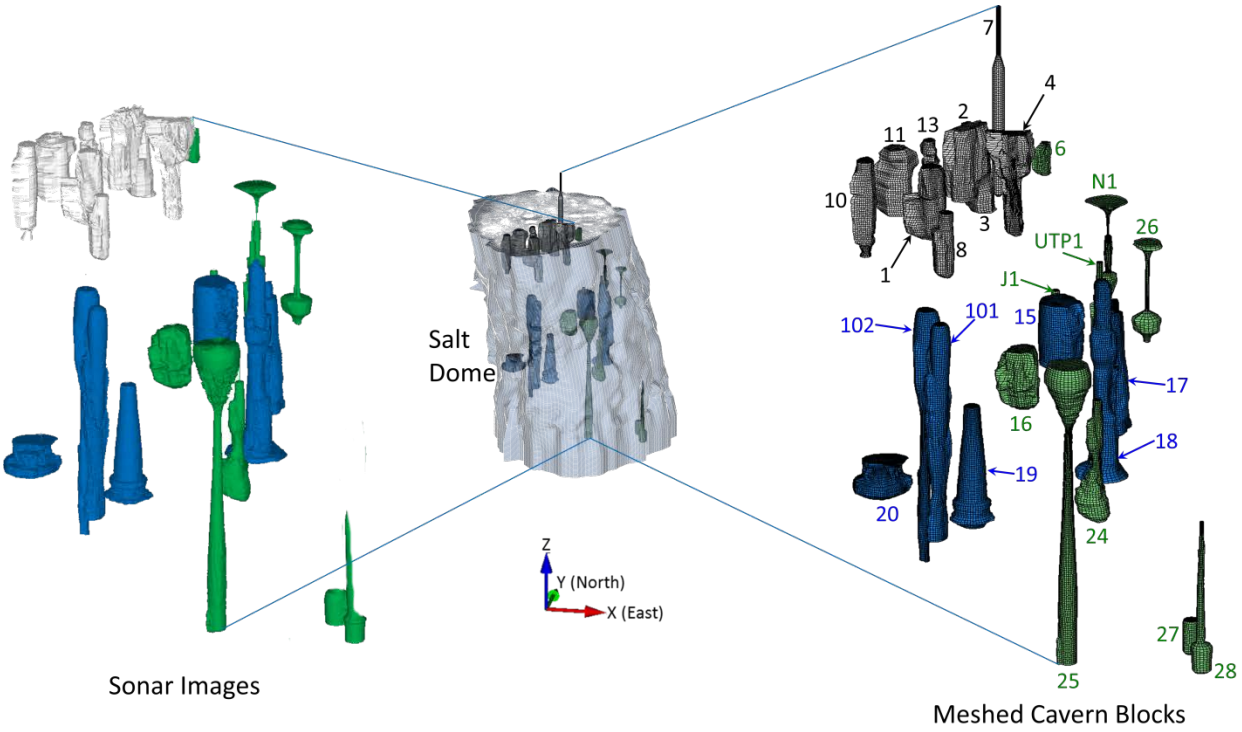

Figure 10 Sonar Images and hexahedral finite element meshed block of 26 caverns in the Bayou Choctaw salt dome. Caverns in gray, green, and blue indicate the abandoned, Boardwalk, and DOE SPR caverns, respectively. The cavern ID numbers are also shown.

3.4.2. Non-SPR Caverns

From a perspective of mesh generation, the caverns in the BC salt dome are classified into two groups, non-SPR and SPR caverns. The non-SPR caverns are classified further into two groups, normal and abnormal caverns.

The following caverns are classified as Non-SPR Caverns:

- Normal group: BC-1, BC-2, BC-3, BC-6, BC-8, BC-10, BC-11, BC-13, BC-16, BC-24, BC-25, BC-26, BC-27, BC-28, BC-J1, BC-N1, and BC-UTP
- Abnormal group: BC-4, BC-7

The normal caverns are those whose entire cavern volumes exist within the salt dome. The abnormal cavern BC-4 was leached into the salt dome and the top of the cavern extended into the caprock layer. BC-7 collapsed in 1954 and was filled with overburden material which formed a lake on the surface above the cavern top. Therefore, the cavern boundary extends into three lithologic layers such as the salt dome, caprock and overburden layers.

Figure 11 shows the BC-1 cavern cavity with an extra skin as an example of normal non-SPR caverns. The non-SPR caverns, because they are abandoned and private caverns, do not require the explicit meshing of a drawdown leach. However, one onion skin (extra skin) is constructed to check the analysis results at the cavern wall, roof, and floor. The cavern skin can be separated from the entire mesh. The amount of numerical result data in the skin block is much less than in the whole mesh. Examining the result in the skin volumes makes storage and analysis efforts

more efficient. The small amount of the data can be handled easily to check various structural behaviors of the cavern. In the same reason, every cavern has an extra skin as the outmost skin. The detailed steps and methodologies to construct the cavern meshes were provided by Park and Roberts [2015].

Figure 11 BC-1 cavern cavity with an extra skin

3.4.3. Abnormal Caverns

BC-4 is an abnormal shape cavern in the non-SPR caverns. The cavern is leached through three lithological layers, i.e. the caprock, interbed and salt layers. BC-4 stability has been the object of continuing concern because of its geologic similarity to collapsed BC-7 (now Cavern Lake). Sonar results in 1992 show minimal change since 1980, suggesting that significant caprock dissolution has not occurred and that overburden collapse is unlikely. However, continuing surveillance is prudent [Neal et al., 1993]. Figure 12 shows the BC-4 cavern cavity with caprock roof, interbed skin and an extra skin.

BC-7 was drilled in 1942 to a total depth of 1951 ft and developed into a cavern for the production of brine. The depth to the original top of the cavern is not known. The cavern volume was calculated from production data to be 2.9 MMB. Normal brining operations continued into the early 1950's when cavern pressure was lost. It is assumed that pressure was lost when the cavern roof was leached to the top of the salt. Brining continued by the airlift method until January, 1954 when the cavern collapsed. This resulted in the formation of a crater on the ground surface about 800 ft in diameter which filled with water and is now called Cavern Lake. The cavern's collapse resulted from leaching of the salt to the salt/caprock contact followed by the failure of the caprock and overlying sediments [Hogan, 1980]. Cavern 7 collapse began at the wellhead, eventually filling the cavern with overburden [Hogan, 1980; Neal et al., 1993]. In this model, the elevation of the top of BC-7 is assumed to be the same as the elevation of the caprock top, -500 ft then, the height of the cavern is calculated to be 1451 ft. Based on production records, the diameter of BC-7 is calculated to be 120 ft. The coordinates of BC-7 well is estimated to be (-719, 1710) from Figure 2. The measured depth of the lake was -100 ft in 1956 [The Aerospace Corporation, 1980]. The lake depth (about 100 ft) is small relative to the model

height (6400 ft) and the lake diameter (about 800 ft) is large relative to the lake depth, so the lake can be regarded as a part of the surface, and the lake geometry is simplified as flat in the surface of this model. The cavern is assumed to be cylinder shape with 120 ft diameter. The cavern roof in the caprock layer is assumed to be a conical frustum with 40 ft top diameter. A 40 ft diameter cylinder extends through the overburden layer from the ground surface to the top of the caprock. The cavern slice blocks in the caprock and interbed layers are separated from the cavern body in salt due to different material properties. The cavern height is 1460 ft rather than 1451 ft because the model meshes are discretized by 20 ft element level. The frustum shape with 120 ft and 40 ft diameters is used for the cavern roof and floor, so the amount of the cavern volume is close to 2.9 MMB. Figure 13 shows BC-7 cavern cavity with overburden, caprock, interbed and salt extra skins. The detailed steps and methodologies to construct the cavern meshes were provided by Park and Roberts [2015].

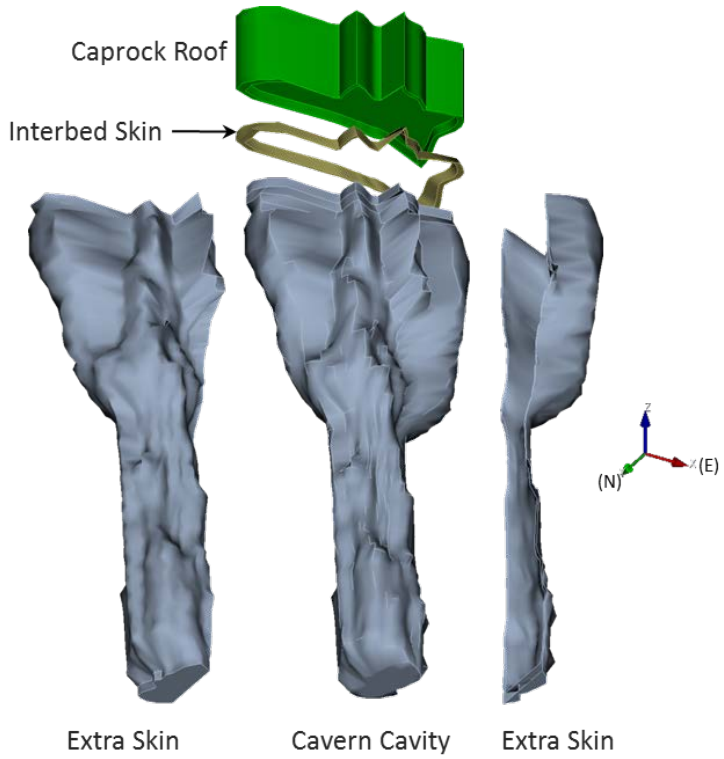

Figure 12 BC-4 cavern cavity with cavern roof, interbed skin and an extra skin

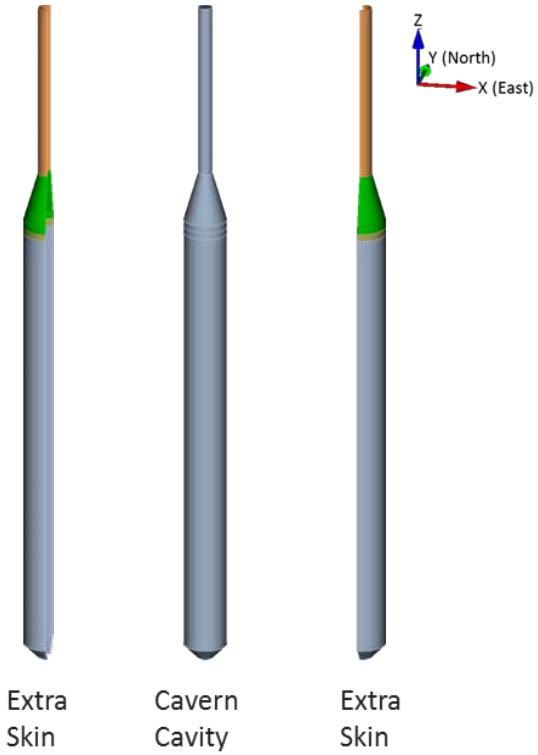

Figure 13 BC-7 cavern cavity with overburden, caprock, interbed and salt extra skins

3.4.4. SPR Caverns

As mentioned in Section 3.1, modeling of the leaching process of the caverns is performed by deleting a pre-meshed block of elements along the walls of the cavern so that the cavern volume is increased by 15 percent per drawdown. Figure 14 through Figure 20 show the volumes for each SPR cavern as developed from sonar data, along with drawdown skins (leaching layers) and extra skin. In this simulation, each SPR cavern is modeled as having five drawdown layers to be removed to account for the future oil drawdown activities. However, BC-15 and 17 are close to each other. More than four onion skins would induce poor mesh element shapes. Thus, three drawdown leaches are considered. BC-20, is close to the dome edge (less than 100 feet away). This close proximity creates two problems. The first is a physical problem, in that the closeness to the salt dome boundary poses potential cavern collapse issues (this issue is one of the driving factors for developing the meshing technique). The second is a meshing problem; the addition of even one onion skin in the narrow pillar between the cavern wall and the dome edge will probably induce generation of poor mesh element shapes. Thus, BC-20 is considered a zero drawdown-leach cavern like the non-SPR caverns.

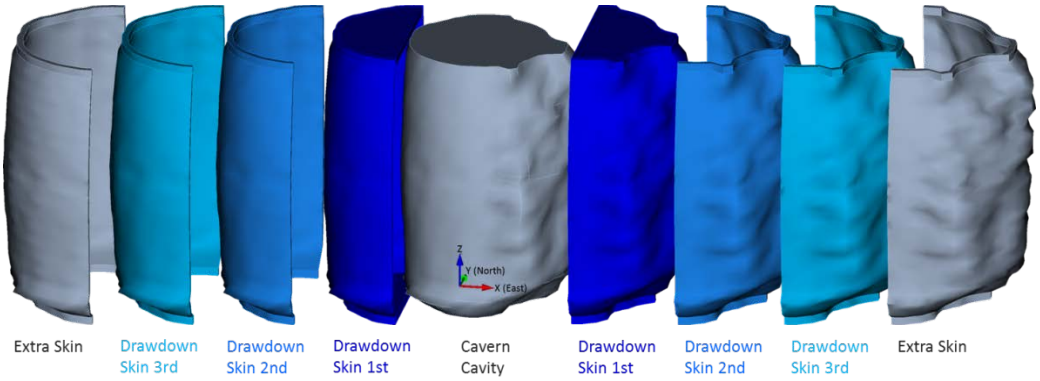

Figure 14 BC-15 cavern cavity with three drawdown skins (leaching layers) and extra skin

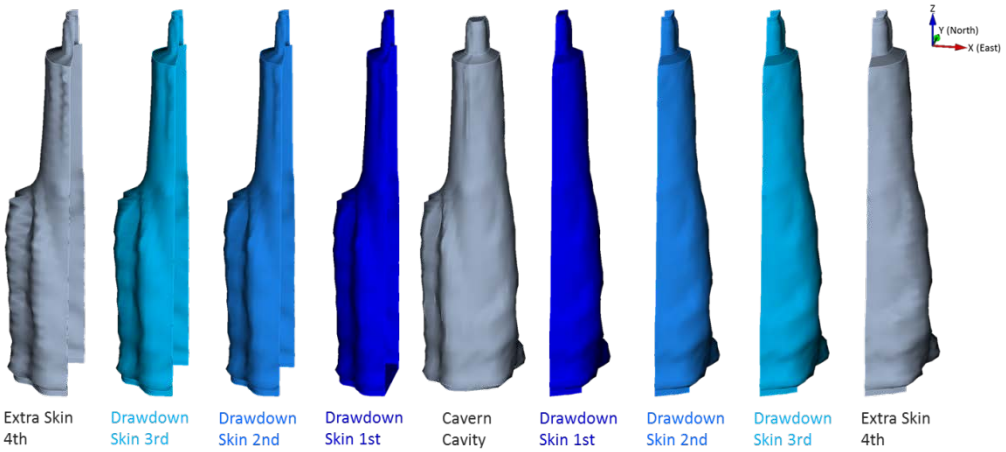

Figure 15 BC-17 cavern cavity with three drawdown skins (leaching layers) and extra skin

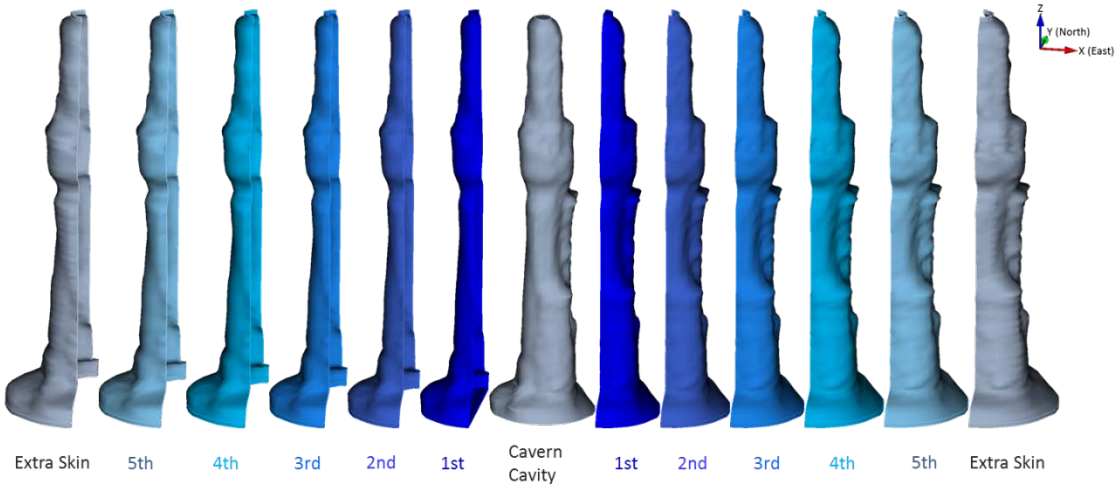

Figure 16 BC-18 cavern cavity with five drawdown skins (leaching layers) and extra skin

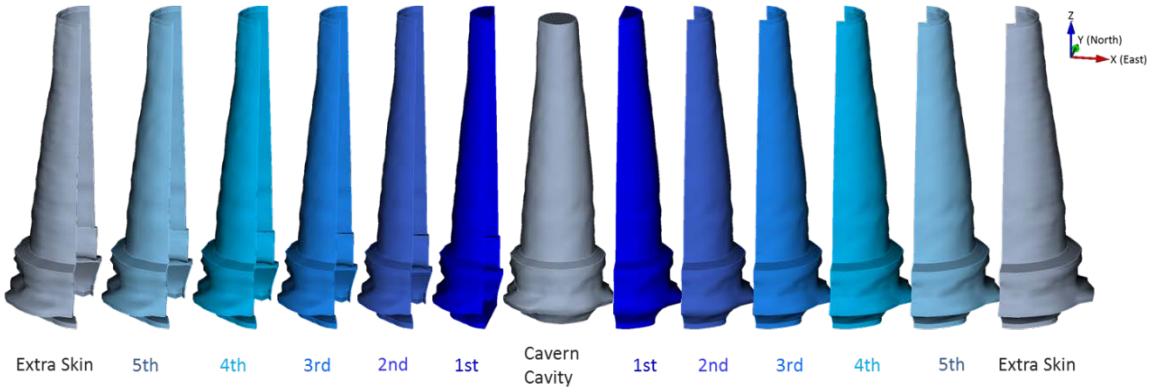

Figure 17 BC-19 cavern cavity with five drawdown skins (leaching layers) and extra skin

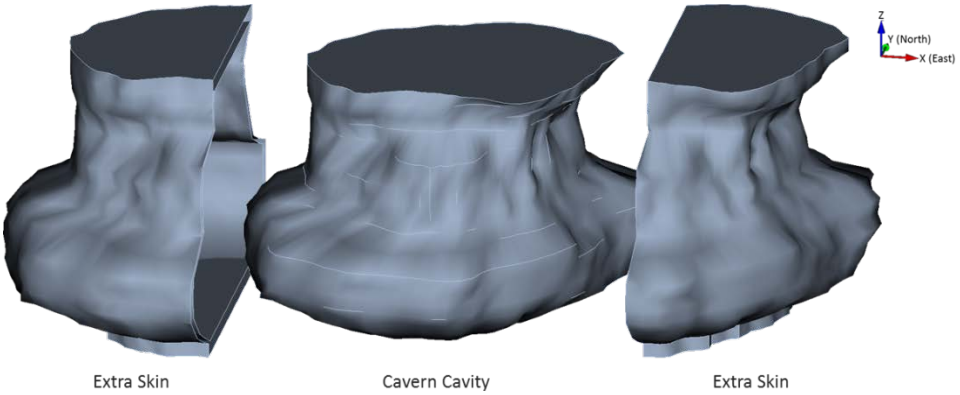

Figure 18 BC-20 cavern cavity with extra skin

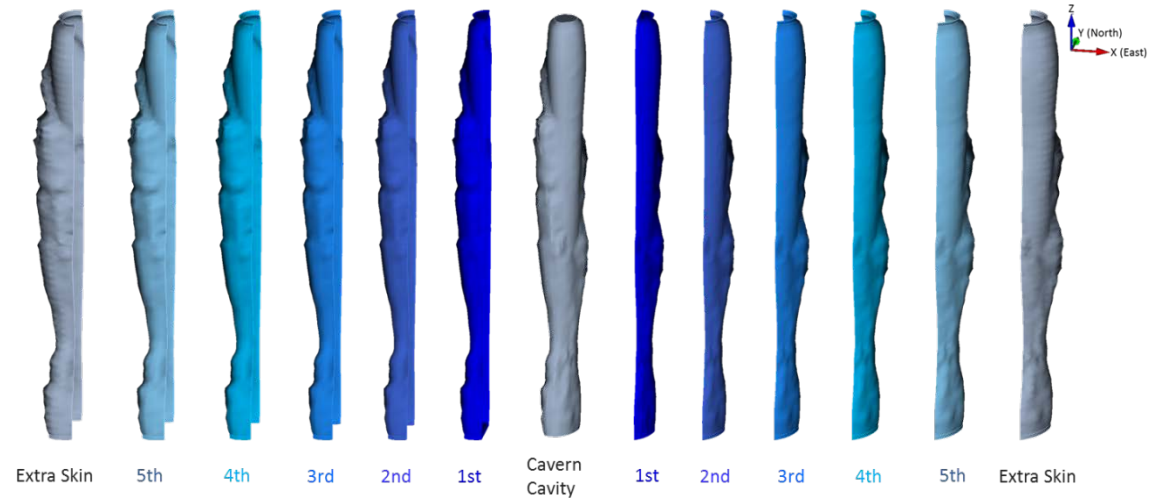

Figure 19 BC-101 cavern cavity with five drawdown skins (leaching layers) and extra skin

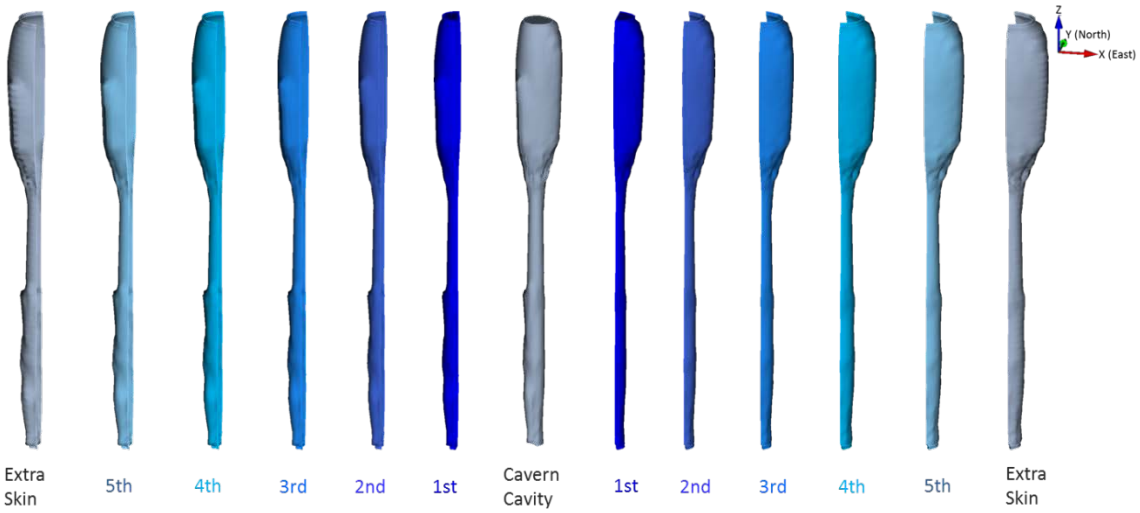

Figure 20 BC-102 cavern cavity with five drawdown skins (leaching layers) and extra skin

3.5. Entire Mesh

The BC-dome, caverns, caprock, interbed, interface, and surrounding rock blocks are combined into the entire BC-model as shown Figure 21, which also shows the overview of the hexahedral finite element mesh of the stratigraphy and cavern field at BC SPR site. The mesh consists of 7,796,127 nodes and 7,758,720 elements with 170 element blocks, 3 node sets (on the boundaries of the entire mesh, to enforce zero normal displacement boundary conditions), and 55 side sets (on the interior surfaces of the caverns and skin layers, to enforce cavern pressure boundary conditions).

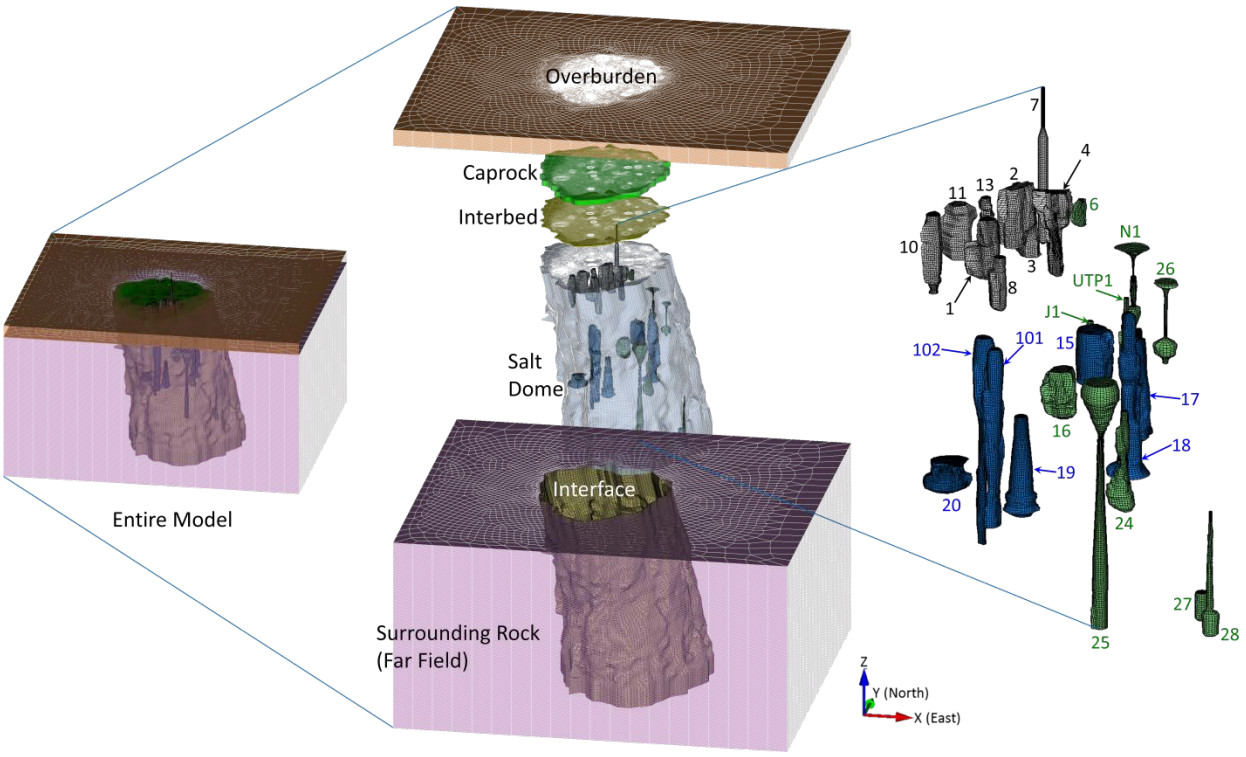

Figure 21 Finite element mesh capturing realistic geometries of Bayou Choctaw site (left), an overview of the meshes of the stratigraphy (middle), and caverns (right). The U.S. Strategic Petroleum Reserve stores crude oil in the seven blue caverns. The other caverns are the Boardwalk caverns (green) and abandoned caverns (gray). The cavern ID numbers are also shown.

4. MECHANICAL CONDITIONS

4.1. Wellhead Pressure

4.1.1. SPR Caverns

The modeling simulates the cavern responses forward in time from the cavern's initial creation. The real wellhead histories of BC-15, 17, 18, 19, and 20 were recorded from 1/1/1990 as shown Figure 22. For the purposes of the present simulation, it is assumed that the initial leaches of the caverns started on 1/1/1989 and that they were leached to full size over a one-year period.

The wellhead pressure of BC-101 was recorded from 6/1/1991, so it is assumed that the initial leach of BC-101 started on 6/1/1990, also with one year leaching period.

BC-102 was previously owned by Boardwalk. The DOE purchased BC-102 to use for SPR in 2012. The wellhead pressure has been recorded since 11/9/2012. BC-102 was filled with ethane while operated by Boardwalk. The wellhead pressure history data during Boardwalk's operations has not been obtained yet due to ongoing litigation between the U.S. government and Boardwalk. In this simulation, it is assumed that the initial leaches of the caverns started on 1/1/1989, were leached to full size over a one-year period, and the wellhead pressure was a constant 900 psi during Boardwalk's operations until 11/8/2012. The recorded wellhead pressure since 11/9/2012 is applied in the simulation.

The peak wellhead pressures over 1000 psi in Figure 22 were created by mechanical integrity tests (MIT). To investigate well casing integrity for oil leakage, nitrogen gas is injected into the well. Nitrogen gas pressure at the wellhead causes pressure peaks because the nitrogen density is much smaller than oil density. The nitrogen gas pushes the oil-nitrogen interface (ONI) down to the casing shoe, so the nitrogen replaces the oil between the wellhead and ONI. The density difference between oil and nitrogen can be offset by increased wellhead pressure, and then the resulting cavern pressure is only slightly different than under normal oil wellhead pressure. The cavern volumetric closure rate due to salt creep depends on the difference between cavern internal and lithostatic pressures. The peak pressures due to MIT do not affect the cavern internal pressure much, so the peak pressures can be ignored. The wellhead histories in Figure 22 were modified for use in the simulation as shown Figure 23. The real wellhead pressure plus oil/brine pressure gradient were applied on the inside boundary of each SPR cavern.

The most recent five-year (3/20/2010 ~ 3/19/2015) wellhead pressure history of each cavern was replicated to simulate the next five years in which no drawdown is assumed to take place, and the five future times drawdown cycles thereafter. The first drawdown leach is assumed to start at 3/20/2020 in this analysis. Figure 24 shows the wellhead histories, which consist of the real (1/1/1990 ~ 3/19/2015) and the assumed future (3/20/2015 ~ 3/19/2045) pressures used for seven SPR caverns in the simulation. BC-102 does not have an entire record for the previous five-year (3/20/2010 ~ 3/19/2015) period, so the concurrent five year history from BC-101 is used instead. This assumption seems reasonable based on the two caverns' locations, i.e. the depths of the cavern tops are similar.

Before a cavern's initial leach starts, the model has a stabilization period (1/1/1900 ~ 12/31/1988). To avoid the numerical shock, gravity is applied gradually into the mesh for ten seconds. After that, the model is allowed to consolidate with gravity for 89 years so that every element is stabilized numerically.

The analysis simulates caverns that were leached to full size over a one-year period by means of gradually switching from salt to fresh water in the caverns. It was assumed that the SPR caverns were filled with petroleum and non-SPR caverns were filled with either brine or a liquid or gas petroleum product after the initial leaching. Creep is then permitted to occur over the entire simulation period (1/1/1990 ~ 3/19/2045). On 3/20/2020, and subsequently every 5 years thereafter, the SPR caverns are instantaneously leached to produce an increased volume of 15% during each leach cycle to simulate drawdowns. Modeling of the leaching process in the caverns was accomplished by deleting elements along the walls of the caverns so that the volume increased by 15% with each leach. Leaching is assumed to occur uniformly along the entire height of the cavern. However, leaching is not simulated in the floor or roof of the caverns. The 5-year period between each drawdown allows the stress state in the salt to return to a steady-state condition, as will be evidenced in the predicted closure rates. The simulation was run to the time 3/19/2045 to investigate the structural behavior of the dome for 55 years, as the process of salt creep continues to reduce the cavern volumes.

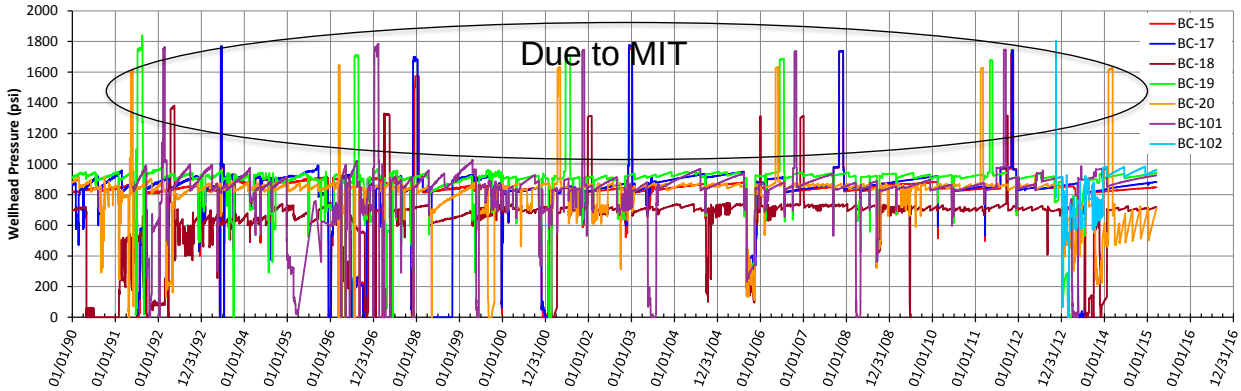

Figure 22 Wellhead pressure histories for the seven Bayou Choctaw SPR caverns provided by the field office

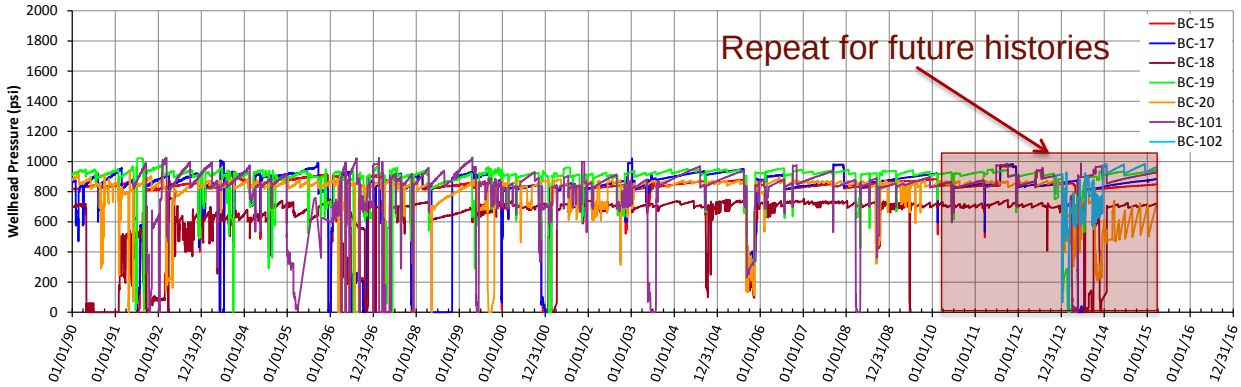

Figure 23 Modified wellhead pressure histories for the seven Bayou Choctaw SPR caverns

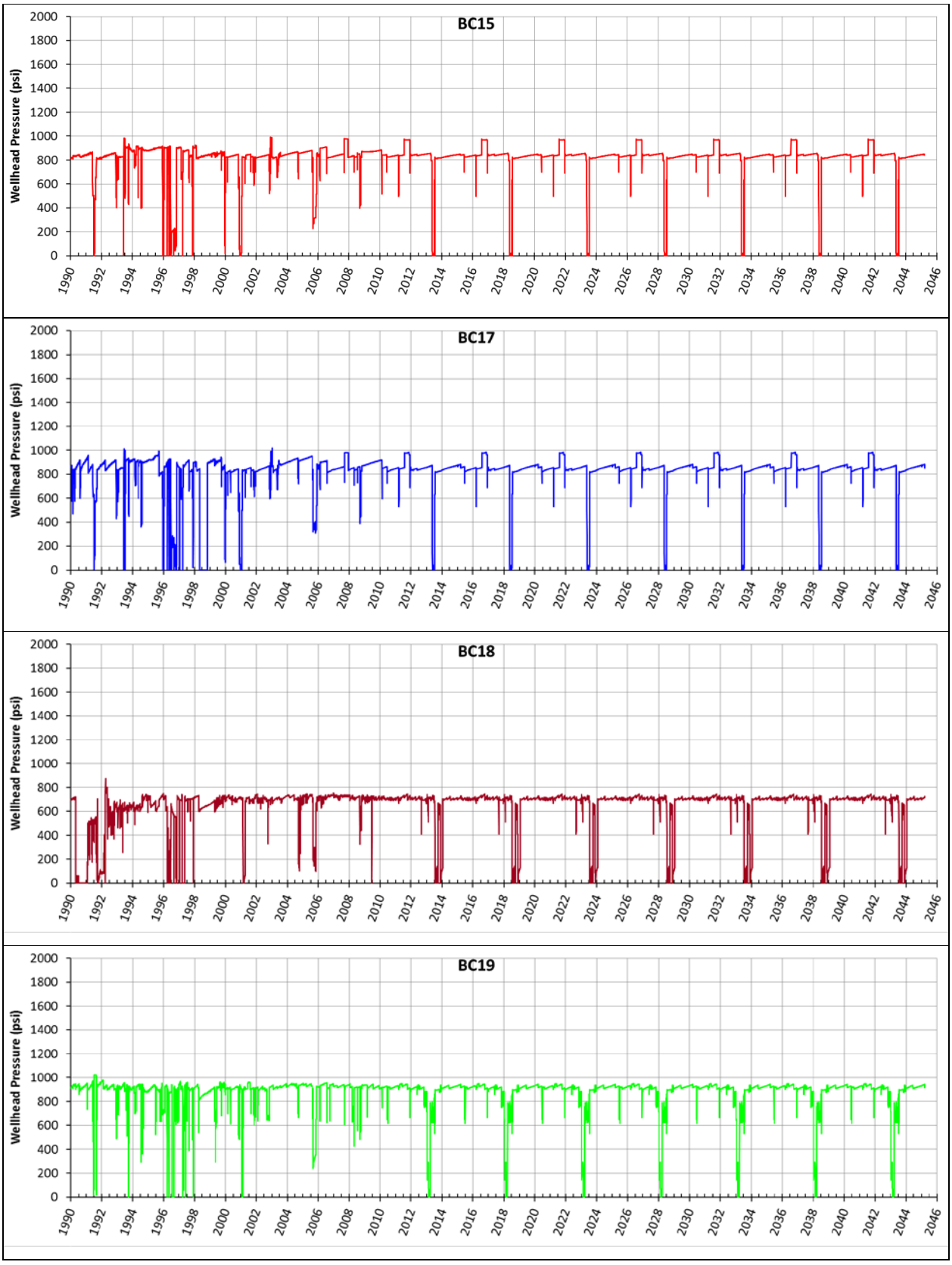
BC15
BC17
BC18
BC19
Wellhead Pressure (psi)
0
200
400
600
800
1000
1200
1400
1600
1800
2000
1990
1992
1994
1996
1998
2000
2002
2004
2006
2008
2010
2012
2014
2016
2018
2020
2022
2024
2026
2028
2030
2032
2034
2036
2038
2040
2042
2044
2046

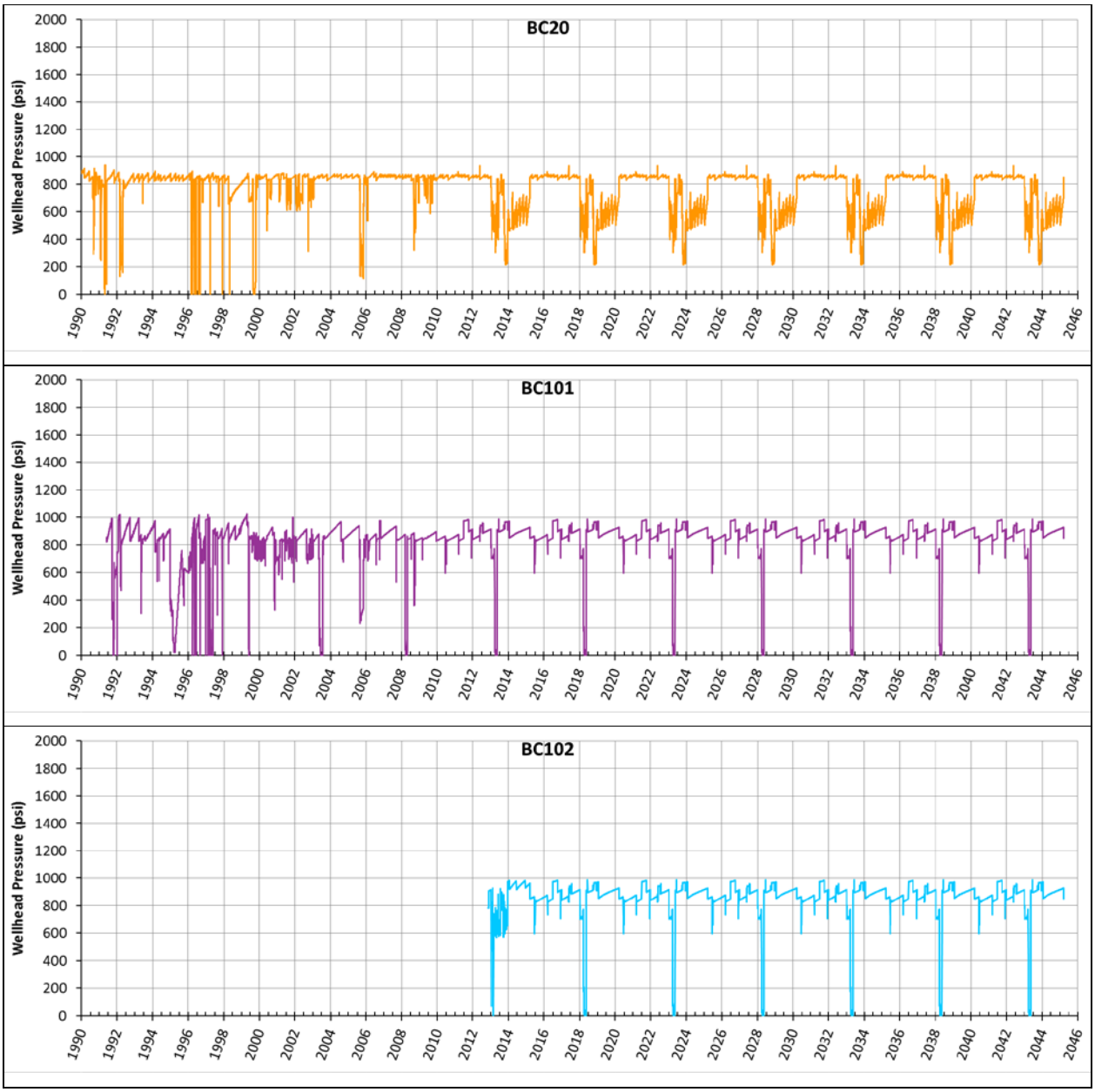

Figure 24 Individual Bayou Choctaw SPR caverns' wellhead pressure histories used in this analysis

4.1.2. Boardwalk Caverns

BC-6, 16, 24, 25, 26, 27, 28, J1, N1, and UTP1 are owned by Boardwalk. The wellhead pressure history data has not yet been provided by Boardwalk because of ongoing litigation between the government and Boardwalk. In this simulation, it is assumed that the initial leaches of the caverns started on 1/1/1989 and they were leached to full size over a one-year period. The wellhead pressure is assumed to be a constant 900 psi over time.

4.1.3. Abandoned Caverns

The abandoned caverns were all plugged with the exception of BC-4. The wellheads were cut off below the surface and buried.

The abandoned caverns were filled fully with brine before plugging. Figure 25 shows pressure distributions on the inside and outside of BC-1 before and after plugging as an example. The lithostatic pressure gradient with depth (1.0 psi/ft) is larger than the brine pressure gradient (0.52 psi/ft). The gradient difference drives the cavern volumetric closure due to salt creep. The brine volume does not decrease over time because there are no leaks, while the cavern volume decreases due to creep until an equilibrium state is reached. The hydrostatic pressure in the cavern increases until pressure equilibrium, i.e. the pressure head increases for some time after the plugging. The pressure head, which is an additional hydrostatic pressure due to the cavern volumetric closure, is calculated to be 578 psi at equilibrium. The calculation sheet for BC-1, as an example, is provided in Appendix I. In the same manner, the pressure heads of the abandoned caverns at equilibrium state are calculated as listed in Table 2. These values are used over time as wellhead pressures in the analysis. Although there are no more pressure increases after equilibrium is reached, pressure differences do occur on the top and bottom of cavern due to gradient with depth (1.0 psi/ft vs. 0.52 psi/ft). Therefore, the bottom area shrinks while the top area expands like a bubble, so a risk of fracturing in the roof could occur.

BC-4 still has a wellhead and is actively monitored with sonars and well logging runs. It cannot hold fluid due to communication with the caprock, so zero wellhead pressure is applied in the analysis conservatively.

BC-7 was drilled in 1942 to a depth of 1951 ft. The depth to the original top of the cavern is not known. The cavern volume was calculated from production data to be 2.9 MMB. Normal brining operations continued into the early 1950's when cavern pressure was lost. It is assumed that pressure was lost when the cavern roof was leached to the top of the salt. Brining continued by the airlift method until January 1954 when the cavern collapsed. This resulted in the formation of a crater about 800 ft in diameter which filled with water and is now called Cavern Lake. The measured depth of the lake was 100 ft in 1956 [The Aerospace Corporation, 1980]. The lake depth is small relative to the model height (6400 ft) and the lake diameter (about 800 ft) is large relative to the lake depth, so the lake is regarded in this model as a part of the surface and its geometry is simplified as flat. The cavern's collapse resulted from leaching of the salt to the salt/caprock contact followed by the failure of the caprock and overlying sediments [Hogan, 1980]. Cavern BC-7's collapse began at the well-head and the void filled with overburden [Hogan, 1980; Neal et al., 1993]. In this model, it is assumed that the cavern volume no longer decreases due to salt creep because the overburden material in the cavern void has been compacted by salt lithostatic pressure to be able to counteract the salt's movement. Therefore, the cavern internal is regarded as a solid made of overburden material in this model.

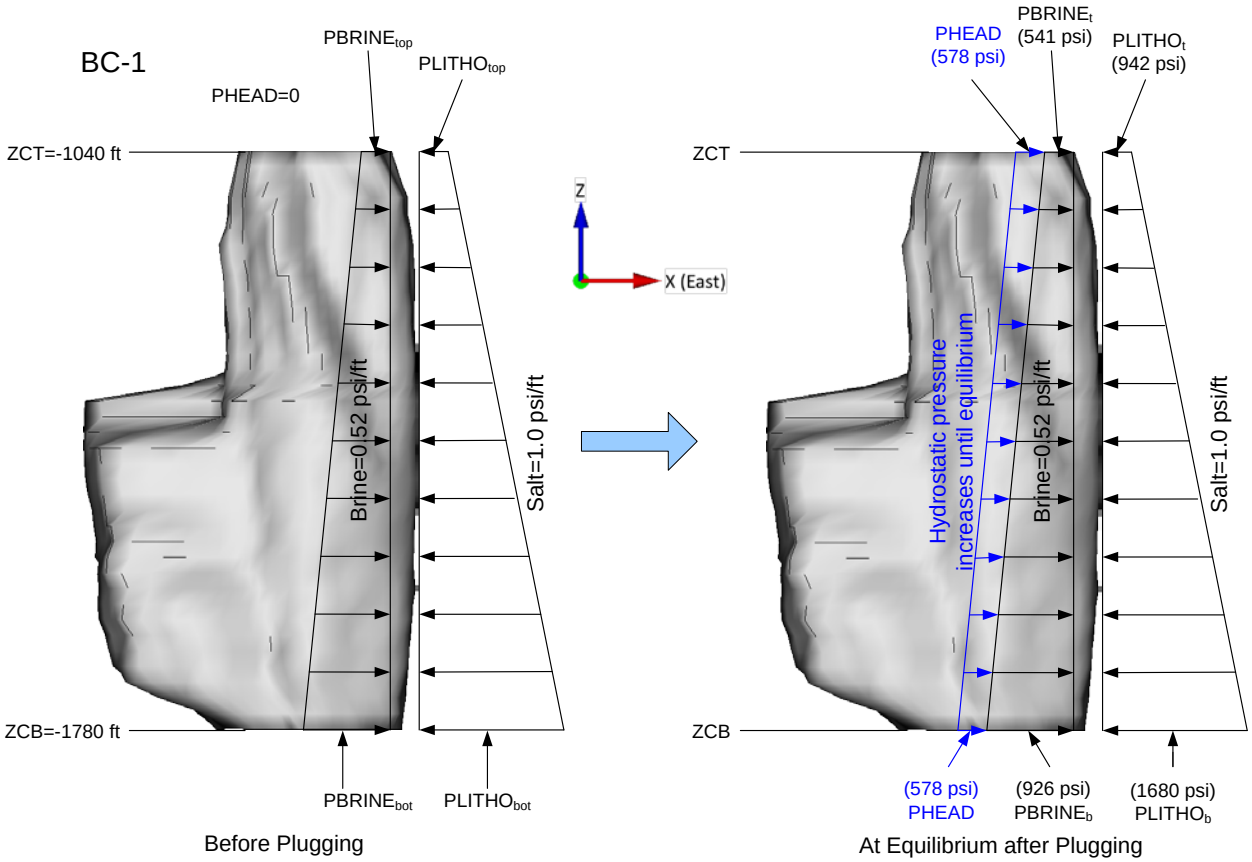

Figure 25 Pressure distribution change before and after plugging in BC-1

Table 2 Calculated pressure heads for the abandoned caverns at equilibrium state

Cavern ID	Depth of cavern top (ft)	Depth of cavern bottom (ft)	Lithostatic pressure at cavern top (psi)	Lithostatic pressure at cavern bottom (psi)	Brine pressure at cavern top (psi)	Brine pressure at cavern bottom (psi)	Pressure head at equilibrium (psi)
BC-1	-1040	-1780	942	1680	541	926	578
BC-2	-780	-1520	683	1421	406	791	454
BC-3	-1020	-1840	922	1740	531	957	587
BC-8	-1300	-1960	1202	1860	676	1020	683
BC-10	-1000	-1980	902	1880	520	1030	616
BC-11	-1080	-1740	982	1640	562	905	578
BC-13	-1120	-1860	1022	1760	583	968	616

4.2. Oil-Brine Interface

4.2.1. SPR Caverns

Previous analyses [Part et al., 2006; Park and Ehgartner, 2008; Park and Ehgartner, 2010] assumed that the SPR caverns were filled fully with oil. In actuality, however, the caverns were not always fully filled with oil. Brine filled the bottom of cavern and the portion changes with time depending on cavern operations. The difference between pressure gradients of oil (0.37

psi/ft of depth) and brine (0.52 psi/ft of depth) cannot be ignored. So, the amounts of oil and brine in a cavern over time needs to be considered. The effect of the oil-brine interface (OBI) depth change will be described in Section 6.1.

Figure 26 shows the OBI depth histories used in this analysis. The history data (1/1/1990 ~ 3/19/2015) were obtained from the field office. It is assumed that the OBI depth of each cavern does not change after 3/19/2015 for the future simulation (3/20/2015 ~ 3/19/2045).

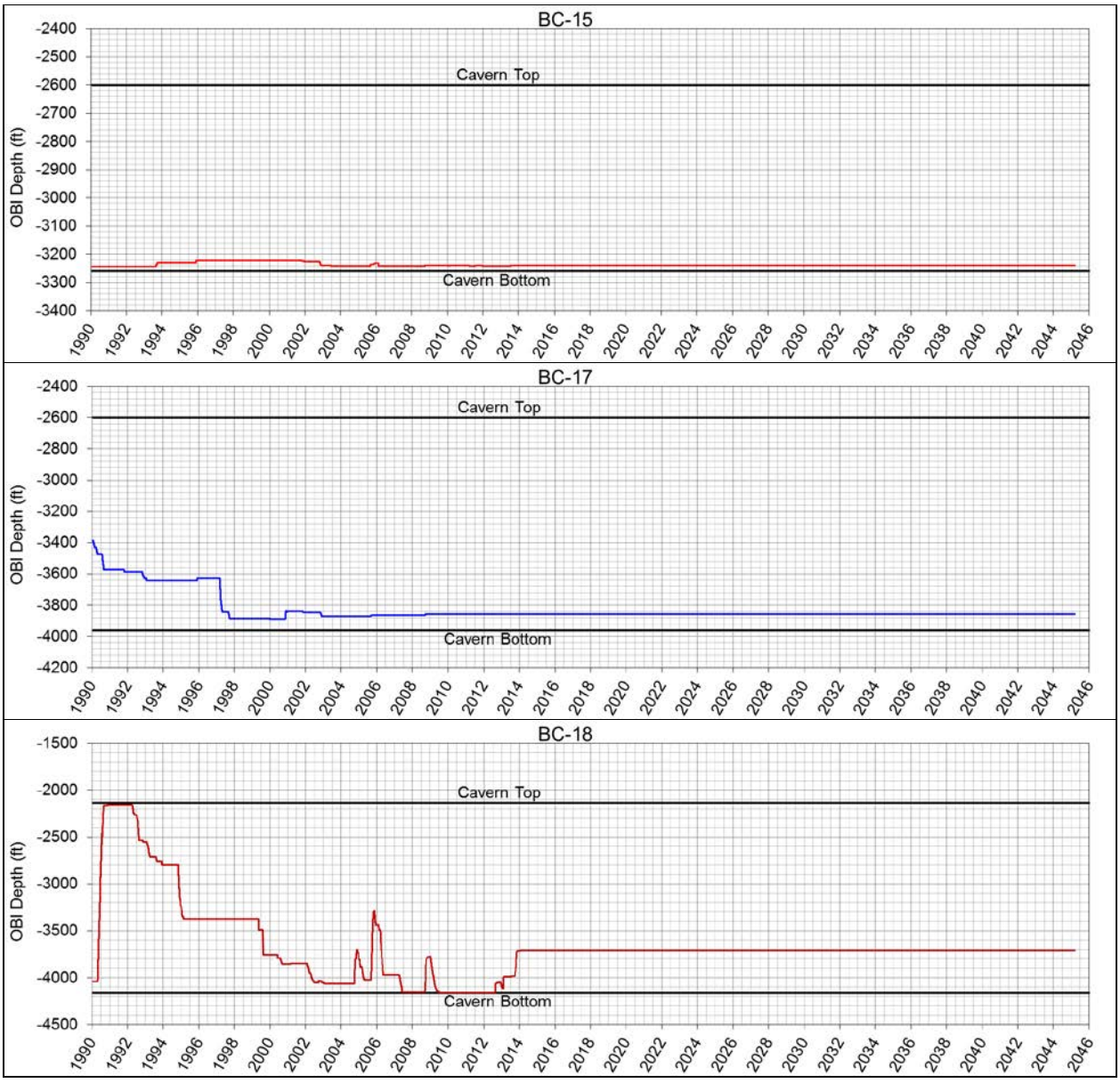

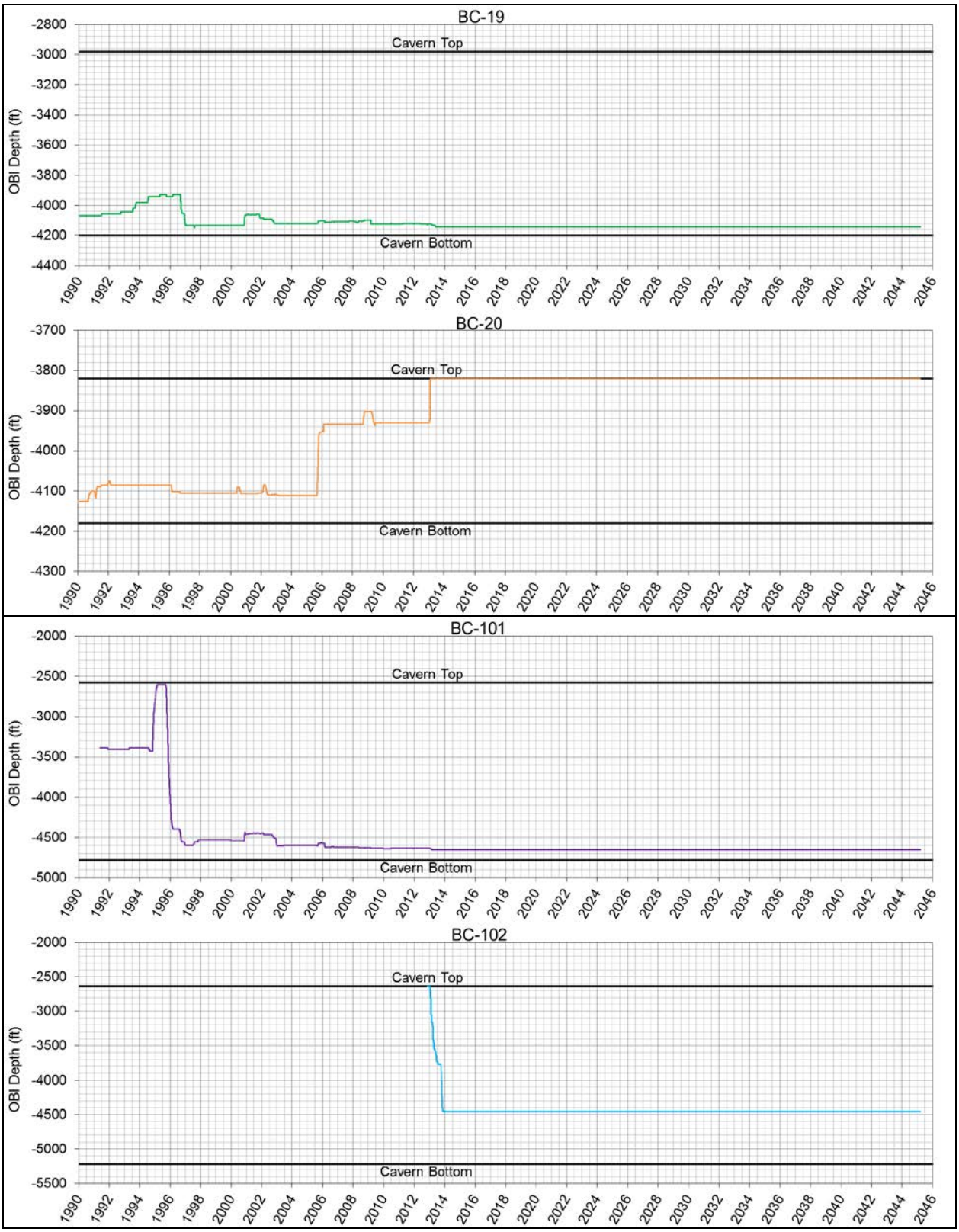

Figure 26 Oil-Brine Interface depth histories to apply into the simulation for seven Bayou Choctaw SPR caverns

4.2.2. Boardwalk Caverns

BC-6, 16, 24, 25, 26, 27, 28, J1, N1, and UTP1 are owned by Boardwalk. The wellhead pressure history data has not yet been provided by Boardwalk, due to ongoing litigation between the U.S. government and Boardwalk. In this simulation, it is assumed that the initial leaches of the caverns started on 1/1/1989, that the caverns were leached to full size over a one-year period, and that the wellhead pressure was a constant 900 psi over time. The products held within Boardwalk caverns and their pressure gradients with depth applied in the analysis are listed below in Table 3.

Table 3 Products held within Boardwalk caverns and pressure gradient of depth

Cavern ID	Product	Pressure gradient of depth (psi/ft)
BC-6	Propylene	0.22
BC-16, N1, UTP1	Ethylene	0.54
BC-24	Natural gas	0.18
BC-J1	Ethane	0.25
BC-25, 26, 27, 28	Brine	0.52

4.3. Temperature

The finite element model includes a depth-dependent temperature gradient which starts at 84.0°F (28.9°C) at the surface and increases at the rate of 1.38°F/100 ft (2.51°C/100 m). The temperature profile is based on the average temperature data recorded in well logs from BC prior to leaching [Ballard and Ehgartner, 2000]. The temperature distribution is important because the creep response of salt is temperature dependent. Radial temperature gradients due to cavern cooling effects from the cavern contents are not considered in these calculations. Previous 2D cavern studies have shown the predicted cavern deformation to be insensitive to the developed radial thermal gradients [Hoffman, 1992].

4.4. Boundary Condition

Figure 27 shows the assembled mesh and the boundary conditions. The lengths of the confining boundaries are 11,000 ft in the N-S direction and 12,000 ft in the E-W direction. The boundary dimensions are determined by more than two times of the dome's range in each direction. The salt dome is modeled as being subject to a regional far-field stresses acting from an infinite distance away. The sizes of the caverns are horizontally much smaller than the dome. Therefore, the North and South sides of far-field boundary are fixed in Y-direction, and the East and West sides are fixed in X-direction. The bottom is fixed vertically. The top surface and four sides are vertically free. The acceleration of gravity used in the model is 9.81 m/s^2 (32.174 ft/s^2).

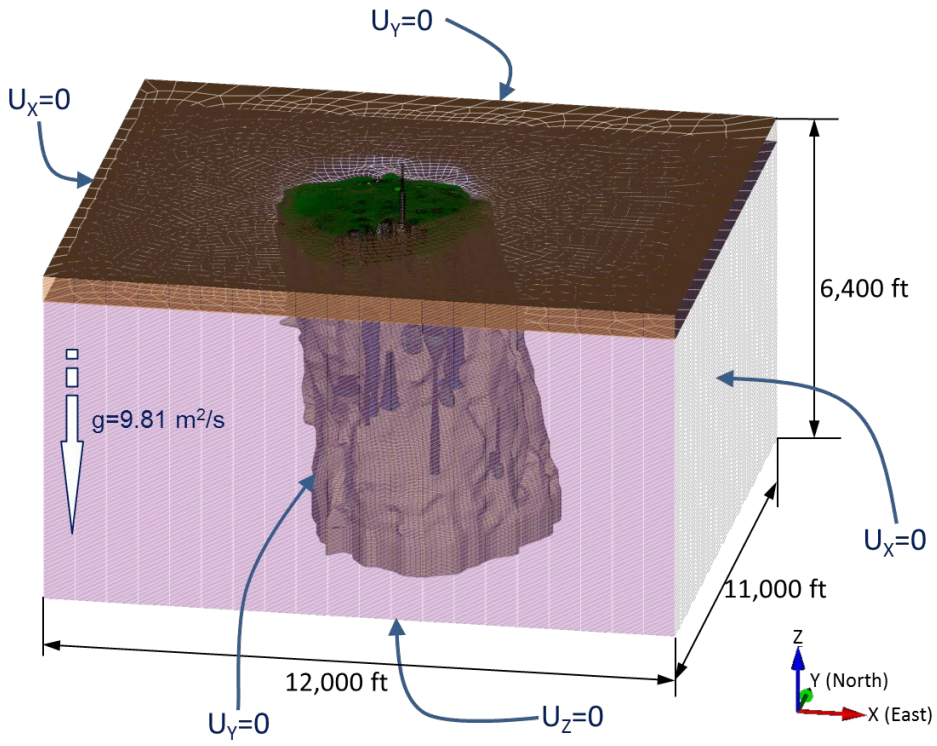

Figure 27 Boundary conditions of Bayou Choctaw Model

5. MATERIAL MODEL AND PROPERTIES

5.1. Salt

The previous BC analyses [Part et al., 2006; Park and Ehgartner, 2008; Park and Ehgartner, 2010] were conducted using the PLC model, a simplified creep model that calculates the secondary steady-state creep mechanism, a subset of the more complete multi-mechanism deformation (M-D) model of salt creep. The PLC considers only the secondary creep rate (steady-state, long term), while M-D considers not only the secondary but also the primary (initial stage, short term) and the tertiary (beyond steady-state) as shown Figure 28. The implementation of the power law creep model included the use of a reduced elastic modulus to simulate the transient response of the salt to pressure changes. The resulting simulations provided satisfactory predictions of long-term creep behavior, but not of transient response to pressure changes. The geological concerns issued recently require more accurate numerical predictions. For a higher-resolution geomechanical simulation, the FE mesh capturing realistic geometries of the salt dome and caverns and M-D salt constitutive model are required. The M-D model proposed by Munson and Dawson [1979, 1982, 1984] and extended by Munson et al. [1989], has been included in ADAGIO to model the creep behavior of rock salt.

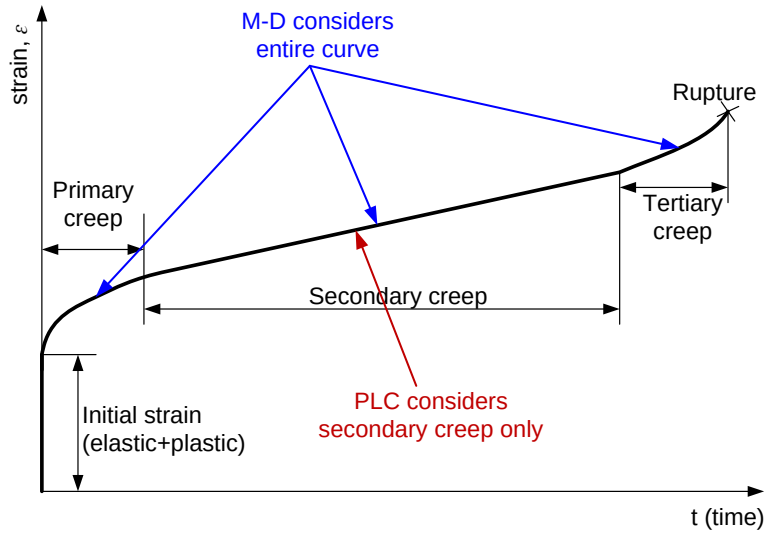

Figure 28 Comparison between M-D and Power Law Creep models

Creep is the time-dependent deformation of a material. Traditionally, a creep curve is thought to consist of three stages as shown in Figure 28. Experimental data obtained from a uniaxial stress laboratory creep test where the stress is held constant are typically of this form. In the first stage (primary), the creep rate decreases with time. In the second stage (secondary), the creep rate is constant (steady-state), and in the third stage (tertiary), the creep rate increases through progressive fracture formation and eventually terminates by failure of the specimen. Most uniaxial and triaxial compression tests do not reach the tertiary creep stage simply because of the amount of time required to get there. Empirically derived creep laws historically have described the shape of the creep curve through mathematical functions that consider the creep as the sum of transient and steady-state contributions. Transient creep is in general the response of the material

to incremental and decremental stress changes. This definition, thus, includes the transient of primary creep response to the initial loading in a standard creep test [Munson and Dawson, 1982].

Principles gained from our understanding of the constitutive behavior of WIPP salt will form the principal basis for the analysis strategy. Not only do the constitutive equations of the M-D model define the necessary material parameters, but they also permit the formulation of rules of the analysis. In developing the constitutive description, we concern ourselves only with the temperature and stress range encountered in mining and storage cavern operations, typically low temperature and low to moderately high stresses. For these conditions, creep is envisioned as arising from the contributions of three appropriate micromechanical mechanisms as determined from salt deformation mechanism-map [Munson, 1979]. These mechanisms are (1) a dislocation climb controlled creep mechanism at high temperatures and low stresses, (2) an empirically specified, but undefined mechanism at low temperatures and low stresses, and (3) a dislocation slip controlled mechanism at high stresses [Munson, et al., 1989]. These mechanisms act in parallel, which means the individual steady-state creep rates can be summed over the three mechanisms to give the total steady-state creep rate, as follows [Munson, 1998]:

$$\dot{\varepsilon}_s = \sum_{i=1}^{3} \dot{\varepsilon}_{s_i} \tag{1}$$

The steady-state creep rates for the individual mechanisms, respectively, are given by:

$$\dot{\varepsilon}_{s_1} = A_1 e^{-\frac{Q_1}{RT}} \left[\frac{\sigma}{\mu(1-\omega)}\right]^{n_1} \tag{2}$$

$$\dot{\varepsilon}_{s_2} = A_2 e^{-\frac{Q_2}{RT}} \left[\frac{\sigma}{\mu(1-\omega)}\right]^{n_2} \tag{3}$$

$$\dot{\varepsilon}_{s_3} = |H(\sigma-\sigma_0)| \left(B_1 e^{-\frac{Q_1}{RT}} + B_2 e^{-\frac{Q_2}{RT}}\right) \sinh\left[\frac{q\left(\frac{\sigma}{1-\omega}-\sigma_0\right)}{\mu}\right] \tag{4}$$

where the numerical subscripts refer to the appropriate mechanism, the *A*'s and *B*'s are structure factors, *Q*'s are activation energies, *R* is the universal gas constant, *T* is the absolute temperature, μ is the shear modulus, q is the stress constant, σ_0 is a stress limit, and H is a Heaviside step function with argument (σ - σ_0). It has been shown [Munson, et al., 1989] through multiaxial experiments that the proper equivalent stress measure is $\sigma = |\sigma_1 - \sigma_3|$.

The equivalent total strain rate is treated through a multiplier on the steady-state rate, as

$$\dot{\varepsilon}_{eq} = F\dot{\varepsilon}_s \tag{5}$$

where the multiplier involves three branches of the transient creep curve: work-hardening, steady-state, and recovery, respectively, as follows:

$$F = \begin{cases} e^{\Delta\left(\left(1-\frac{\zeta}{\varepsilon_t^*}\right)^2\right)}; & \zeta < \varepsilon_t^* \\ 1 \qquad\qquad\quad ; & \zeta = \varepsilon_t^* \\ e^{-\delta\left(\left(1-\frac{\zeta}{\varepsilon_t^*}\right)^2\right)}; & \zeta > \varepsilon_t^* \end{cases} \tag{6}$$

Here, Δ is the work-hardening parameter, δ is the recovery parameter, ζ is the state parameter, and ε^*_t is the transient strain limit. The state parameter rate is given by

$$\dot{\zeta} = (F - 1)\dot{\varepsilon}_s \tag{7}$$

The transient strain limit is defined by

$$\varepsilon_t^* = K_0 e^{cT} \left(\frac{\sigma}{\mu(1-\omega)} \right)^m \tag{8}$$

where K_0 and c are constants and m is a material constant.

The work-hardening, Δ, and recovery, δ, parameters are described through linear functions, as follows:

$$\Delta = \alpha_w + \beta_w \log \frac{\sigma}{\mu(1-\omega)} \tag{9}$$

$$\delta = \alpha_r + \beta_r \log \frac{\sigma}{\mu(1-\omega)} \tag{10}$$

where the α's and β's are constants. Throughout these equations, although it is taken as zero for our purposes here, ω is the damage parameter.

Fundamentally, salt creep behavior has common micromechanical constitutive features regardless of the origin of the salt, all that differs is the exact value of the parameters. In particular, those critical parameters that primarily distinguish one salt material from another salt material are the steady-state responses as represented by the structure factors (A's and B's) and the transient strain rate limits (ε_t^*) as represented by K_0. By using the analysis criteria given above and the known behavior from the well-documented tests of clean WIPP salt as a baseline response, it may be possible on the one hand to construct reasonable steady-state responses for the domal salts. On the other hand, determination of the transient strain limit depends critically upon having the complete transient strain curves, i.e., complete conventional raw creep curves. In the absence of these curves, only uncertain estimates can be made for values for this parameter. Often, the only recourse in this case is to estimate the transient strain limit values based on the particle impurity level and the measured values from the clean and argillaceous WIPP salts. Remaining parameters are either unaffected by or insensitive to the specific salt material [Munson, 1998].

Neal et al. [1993] analyzed the geology of the Bayou Choctaw dome and reported on some of the mineralogy. Core taken down to 728 m (2390 ft) from Well 101 was clear with 10 to 20 mm (0.4 to 0.8 inch) diameter grains, and 1 mm (0.04 inch) gray anhydrite bands. Core from 1446 m (4743 ft) was black with 5 mm (0.2 inch) crystals and about 5% anhydrite in wavy bands.

The creep response from one specimen of Bayou Choctaw salt prepared from core obtained from Well 19A was determined using an incremental stress and temperature change procedure [Wawersik and Zeuch, 1984]. This material was medium grained, with the maximum grain size of 19 mm (0.75 inch) and with uniformly distributed anhydrite crystals as the principal impurity. The anhydrite concentration in this specimen probably was no more than 4.2 %, based on dissolution of specimen remains. The incremental creep rates are shown in Figure 29. Unfortunately, the incremental tests involved several stress drops. If the stress drop increment results are eliminated (we do not show a plot of this), the 60°C minimum data are essentially identical to the 25°C WIPP clean salt baseline. The 80°C data are consistent, being offset

somewhat above the 22°C Bayou Choctaw test results. As a consequence, the Bayou Choctaw material appears to be more creep resistant than the WIPP clean salt by about a factor of 0.17 [Munson, 1998].

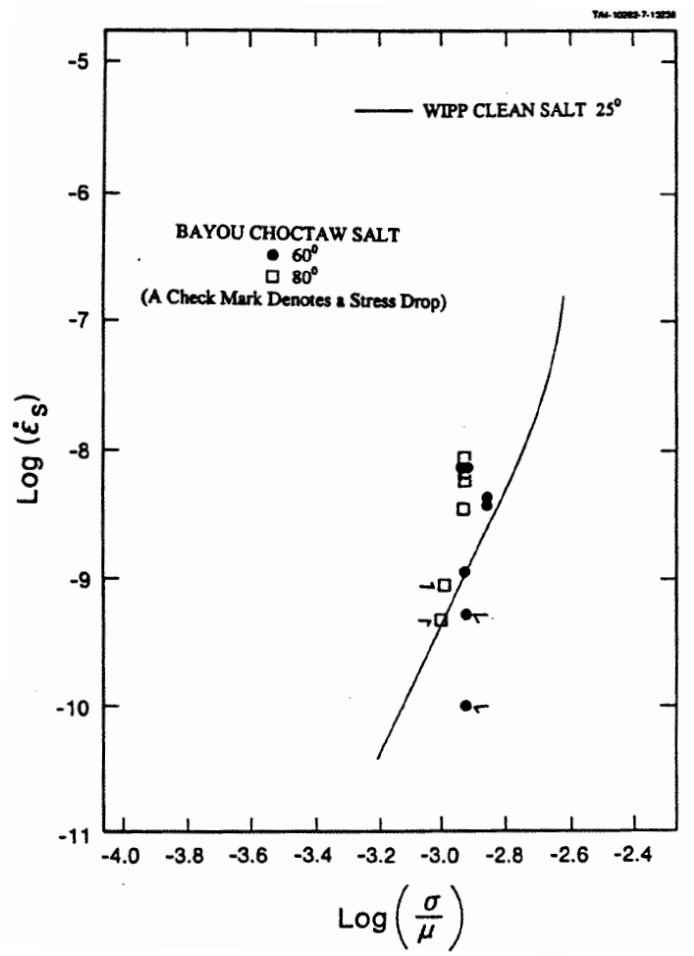

Figure 29 Incremental test creep rates for Bayou Choctaw [Data of Wawersik and Zeuch, 1984]

Indirect substantiation of the effect of differences in the creep response of domal salt is found in the work of Ehgartner et al. [1995] on loss of volume of petroleum storage caverns of the SPR. These results are produced from a CAVEMAN simulation methodology based on the M-D creep equations. The methodology generates a set of "effective" fitting parameters for material, geometry, pressurization, and stress in the cavern setting as determined from cavern fluid loss histories and can be used to predict "effective" SPR cavern creep rates. These rates have been reported [Linn, 1997] from an ullage study. The effective creep rates in volume loss percentage per year (the same as a linear rate) are shown in Figure 30. Of the four facilities studied, Big Hill and West Hackberry show the highest creep volume loss rates; whereas, Bryan Mound and Bayou Choctaw show the lowest creep volume loss rates [Munson, 1998].

By applying ratios determined from the creep results, we can establish some suggested M-D creep parameters. However, the limited database permits only structure factors to be determined; all other parameters must be established on the basis of the clean WIPP salt database and the

logical extension of the WIPP parameters, considering how material variation can affect the parameter. These results are given in Table 4 for clean WIPP salt and the Bayou Choctaw salt [Munson, 1998].

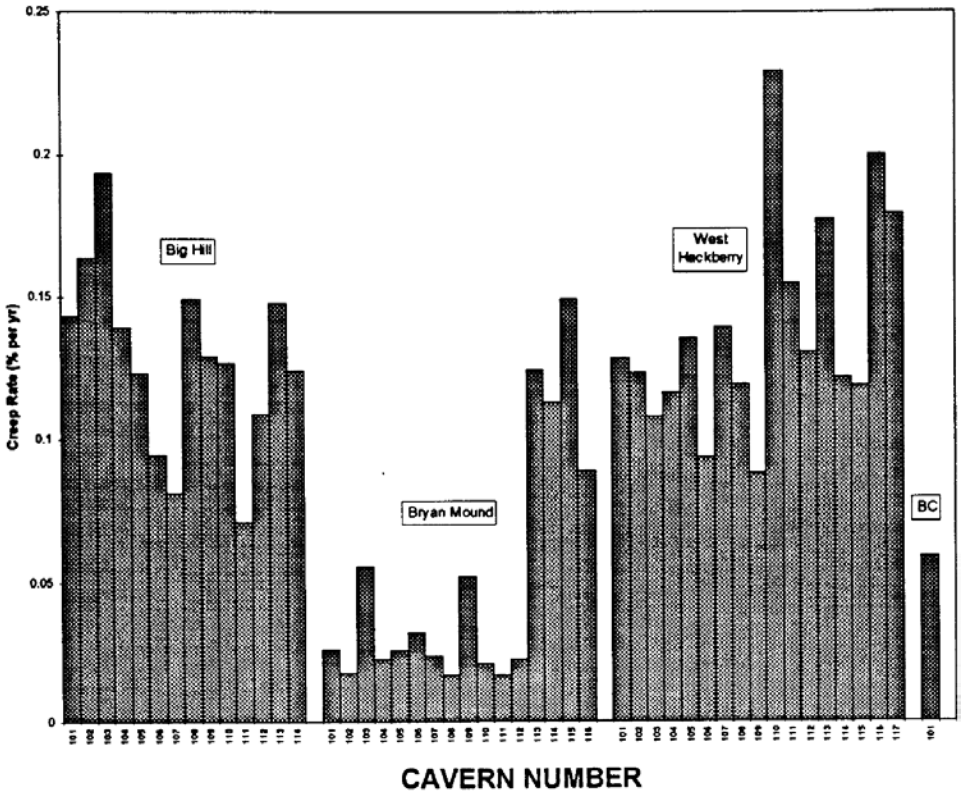

Figure 30 CAVEMAN calculated volume creep rates for SPR caverns [Linn, 1997]

Table 4 Suggested parameter values for the M-D model of Bayou Choctaw salt [Munson, 1998]

Mechanism	Parameter	Symbol	Unit	WIPP Salt Baseline	BC Salt
Conventional	Density	ρ	lb/ft^3	**143.58 (2300 kg/m^3)**	143.58
Elasticity	Young's Modulus	E	psf	**647447400 (31.0 GPa)**	647447400
	Shear Modulus	μ	psf	**258978960 (12.4 GPa)**	258978960
	Poisson's Ratio	ν	-	**0.25**	0.25
Dislocation climb controlled creep mechanism at high temperatures and low stresses (Eq. 2)	Structure factor	A_1	1/s	**8.386×10^{22}**	1.445×10^{22}
	Activation energy	Q_1	cal/mol	**25000**	25000
	Stress exponent	n_1	-	**5.5**	5.5
Empirically specified but undefined mechanism at low temperatures and low stresses (Eq. 3)	Structure factor	A_2	1/s	**9.672×10^{12}**	**1.667×10^{12}**
	Activation energy	Q_2	cal/mol	**10000**	10000
	Stress exponent	n_2	-	**5.0**	**5.0**
Dislocation slip controlled mechanism at high stresses (Eq. 4)	Structure factor	B_1	1/s	**6086000**	1048941
	Structure factor	B_2	1/s	**0.03034**	0.005229
	Stress limit	σ_0	psf	**429613 (20.57 MPa)**	429613
	Stress constant	q	-	**5335**	5335
Transient strain (Eq. 8)	Material constant	m	-	**3.0**	3.0
	Constant	K_0	-	**627500**	(627500)
	Constant	c	1/K	**0.009198**	0.009198
Work-hardening and recovery (Eq. 9&10)	Constant	α	-	**-17.37**	-17.37
	Constant	β	-	**-7.738**	-7.738
	Recovery	δ	-	**0.58**	0.58
	Damage	ω	-	**0.0**	0.0
Structure factor multiplication factor from WIPP 25°C salt		*SMF*	-	**-**	0.172353*

Note:
- Bold numbers are determined from creep data for that specific salt material.
- Underlined value is theoretical micro-mechanism constants and are the same as WIPP clean salt values.
- K_0 value in parentheses is assumed.
- All other values are assumed to be the same as the WIPP salt values or adjusted from the WIPP salt value in proportion to the A_2 value obtained experimentally for Bayou Choctaw salt.
- Because the Multi-mechanism Deformation (M-D) model is used, the equations given in this report require a zero value of ω
- * - = $A_{2\,\text{BC Salt}}$ / $A_{2\,\text{WIPP Salt}}$, A_1, B_1, and B_2 of BC salt are multiplied those of WIPP salt by *SMF*

5.2. Lithologies Encompassing Salt

An elastic model is assumed for the lithologies encompassing the salt dome. The surface overburden layer, which is mostly comprised of sand, is assumed to exhibit elastic material behavior. The sand layer is considered isotropic, and has no assumed failure criteria. The values of the required model parameters for the overburden are not available for BC, so the McCormick Ranch Sand properties used in the West Hackberry (WH) analysis [Ehgartner and Sobolik, 2002] were used. The caprock layer, consisting of gypsum, anhydrite and sand, is also assumed to behave elastically. Samples of caprock from core holes at BC were tested by Dames and Moore [1978] to determine physical properties. The tested samples were from massive gypsum-anhydrite units at depths of 602 ft and 645 - 648 ft in Core Hole 1 and 558 - 642 ft in Core Hole 2 [Hogan, 1980]. The rock surrounding the salt dome is sedimentary rock that consists mostly of sandstone and shale, which is assumed isotropic, homogeneous, elastic rock. The values of the

required model parameters of the surrounding rocks are also not available. Typical values for the Young's moduli of sandstones and shales range from 6×10^4 to 1×10^7 psi [Carmichael, 1984]. For simplifying the analysis, a median value of the Young's modulus of sandstone, 5.076×10^6 psi, is assumed. The mechanical properties used in the present analysis are listed in Table 5.

Table 5 Material properties of the lithologies encompassing the salt dome used in the analysis [Park et al., 2006]

	Unit	Overburden	Caprock	Surrounding Rock
Young's modulus	psf	2.0885×10^6 (0.1 GPa)	3.2832×10^8 (15.72 GPa)	7.3099×10^8 (35.0 GPa)
Density	lb/ft^3	116.99 (1874 kg/m^3)	144.77 (2319 kg/m^3)	156.07 (2500 kg/m^3)
Poisson's ratio	-	0.33	0.288	0.33

5.3. Interbed and Interface

The interbed and interface are pseudo materials which represent contact surface. ADAGIO has a contact surface algorithm for modeling contact and sliding behavior between two solid surfaces. However, this algorithm has a limitation on the number of elements in the model. The current model is over that limitation. In place of a contact surface, a thin soft layer of elements is used for the interbed between the caprock and salt top. The thin soft element layer uses the overburden material properties and is assumed to behave mechanically like a contact surface with friction coefficient of 0.2 from a perspective of relative displacement between two lithologies. Thus the overburden material properties (Table 6) are used for the interbed layer.

The interface between the dome and surrounding rock is a vertical layer, while the interbed is a horizontal layer. In this analysis, it is assumed that the interface behaves like a thin soft element layer in a manner similar to the interbed, but the horizontal pressure applied on the dome surface has to be the same as it arise from the surrounding rock. Therefore, the density and Poisson's ratio of the surrounding rock are used for the pseudo material of the interface. To implement a soft element, 1% of the surrounding rock's elastic modulus is used for the interface. The mechanical properties used in the analysis are listed in Table 6.

Table 6 Material properties of the interbed and interface used in the analysis

	Unit	Interbed	Interface
Young's modulus	psf	2.0885×10^6 (0.1 GPa)	7.3099×10^6 (0.35 GPa)
Density	lb/ft^3	116.99 (1874 kg/m^3)	156.07 (2500 kg/m^3)
Poisson's ratio	-	0.33	0.33

Intentionally Blank

6. PARAMETER EFFECT

6.1. Oil-Brine Interface Effect

Previous analyses [Part et al., 2006; Park and Ehgartner, 2008; Park and Ehgartner, 2010] assumed that the SPR caverns were filled fully with oil. In actuality, however, the caverns were not always fully filled with oil. The caverns were usually filled with both brine and oil, with brine on the bottom. The amount of brine changes with time. The difference between pressure gradients of oil (0.37 psi/ft of depth) and brine (0.52 psi/ft of depth) cannot be ignored. So, both the cavern's oil and brine volumes over time need to be considered.

For BC-15, 17, 18, 19, 20, and 101, respectively, Figure 31 through Figure 36 show the wellhead pressure history (top plot), oil-brine interface (OBI) depth history (middle plot), the volumetric closures normalized to initial volume predicted by the numerical model and CAVEMAN (bottom plot), and the initial meshed geometries. The dashed curve in the normalized volumetric closure plots (bottom plots of Figure 31 through Figure 36) indicates the predicted volumetric closure of the cavern filled fully with oil. The red curve indicates the predicted volumetric closure considering OBI depth history.

As an example, during the beginning interval (between mid-1990 and mid-1992) of BC-18 (Figure 33), the cavern was filled fully with brine. Since brine density is greater than oil, the pressure on the walls and bottom of cavern filled with brine is larger than one filled with oil. The internal pressure impedes the cavern volumetric closure due to salt creep. As a result, the two liquid pressures produce a difference in the amount of cavern volumetric closure. The curve slopes are similar except at the beginning stage. This implies that the salt constitutive model used in the analysis is predicting cavern behavior in reasonable manner. The red curve is close to the CAVEMAN prediction but does not match, it because CAVEMAN assumes the cavern shape is cylindrical, not the actual geometry of the cavern. As another example, the prediction considering OBI (red curve) for BC-101 is closer to CAVEMAN's (black curve) as shown Figure 36, because the shape of BC-101 is close to cylindrical.

As for BC-15, 17, and 19, the cavern was filled fully with oil since the beginning stage, so the red and dashed curves are close each other. As for BC-20, the brine volume jumped up at 9/5/2005, and then brine has filled fully the cavern since 2/7/2013. Therefore, the gap between the red and dashed curves increases with time since then as shown in Figure 35.

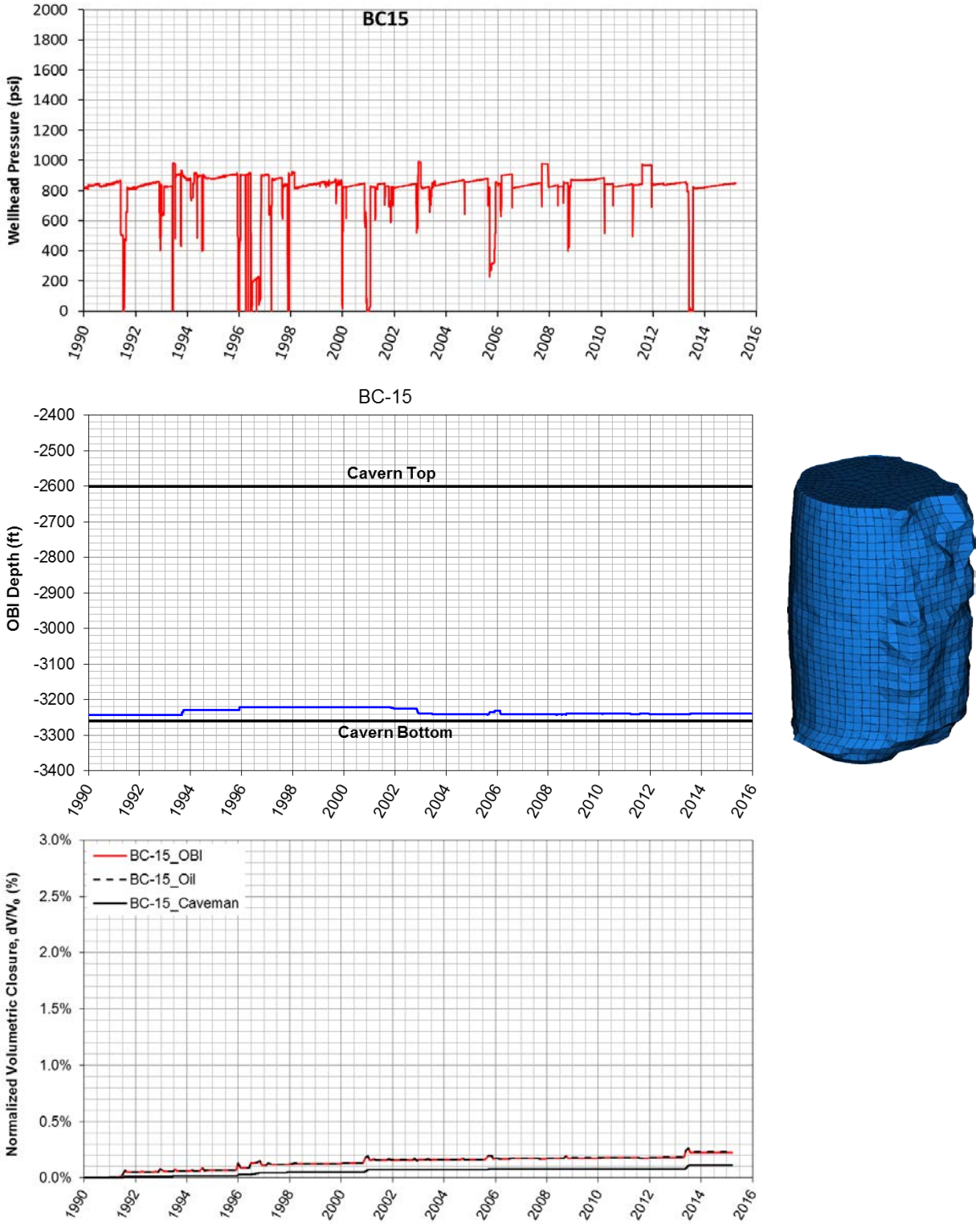

Figure 31 Wellhead pressure history (top), Oil-Brine Interface history (middle), volumetric closure normalized to initial volume (bottom) calculated from this analysis and Caveman, and initial meshed cavity (right) of BC-15 based on sonar survey data

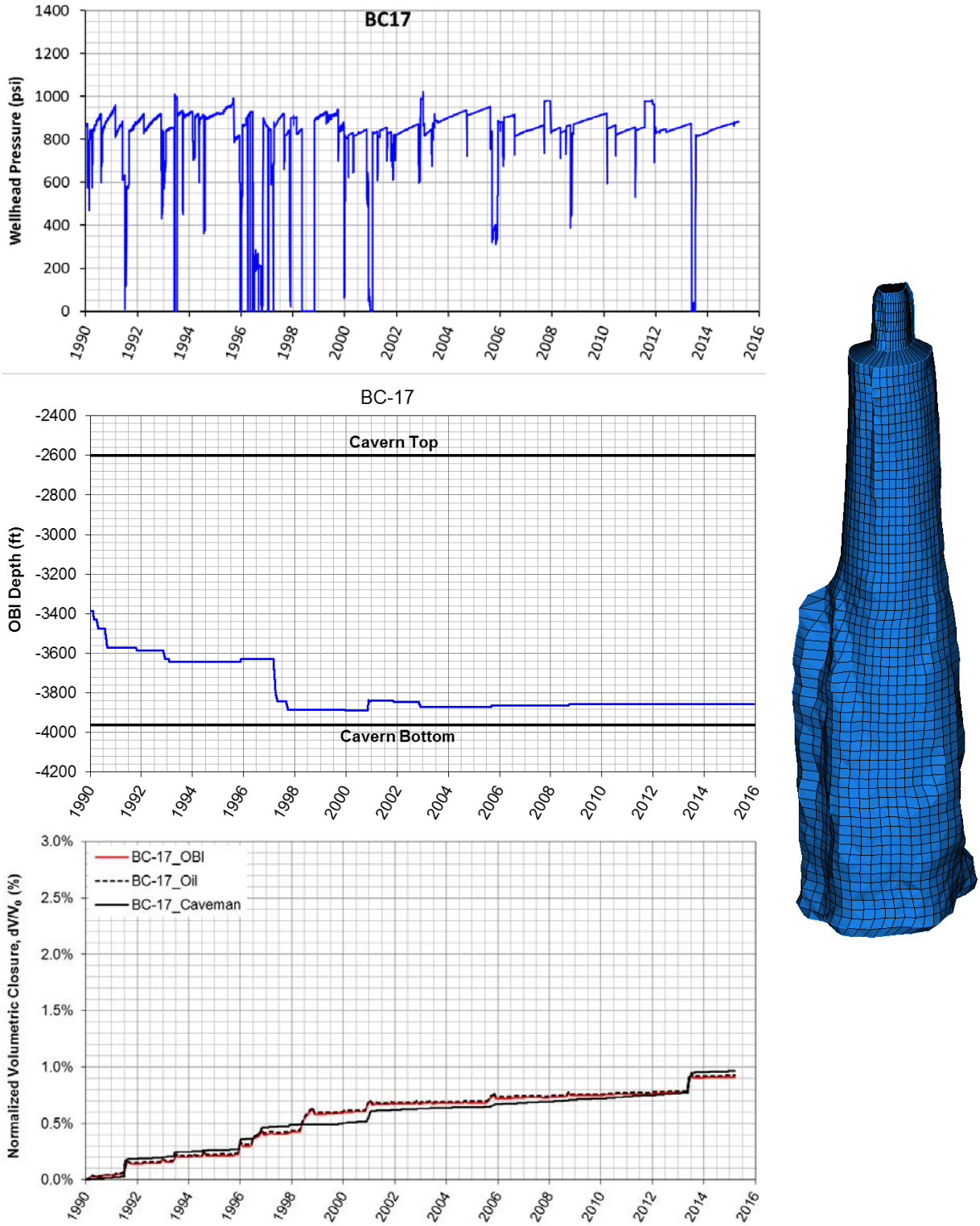

Figure 32 Wellhead pressure history (top), Oil-Brine Interface history (middle), volumetric closure normalized to initial volume (bottom) calculated from this analysis and Caveman, and initial meshed cavity (right) of BC-17 based on sonar survey data

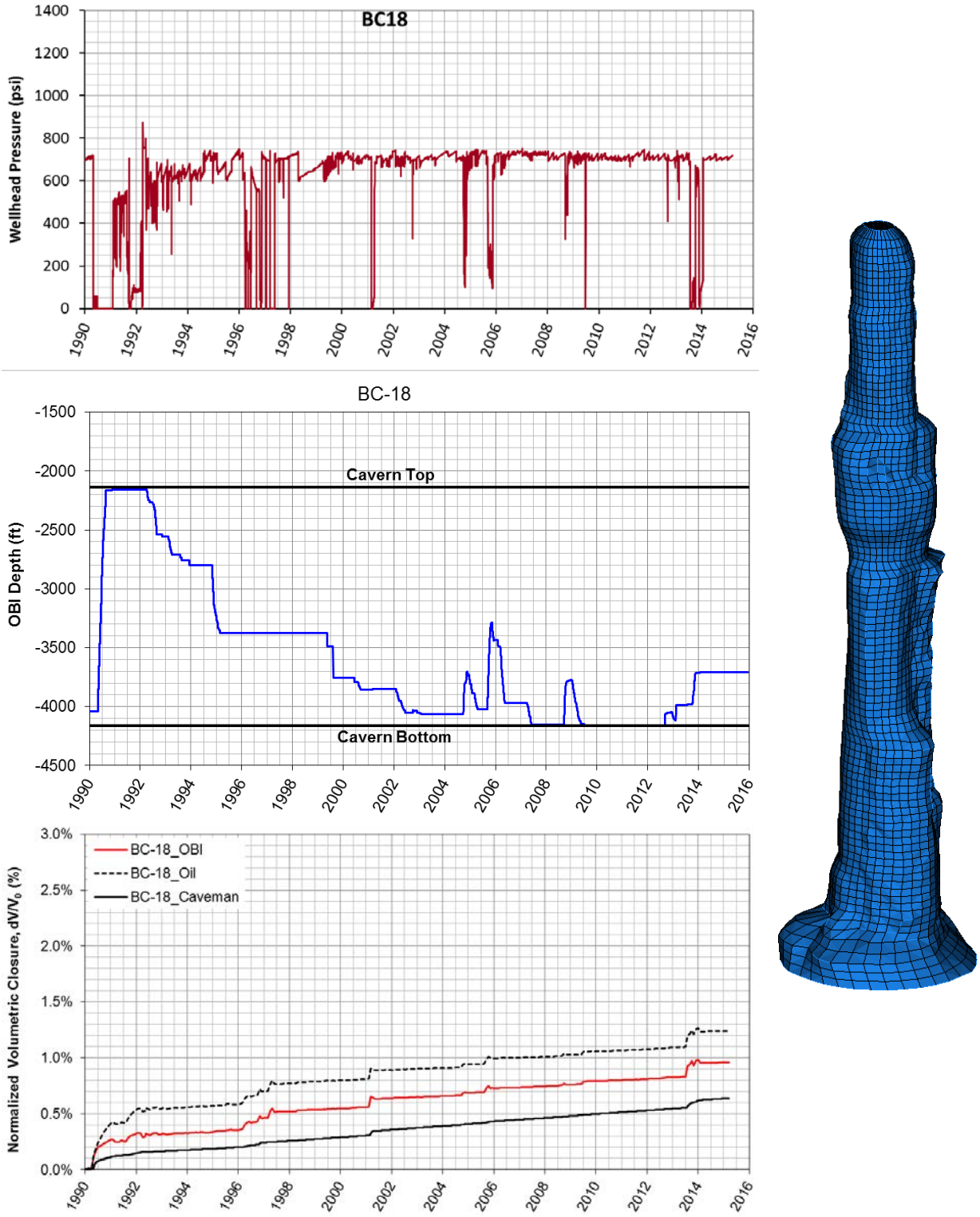

Figure 33 Wellhead pressure history (top), Oil-Brine Interface history (middle), volumetric closure normalized to initial volume (bottom) calculated from this analysis and Caveman, and initial meshed cavity (right) of BC-18 based on sonar survey data

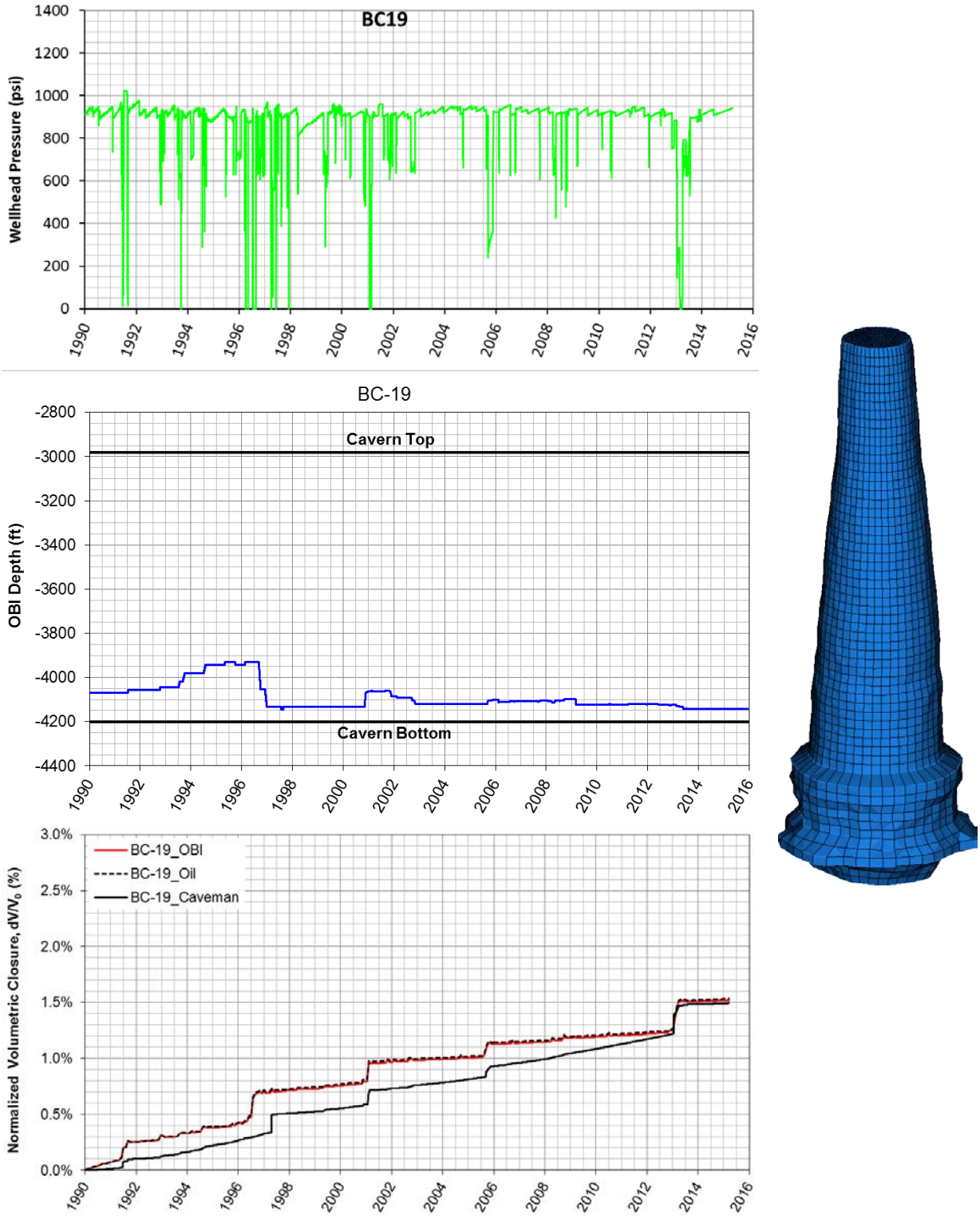

Figure 34 Wellhead pressure history (top), Oil-Brine Interface history (middle), volumetric closure normalized to initial volume (bottom) calculated from this analysis and Caveman, and initial meshed cavity (right) of BC-19 based on sonar survey data

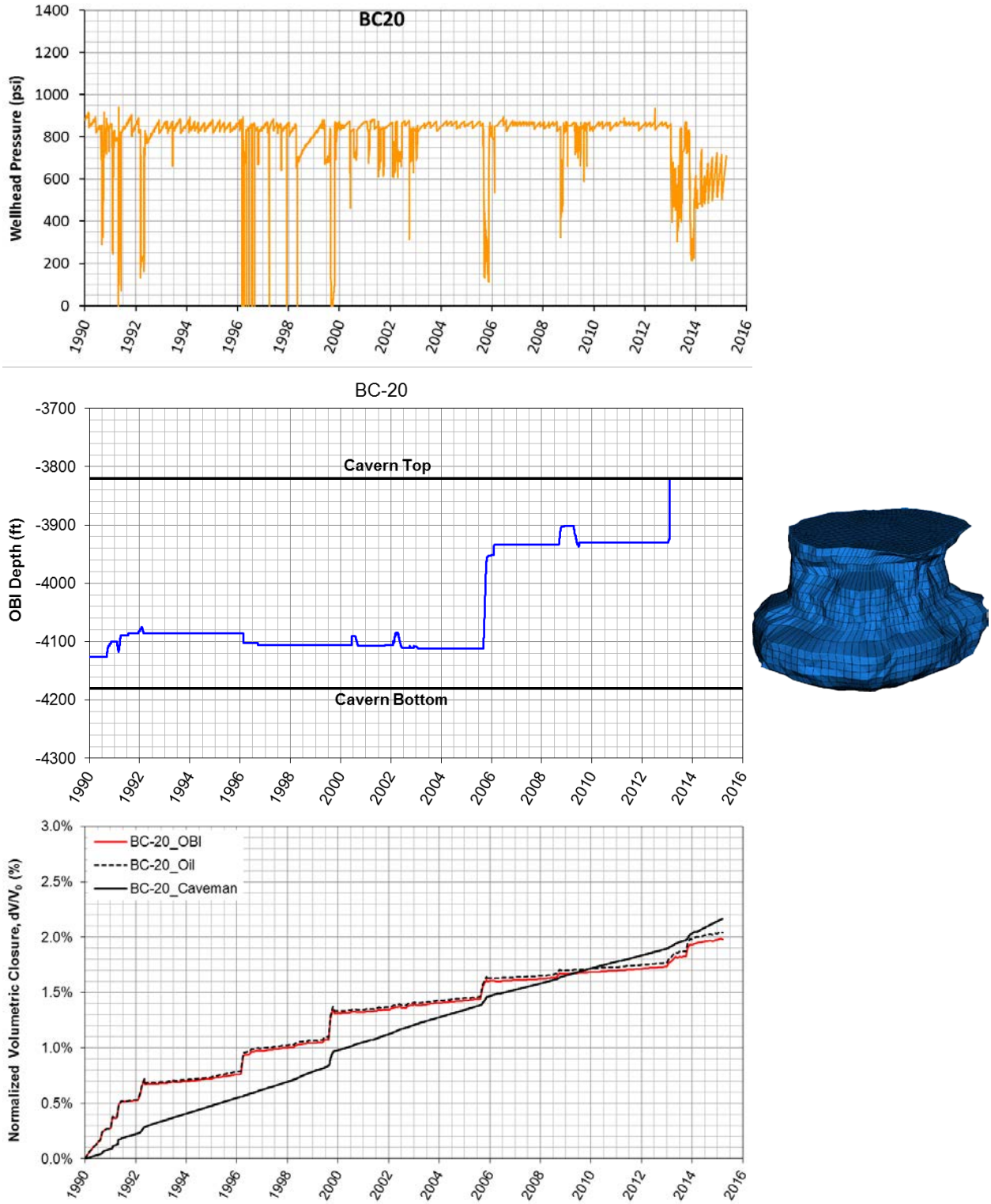

Figure 35 Wellhead pressure history (top), Oil-Brine Interface history (middle), volumetric closure normalized to initial volume (bottom) calculated from this analysis and Caveman, and initial meshed cavity (right) of BC-20 based on sonar survey data

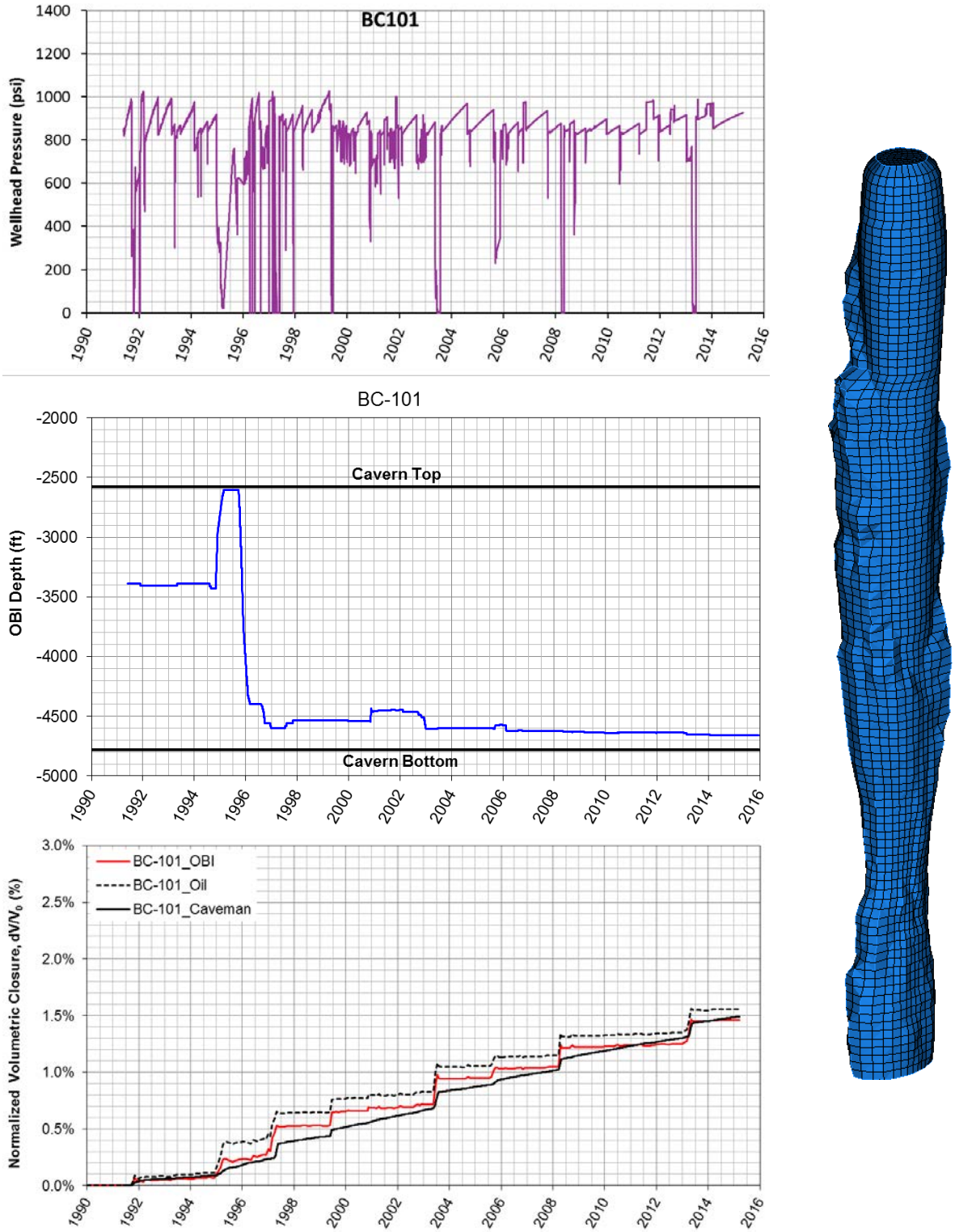

Figure 36 Wellhead pressure history (top), Oil-Brine Interface history (middle), volumetric closure normalized to initial volume (bottom) calculated from this analysis and Caveman, and initial meshed cavity (right) of BC-101 based on sonar survey data

6.2. Caveman

One of the challenges of operating the SPR caverns is ensuring that none of the fluids in the caverns are leaking into the environment. The approach until 2000 was to test the mechanical integrity of all the wells entering each cavern approximately once every five years. An alternative approach to detecting cavern leaks is to monitor the cavern pressure, since leaking fluid would act to reduce cavern pressure. Leak detection by pressure monitoring is complicated by other factors that influence cavern pressure. The most important of these factors are thermal expansion and contraction of the fluids in the cavern as they come into thermal equilibrium with the host salt and cavern volume reduction due to salt creep. Cavern pressure is also influenced by cavern enlargement resulting from salt dissolution following introduction of water or unsaturated brine into the cavern. However, this effect only lasts for a month or two following a fluid injection. In order to implement a cavern pressure monitoring program, a software program called CAVEMAN has been developed. It includes thermal, creep, and salt dissolution models and is able to predict the cavern pressurization rate based on the operational history of the cavern. [Ballard and Ehgartner, 2000].

As for a salt constitutive model, the M-D model has three steady-state creep mechanisms (Eqs. (2)-(4)), of which only one (mechanism 2, Eq.(3)) was selected for use in the cavern model in CAVEMAN, based on its dominant influence over the other mechanisms for SPR caverns. The dominance of a mechanism is determined by the stress and temperature regime for the cavern. Transient creep is included in the model through the function, F in Eq. (6), where the total strain rate (transient and steady-state) is the product of F times the steady-state strain rate (Eq. (5)). CAVEMAN assumes that caverns are right circular cylinders. Available cavern height and cavern volume information were used to calculate an effective radius for each cavern. [Ballard and Ehgartner, 2000].

Cavern volume closure as a function of time is not a directly measured quantity, i.e. day-to-day volume closure due to creep cannot be monitored. Daily cavern volume closure is estimated indirectly using a cavern pressure monitoring code CAVEMAN. Many of the numerous thermal and mechanical parameters in CAVEMAN have been optimized to produce the best match between the field historical data and the model predictions. Therefore, CAVEMAN predictions are regarded as a field-data in this study. The cavern volumetric closures normalized to the initial volumes of BC SPR caverns are calculated using CAVEMAN as shown Figure 37 which will be used for the model calibration baseline.

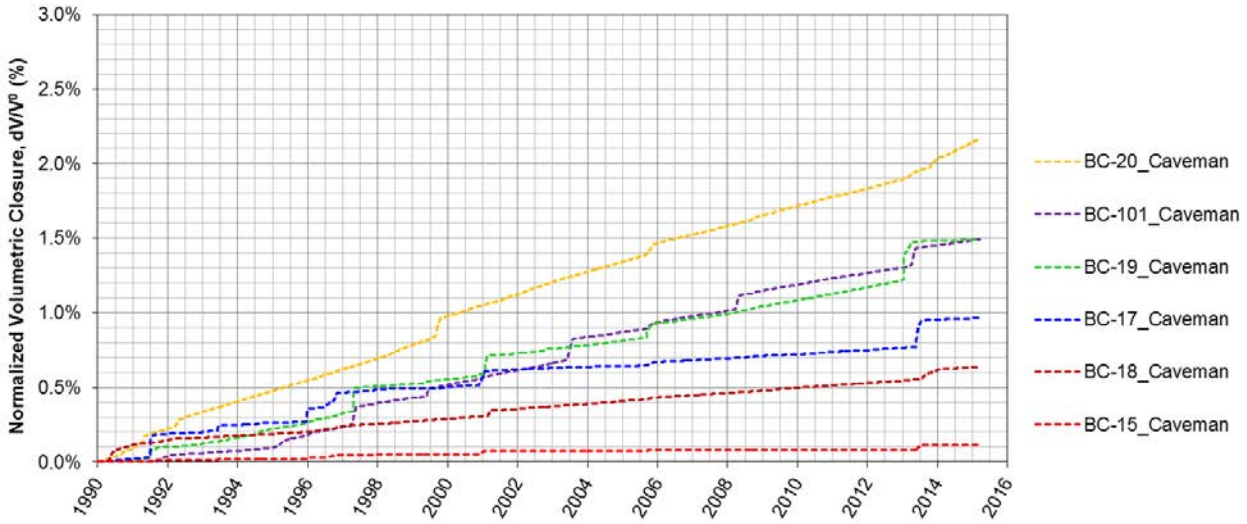

Figure 37 Volumetric closure normalized to initial volume calculated from CAVEMAN

6.3. Baseline

Figure 38 and Figure 39 show the predicted decrease in storage volumes of BC SPR caverns with the CAVEMAN predictions. The solid curves indicate the normalized volumetric closure when the parameter values in Table 4 are used. The dashed curves indicate the normalized volumetric closure predicted from CAVEMAN. The predictions for BC-15 and 18 are close each other, but for other caverns are much different. This implies that the salt behavior is not identical in the entire salt dome. The effective creep rates in volume loss percentage per year differ with cavern locations as shown Figure 30. Therefore, the parameter values in M-D model need to be optimized to produce the best match between the CAVEMAN and model predictions.

To calibrate the parameter values, we need to be aware how each parameter affects the cavern volumetric closure. The structure factors, A's and B's in Eqs. (2)-(4) affect the steady-state creep rates and K_0 in Eq. (8) affect the transient strain rates as mentioned in Section 5.1. Because all of the creep tests were conducted at relatively low stress and low temperature, the creep in terms of the structure factor of just one of the three mechanisms involved in salt creep can be characterized. This is the undefined or empirical mechanism with the structure factor A_2 [Munson, 1998]. Eq. (3) represents the strain rate for an empirically specified but undefined mechanism at low temperatures and low stresses. The structure factor, A_1 in Eq. (2), may also need to be considered, but for the stress and temperature regimes where the SPR caverns are located, mechanism 2 (Eq. (3)) tends to dominate mechanism 1 (Eq. (2)) [Sobolik, 2015]. Therefore, the effect of A_2 in Eq. (2) will be examined for the steady-state creep in this study. The only parameter value that has no basis in the experimental data or a logical extension, and is therefore an assumed value, is the value of K_0, which may indeed depend strongly upon specific salt material [Munson, 1998]. Therefore, the effect of K_0 will be investigated for the transient strain in the next section.

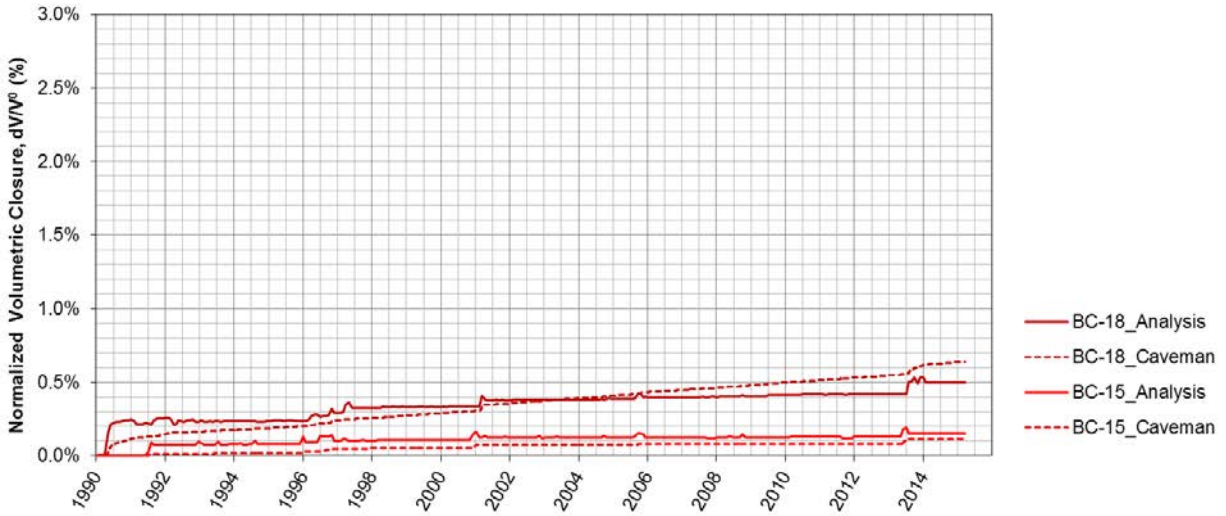

Figure 38 Volumetric closure normalized to initial volume calculated using the baseline parameter values and Caveman predictions for BC-15 and 18

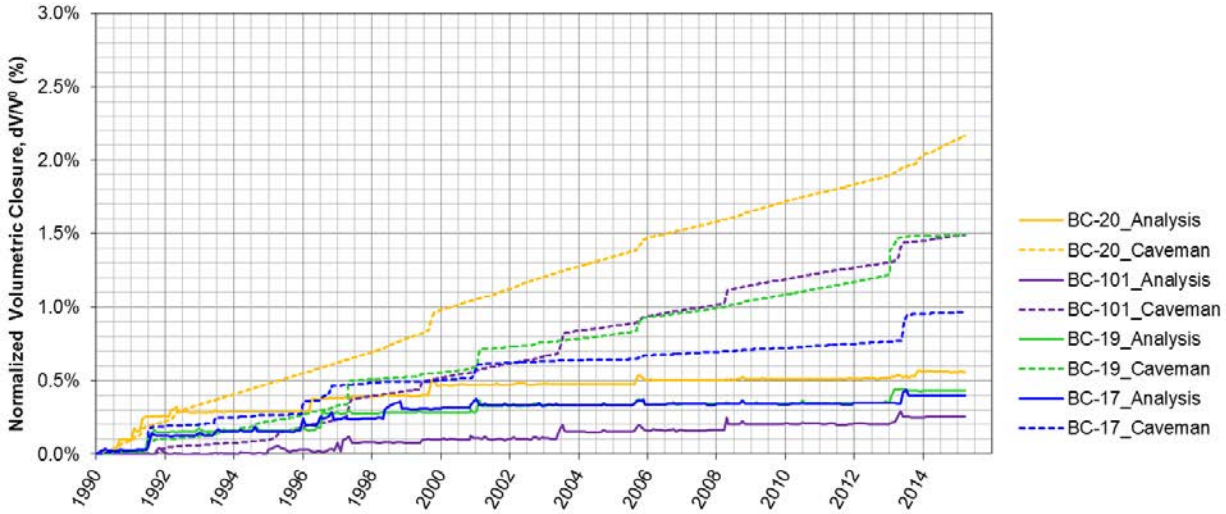

Figure 39 Volumetric closure normalized to initial volume calculated using the baseline parameter values and Caveman predictions for BC-17, 19, 20, and 101

6.4. A_2 Effect

To examine the effect of changing A_2 on cavern volumetric closure, the cavern volume decrease rates are calculated with several A_2 values while other parameter values are not changed. The magnitude of the sudden increases (called "jump" hereafter) in cavern volumetric closure at workovers is a function of both A_1 and A_2, but also of the transient creep phenomenon, which is governed by the factor K_0 in Eq. (8) [Sobolik, 2015]. The slopes of the curves calculated from the analysis for BC-17, 19, 20, and 101 as shown in Figure 38 are much smaller than CAVEMAN's. Thus, ten times constant of A_2 value is used as a start value for the calibration. Then it makes the magnitude of jump larger than CAVEMANS, so 10% constant of K_0 value is used as a start value to reduce the magnitude. The input parameter values in ADAGIO input

values lists in Table 7. The values for BC salt in Table 4 are converted into the ADAGIO input format.

Figure 40 shows the predicted cavern volumetric closure normalized to the initial volume with various A_2 multiplication factor (*A2F*) values when K_0 multiplication factor, *K0F*=0.1which are applied into the entire salt dome. The linear equation on each curve indicates the trend-line (regression) with slope and intercept values in the time interval between 1/2/2006 and 12/30/2012 (6/2/2008 and 12/30/2012 for BC-101) because the interval is longest between workovers. The relationship between the slope and *A2F* could be a reference to calibrate the value of A_2, and then match the cavern volumetric closure to the field observation.

Table 8 and Figure 41 show the relationship between the slope and *A2F*. The slope increases nearly linearly as the *A2F* increases. However, the increase rate is different for each cavern, i.e. it is not uniform throughout the salt dome. When we determine the *A2F* value for the salt around each cavern, Figure 30 could be used for a reference to calibrate the value of A_2.

To examine how A_2 affects the jump, the differences between before and after the workover are calculated from the curves in Figure 40. Table 9 lists the difference between the normalized volumetric closures on the dates before and after the workover for each SPR cavern, i.e. the difference indicates the magnitude of jump due to the workover. The magnitudes are changed with *A2F* values as shown Figure 42. The curve for each cavern has a trend. However, the increase rate is different, i.e. not uniform in the salt dome like the slope trend. When we determine the *A2F* value for the salt around each cavern, Figure 42 also could be used for a reference.

Table 7 Parameter values used in ADAGIO input deck

Mechanism	Parameter	Symbol	Unit	Values in Input Deck
Conventional	Gravity	gr	ft/s^2	32.174
	Universal gas constant	R	cal/(mol·K)	1.986
	Temperature	T	K	Varies with depth*
	Density	ρ/gr	$lb{\cdot}s^2/ft^4$	4.4627** (2300 kg/m^3)
Elasticity	Young's modulus	E	psf	647447400 (31.0 GPa)
	Shear modulus	μ	psf	258978960 (12.4 GPa)
	Bulk modulus	K	psf	431631600 (20.7 GPa)
	Poisson's ratio	v	-	0.25
Dislocation climb controlled creep mechanism at high temperatures and low stresses (Eq. 2)	Structure factor	A_1	1/s	1.445×10^{22}
	Activation energy	Q_1/R	K	12588.89‡
	Stress exponent	n_1	-	5.5
Empirically specified but undefined mechanism at low temperatures and low stresses (Eq. 3)	Structure factor	A_2	1/s	***A2F***†×1.667×10^{12}
	Activation energy	Q_2/R	K	5035.55‡
	Stress exponent	n_2	-	5.0
Dislocation slip controlled mechanism at high stresses (Eq. 4)	Structure factor	B_1	1/s	1048941
	Structure factor	B_2	1/s	0.005229
	Stress limit	σ_0	psf	429613 (20.57 MPa)
	Stress constant	q	-	5335
Transient strain (Eq. 8)	Material constant	m	-	3.0
	Constant	K_0	-	***K0F***††×62750
	Constant	c	1/K	0.009198
Work-hardening and recovery (Eq. 9&10)	Constant	α	-	-17.37
	Constant	β	-	-7.738
	Recovery	δ	-	0.58
	Damage	ω	-	0.0
Structure factor multiplication factor from WIPP 25°C salt		*SMF*	-	0.172353
Scalar multiplier of time step needed for stability		*AMULT*	-	0.95
System parameters for numerical convergence		*ANGLE*	-	0.1
		epstol	-	0.005
		grwfac	-	1.05
		shkfac	-	1.0
		ITHPE		0.0

Note:
- * – Temperature value is assigned on every node in the mesh
- ** -The value (lb/ft^3/gr) will be multiplied by gravity in the system
- ‡ – ADAGIO requests the value be divided by universal gas constant
- † – A_2 multiplication factor to examine the A_2 factor effect
- †† - K_0 multiplication factor to examine the K_0 factor effect

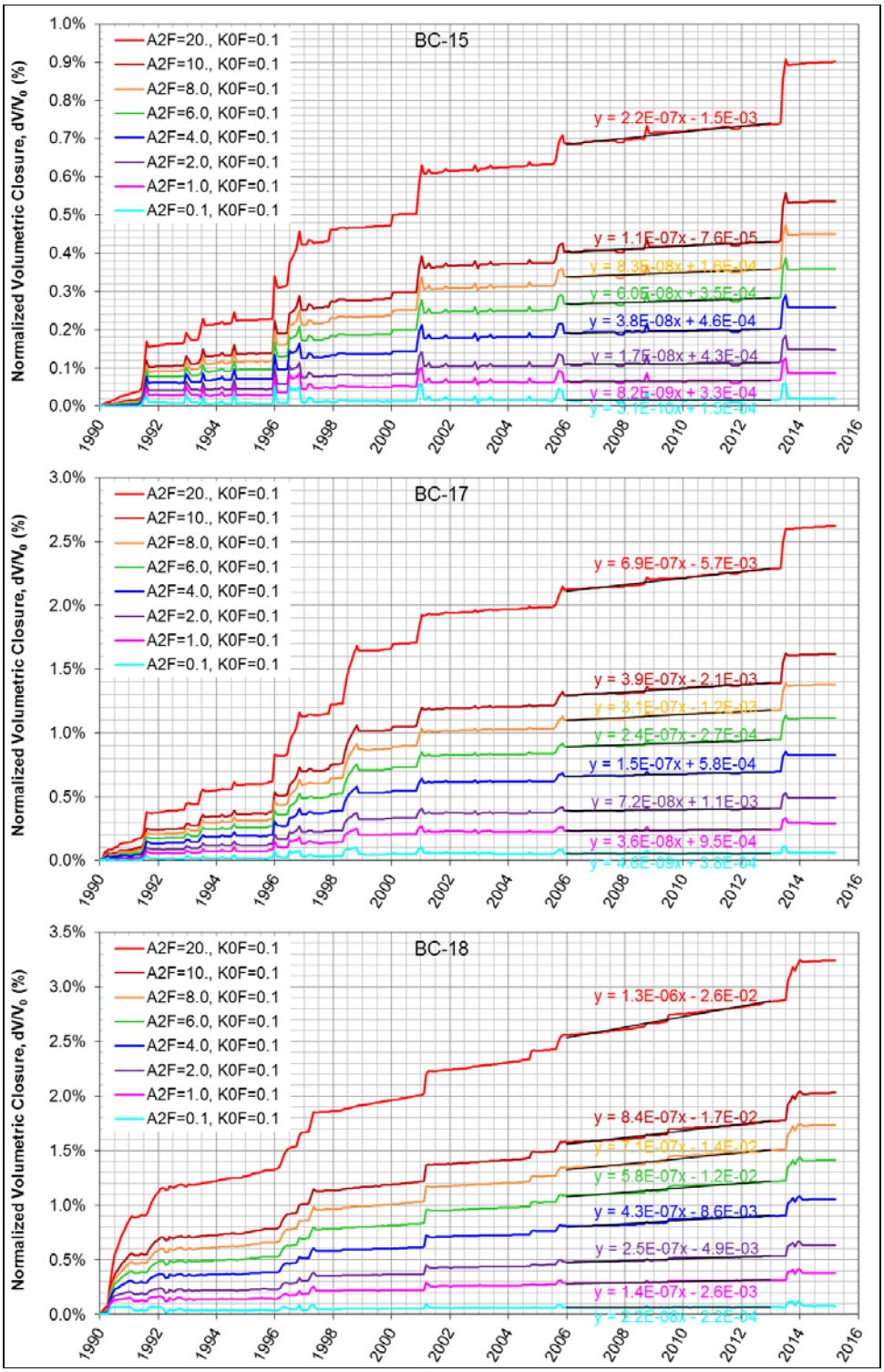
BC-15
A2F=20., K0F=0.1
A2F=10., K0F=0.1
A2F=8.0, K0F=0.1
A2F=6.0, K0F=0.1
A2F=4.0, K0F=0.1
A2F=2.0, K0F=0.1
A2F=1.0, K0F=0.1
A2F=0.1, K0F=0.1
y = 2.2E-07x - 1.5E-03
y = 1.1E-07x - 7.6E-05
y = 8.3E-08x + 1.6E-04
y = 6.0E-08x + 3.5E-04
y = 3.8E-08x + 4.6E-04
y = 1.7E-08x + 4.3E-04
y = 8.2E-09x + 3.3E-04
y = 3.1E-10x + 1.5E-04
Normalized Volumetric Closure, dV/V0 (%)
BC-17
y = 6.9E-07x - 5.7E-03
y = 3.9E-07x - 2.1E-03
y = 3.1E-07x - 1.2E-03
y = 2.4E-07x - 2.7E-04
y = 1.5E-07x + 5.8E-04
y = 7.2E-08x + 1.1E-03
y = 3.6E-08x + 9.5E-04
y = 4.8E-09x + 3.8E-04
BC-18
y = 1.3E-06x - 2.6E-02
y = 8.4E-07x - 1.7E-02
y = 7.1E-07x - 1.4E-02
y = 5.8E-07x - 1.2E-02
y = 4.3E-07x - 8.6E-03
y = 2.5E-07x - 4.9E-03
y = 1.4E-07x - 2.6E-03
y = 2.2E-08x - 2.2E-04

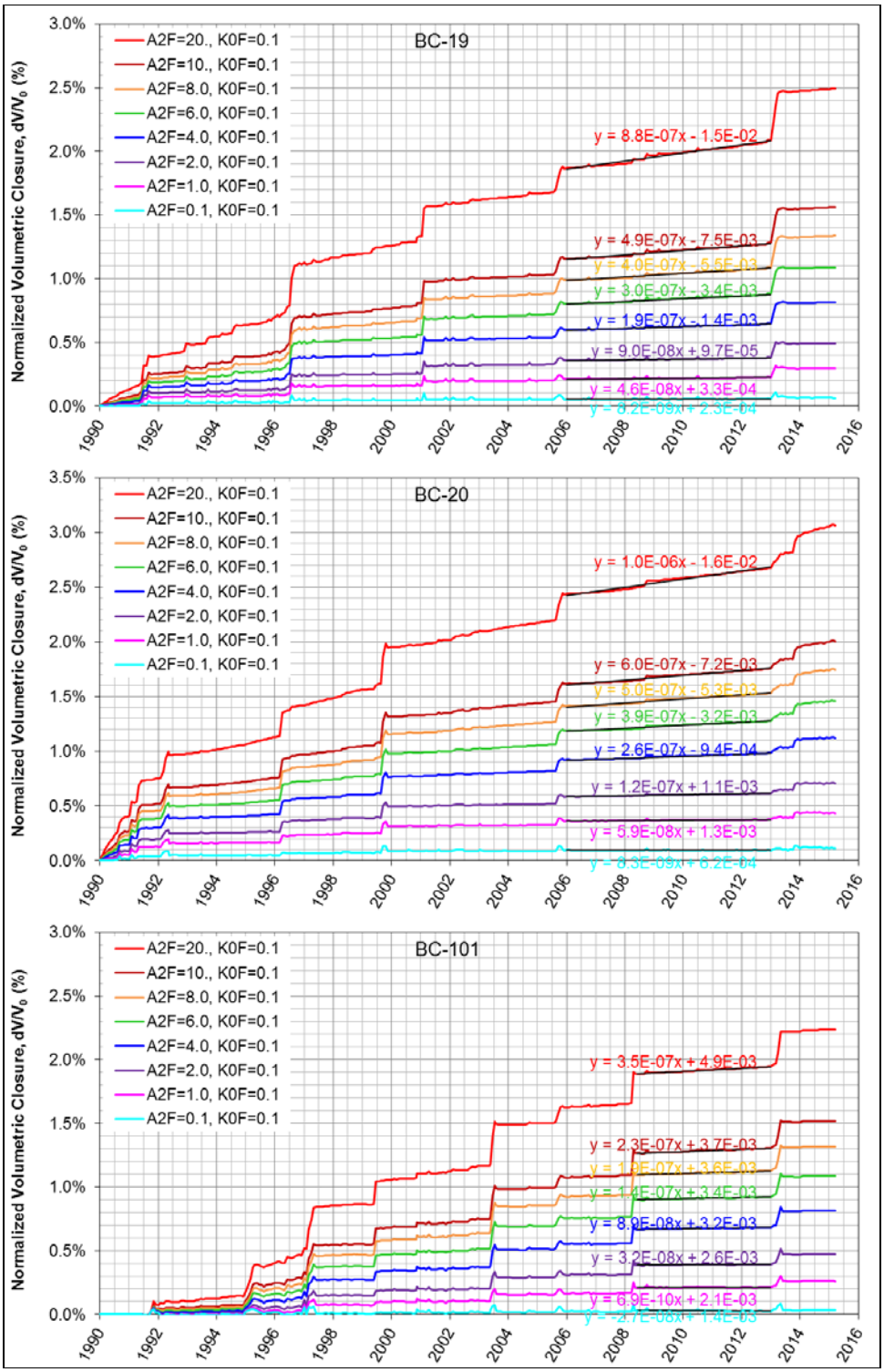

Figure 40 Predicted cavern volumetric closure normalized to initial volume with various A_2 multiplication factor (*A2F*) when K_0 multiplication factor, *K0F*=0.1

Table 8 Slope values of trend lines with *A2F* in the time interval between 1/2/2006 and 12/30/2012 (6/2/2008 and 12/30/2012 for BC-101)

A2F	BC-15	BC-17	BC-18	BC-19	BC-20	BC-101
20	2.17E-07	6.92E-07	1.32E-06	8.76E-07	1.03E-06	3.52E-07
10	1.06E-07	3.87E-07	8.37E-07	4.90E-07	6.02E-07	2.26E-07
8	8.29E-08	3.14E-07	7.15E-07	3.97E-07	4.99E-07	1.87E-07
6	5.99E-08	2.37E-07	5.81E-07	2.96E-07	3.87E-07	1.41E-07
4	3.75E-08	1.55E-07	4.29E-07	1.90E-07	2.61E-07	8.92E-08
2	1.72E-08	7.18E-08	2.48E-07	8.96E-08	1.23E-07	3.21E-08
1	8.17E-09	3.59E-08	1.40E-07	4.64E-08	5.90E-08	6.87E-10
0.1	3.08E-10	4.62E-09	2.15E-08	8.18E-09	8.26E-09	2.67E-08

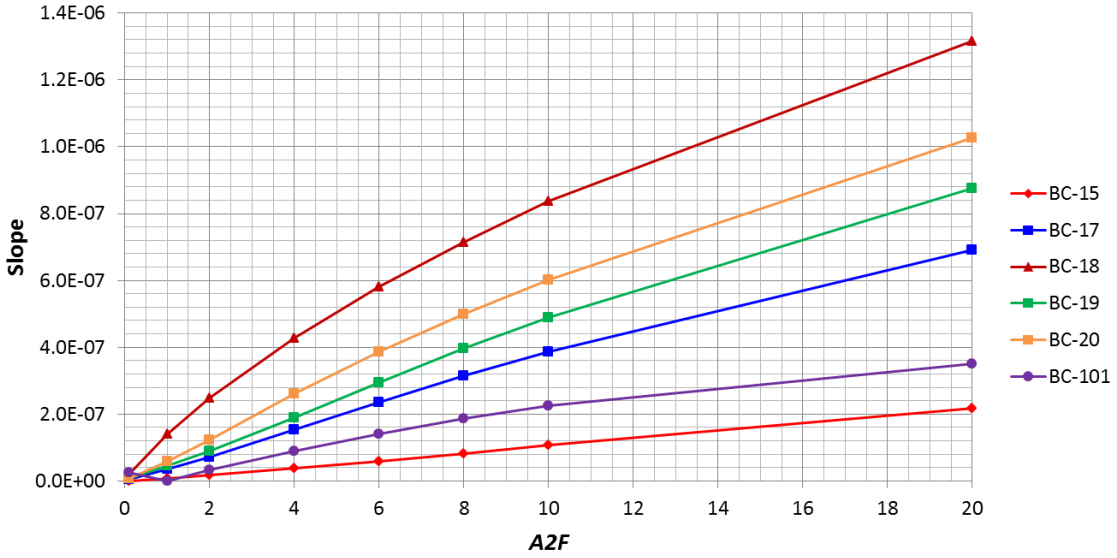

Figure 41 Relationship between *A2F* and slopes in the time interval between 1/2/2006 and 12/30/2012 (6/2/2008 and 12/30/2012 for BC-101)

Table 9 Magnitude of jump due to the workover with *A2F*

		BC-15	BC-17	BC-18	BC-19	BC-20	BC-101
Date before workover		12/30/2012	12/30/2012	4/30/2013	12/30/2012	1/1/1996	12/30/2012
Date after workover		11/2/2013	11/2/2013	1/30/2014	11/2/2013	10/1/1996	11/2/2013
A2F	20	0.16%	0.32%	0.36%	0.38%	0.29%	0.27%
	10	0.10%	0.22%	0.25%	0.27%	0.21%	0.20%
	8	0.09%	0.19%	0.22%	0.24%	0.19%	0.18%
	6	0.08%	0.17%	0.19%	0.20%	0.17%	0.16%
	4	0.06%	0.13%	0.15%	0.16%	0.14%	0.12%
	2	0.04%	0.08%	0.10%	0.11%	0.10%	0.08%
	1	0.02%	0.05%	0.07%	0.07%	0.07%	0.05%
	0.1	0.00%	0.01%	0.01%	0.01%	0.02%	0.00%

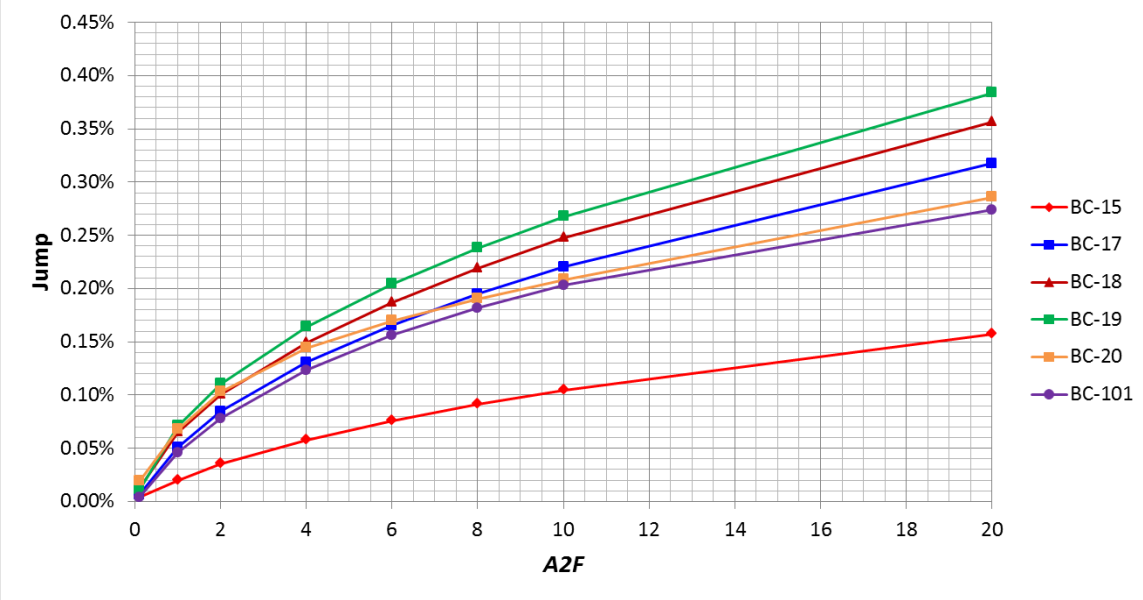

Figure 42 Relationship between *A2F* and magnitude of jump due to the workover

6.5. K_0 Effect

In similar manner, decreased cavern volumetric rates are calculated with several K_0 values while other parameter values are not changed to examine the effect of K_0. A_2 = 10 is used as a start value.

Figure 43 shows the predicted cavern volumetric closure normalized to the initial volume with various K_0 multiplication factor values (*K0F*) when the A_2 multiplication factor is ten, *A2F*=10 which are applied into the entire salt dome. The linear equation on each curve indicates the trend-line (regression) with slope and intercept values in the time interval between 1/2/2006 and 12/30/2012 (6/2/2008 and 12/30/2012 for BC-101). The relationship between the slope and *K0F* could be a reference of the K_0 effect to calibrate the value of K_0, and then match the cavern volumetric closure to the field observation.

Table 10 and Figure 44 show the relationship between the slope and *K0F*. The slope decreases with *K0F*. And the rate tends to decrease further as *K0F* increases. The slope decrease rate is different for each cavern, i.e. it is not uniform throughout the salt dome. When we determine the *K0F* value for the salt around each cavern, Figure 44 could be used for a reference.

To examine how K_0 affects the jumps in cavern volumetric closure at workovers, the differences between before and after the workover are calculated from the curves in Figure 43. Table 11 lists the difference between the normalized volumetric closures on the dates before and after the workover for each SPR cavern, i.e. the difference indicates the magnitude of jump due to the workover. The magnitudes are changed with *K0F* values as shown Figure 45. The magnitude increases with *K0F* value increases except the salt around BC-101. The salt creep rate around BC-101 is unaffected by K_0 values as shown in Figure 43.

The increasing volumetric closure rate tends to decrease as *K0F* values increase. The rate is different at different locations in the salt dome, i.e. not uniform throughout the salt dome. When

we determine the *K0F* value for the salt around each cavern, Figure 45 also could be used for a reference.

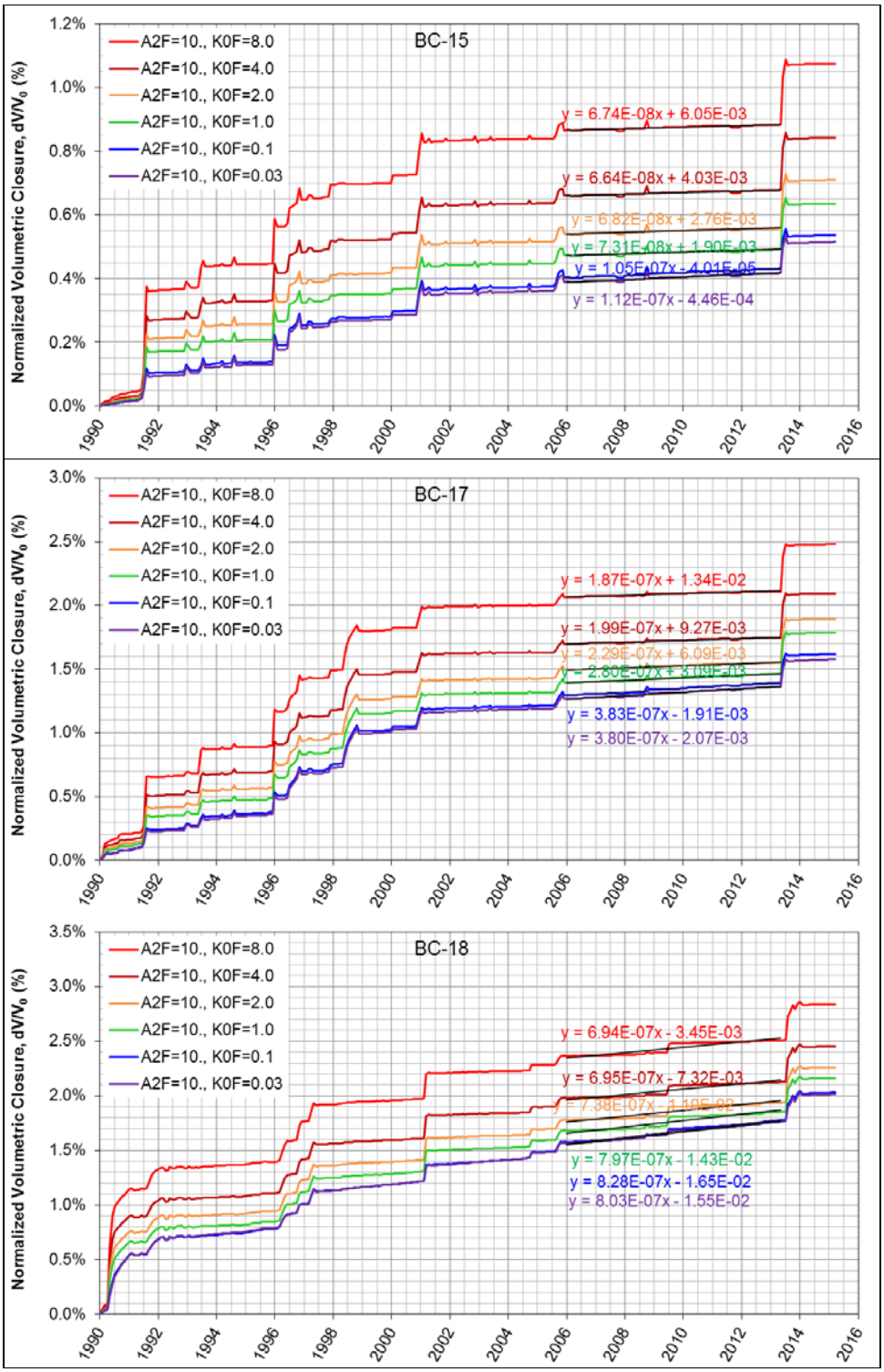

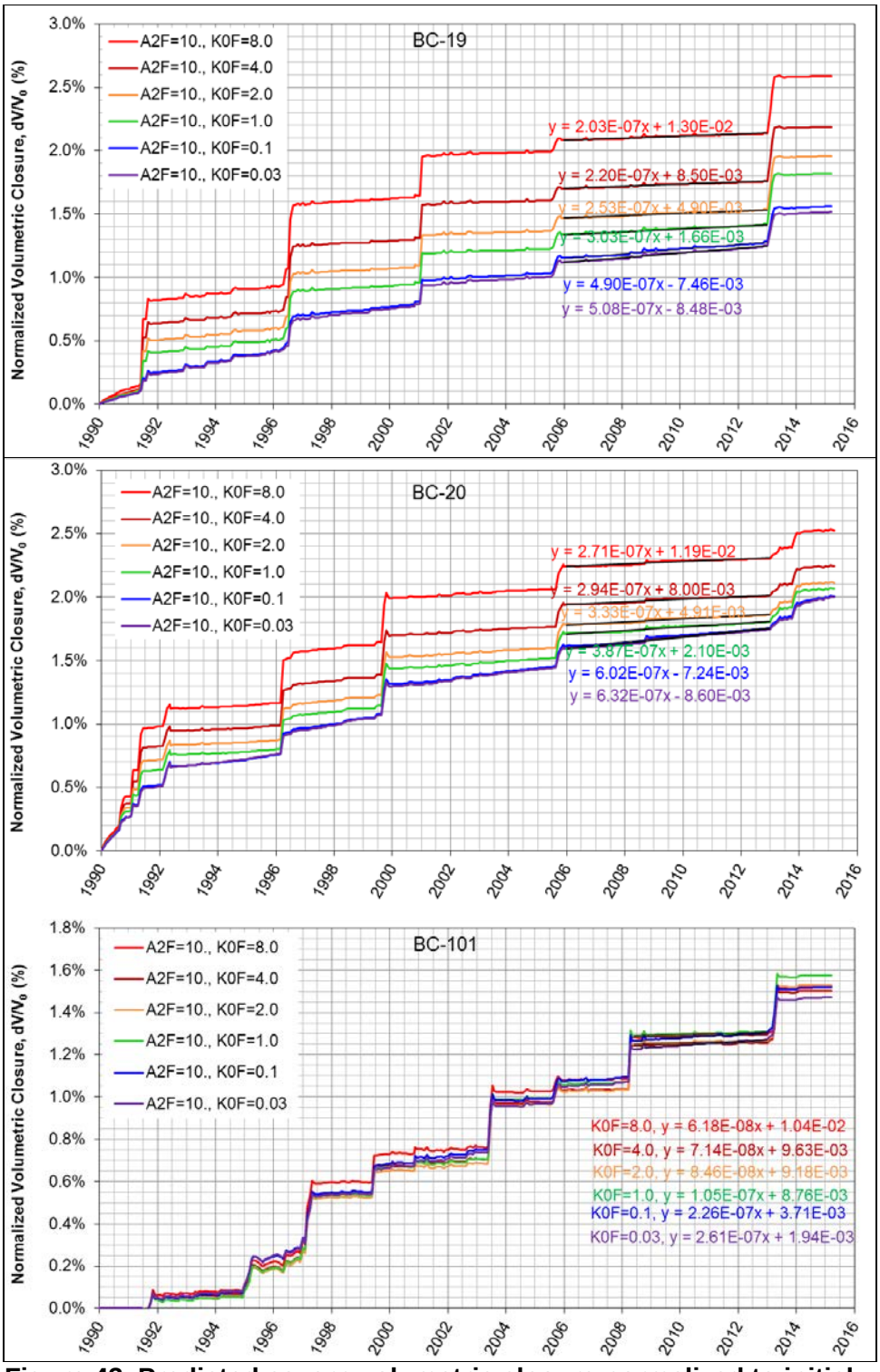

Figure 43 Predicted cavern volumetric closure normalized to initial volume with various K_0 multiplication factor (*K0F*) when A_2 multiplication factor, *A2F*=10

Table 10 Slope values of the trend lines with *K0F* in the time interval between 1/2/2006 and 12/30/2012 (6/2/2008 and 12/30/2012 for BC-101)

K0F	BC-15	BC-17	BC-18	BC-19	BC-20	BC-101
8	6.74E-08	1.87E-07	6.94E-07	2.03E-07	2.71E-07	6.18E-08
4	6.64E-08	1.99E-07	6.95E-07	2.20E-07	2.94E-07	7.14E-08
2	6.82E-08	2.29E-07	7.38E-07	2.53E-07	3.33E-07	8.46E-08
1	7.31E-08	2.80E-07	7.97E-07	3.03E-07	3.87E-07	1.05E-07
0.1	1.05E-07	3.83E-07	8.28E-07	4.90E-07	6.02E-07	2.26E-07
0.03	1.12E-07	3.80E-07	8.03E-07	5.08E-07	6.32E-07	2.61E-07

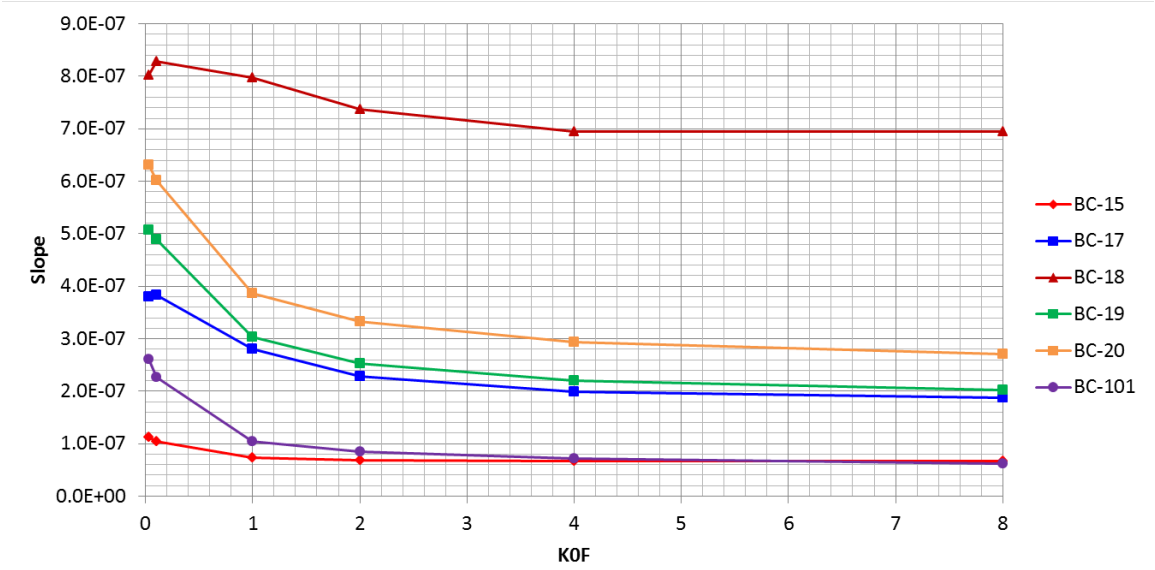

Figure 44 Relationship between *K0F* and slopes of trend lines in the time interval between 1/2/2006 and 12/30/2012 (6/2/2008 and 12/30/2012 for BC-101)

Table 11 Magnitude of jump due to the workover with *K0F*

		BC-15	BC-17	BC-18	BC-19	BC-20	BC-101
Date before workover		12/30/2012	12/30/2012	4/30/2013	12/30/2012	1/1/1996	12/30/2012
Date after workover		11/2/2013	11/2/2013	1/30/2014	11/2/2013	10/1/1996	11/2/2013
K0F	8	0.19%	0.36%	0.33%	0.44%	0.40%	0.22%
	4	0.16%	0.34%	0.32%	0.42%	0.33%	0.24%
	2	0.15%	0.34%	0.32%	0.41%	0.29%	0.25%
	1	0.14%	0.32%	0.31%	0.39%	0.27%	0.26%
	0.1	0.10%	0.22%	0.25%	0.27%	0.21%	0.20%
	0.03	0.10%	0.21%	0.24%	0.25%	0.19%	0.19%

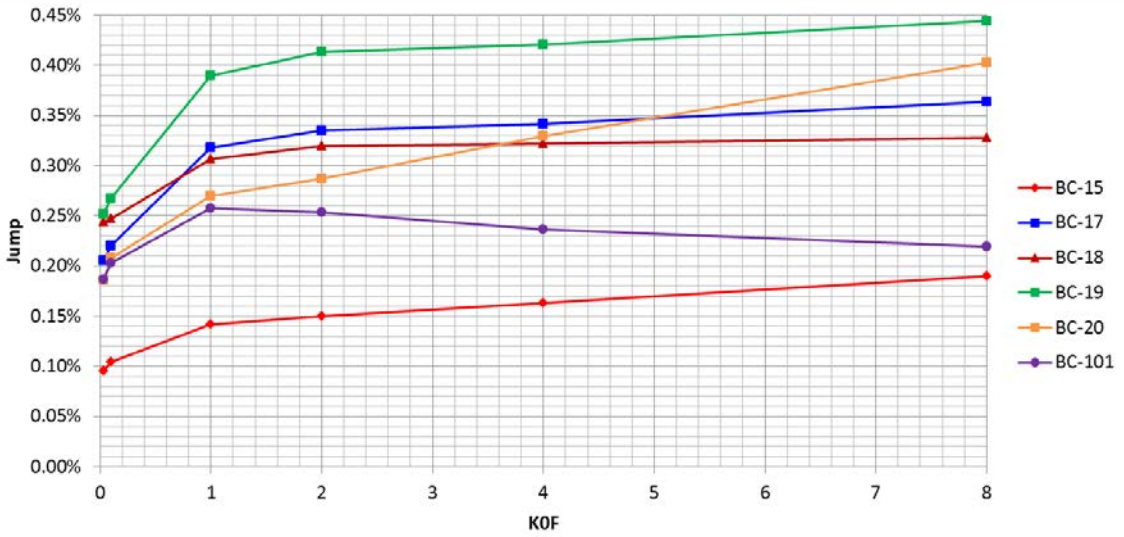

Figure 45 Relationship between *K0F* and magnitude of jump due to the workover

7. MODEL CALIBRATION

7.1. Volumetric Closure

Based on the relationships between slope and jump; and *A2F* and *K0F* in Figure 41, Figure 42, Figure 44, and Figure 45, the values of *A2F* and *K0F* have been calibrated through a number of back-fitting analyses and determined as listed Table 12. *A2F*=10 and *K0F*=0.1 are applied into the entire salt dome except the cavern skins and then each *A2F* and *K0F* values are applied into the salt skins encompassing each cavern cavity as mentioned in Section 3.4.4. The cavern curves normalized to the initial volumes of SPR caverns calculated from CAVEMAN as shown Figure 37 are used as a back-fitting standard.

Table 12 Multiplication factors applied to the A_2 and K_0 values listed in Table 7

Cavern ID	*A2F*	*K0F*
Salt except SPR cavern skins	**10.0**	**0.10**
BC-15 salt skins	0.01	0.03
BC-17 salt skins	0.12	0.10
BC-18 salt skins	0.04	0.03
BC-19 salt skins	10.0	0.10
BC-20 salt skins	25.0	0.03
BC-101 salt skins	10.0	0.10
BC-102 salt skins	10.0	0.10

The values of *A2F* and *K0F* have been determined through two steps:

In the first step, the values of entire salt dome are determined. When *A2F*=1.0 and *K0F*=1.0, the increase rate of normalized volumetric closure calculated from CAVEMAN are much larger than those from the analyses except BC-15 as shown Figure 38 and Figure 39. The curve slopes need to be increased without increasing the size of the jumps. Considering the *A2F* and *K0F* effects in Sections 6.4 and 6.5, *A2F* and *K0F* have been determined as 10 and 0.1, respectively, through a number of computer runs. Figure 46 shows the volumetric closure normalized to initial cavern volume calculated using *A2F*=10 and *K0F*=0.1 with CAVEMAN predictions for six SPR caverns. The solid and dashed curves indicate the results using ADIGIO and CAVEMAN, respectively. For both the CAVEMAN and ADAGIO values, the long time periods with relatively straight slopes in the plots represent period of normal operating conditions (steady-state periods), whereas the sudden jumps in cavern closure represent periods (usually workovers) when the wellhead pressure was much lower than normal. The ADIGIO results for BC-19, 20, 101 are matched well to CAVEMAN's, but the increase rates from the ADAGIO for BC-15, 17, and 18 are larger than CAVEMAN's.

In the second step, the values of the salt skins of each cavern are determined. To reduce the increase rates of normalized volumetric closure of BC-15, 17, and 18, the *A2F* and *K0F* of cavern skins as shown Figure 14 through Figure 20 are calibrated using Figure 41, Figure 42, Figure 44, and Figure 45. Finally, the values of *A2F* and *K0F* of BC-15, 17, and 18 cavern skins have been determined as listed Table 12 through a number of ADAGIO runs. BC-102 was previously owned by Boardwalk. The DOE re-purchased BC-102 to use for SPR in 2012. The wellhead pressure has been recorded since 11/9/2012, so CAVEMAN predictions exist since then which is too short period to catch the trend of cavern volumetric closure and then calibrate the multiplication factors. Therefore, the multiplication factor values of BC-102 skins assume to

be the same as BC-101's because two caverns are not far off and the depths of cavern tops are similar.

Figure 47 shows the volumetric closure normalized to initial cavern volumes calculated using calibrated *A2F* and *K0F* in Table 12 with CAVEMAN predictions for six SPR caverns. The analyses results for six SPR caverns are matched well to CAVEMAN's. However, the gap between them still exists. CAVEMAN assumes that caverns are right circular cylinders rather than real geometries in this model. Available cavern height and cavern volume information were used to calculate an effective radius for each cavern [Ballard and Ehgartner, 2000]. The discrepancies between the predictions from ADAGIO and CAVEMAN for BC-18, 19 and 20 are larger than other caverns' because the cavern shapes are farthest away from a cylinder used in CAVEMAN and contain disc shapes indicated by ellipses as shown in Figure 48. This implies the predictions from this model may be closer to the real geomechanical behavior than CAVEMAN's. Therefore, the numerical finite element model in this study can reliably predict past and future geomechanical behavior of salt containing cavern cavities.

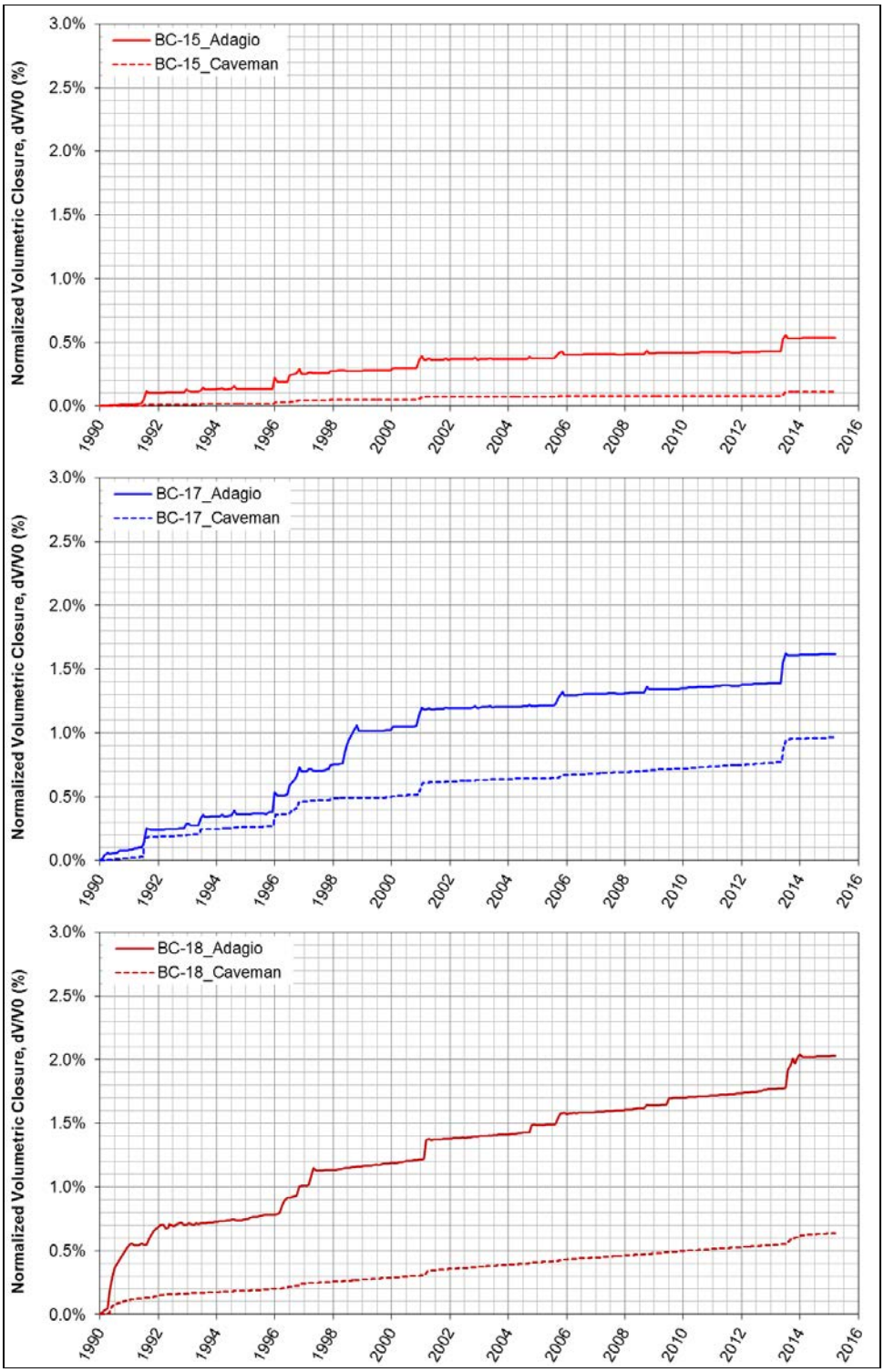
BC-15_Adagio
BC-15_Caveman
Normalized Volumetric Closure, dV/V0 (%)
3.0%
2.5%
2.0%
1.5%
1.0%
0.5%
0.0%
1990
1992
1994
1996
1998
2000
2002
2004
2006
2008
2010
2012
2014
2016
BC-17_Adagio
BC-17_Caveman
Normalized Volumetric Closure, dV/V0 (%)
BC-18_Adagio
BC-18_Caveman
Normalized Volumetric Closure, dV/V0 (%)

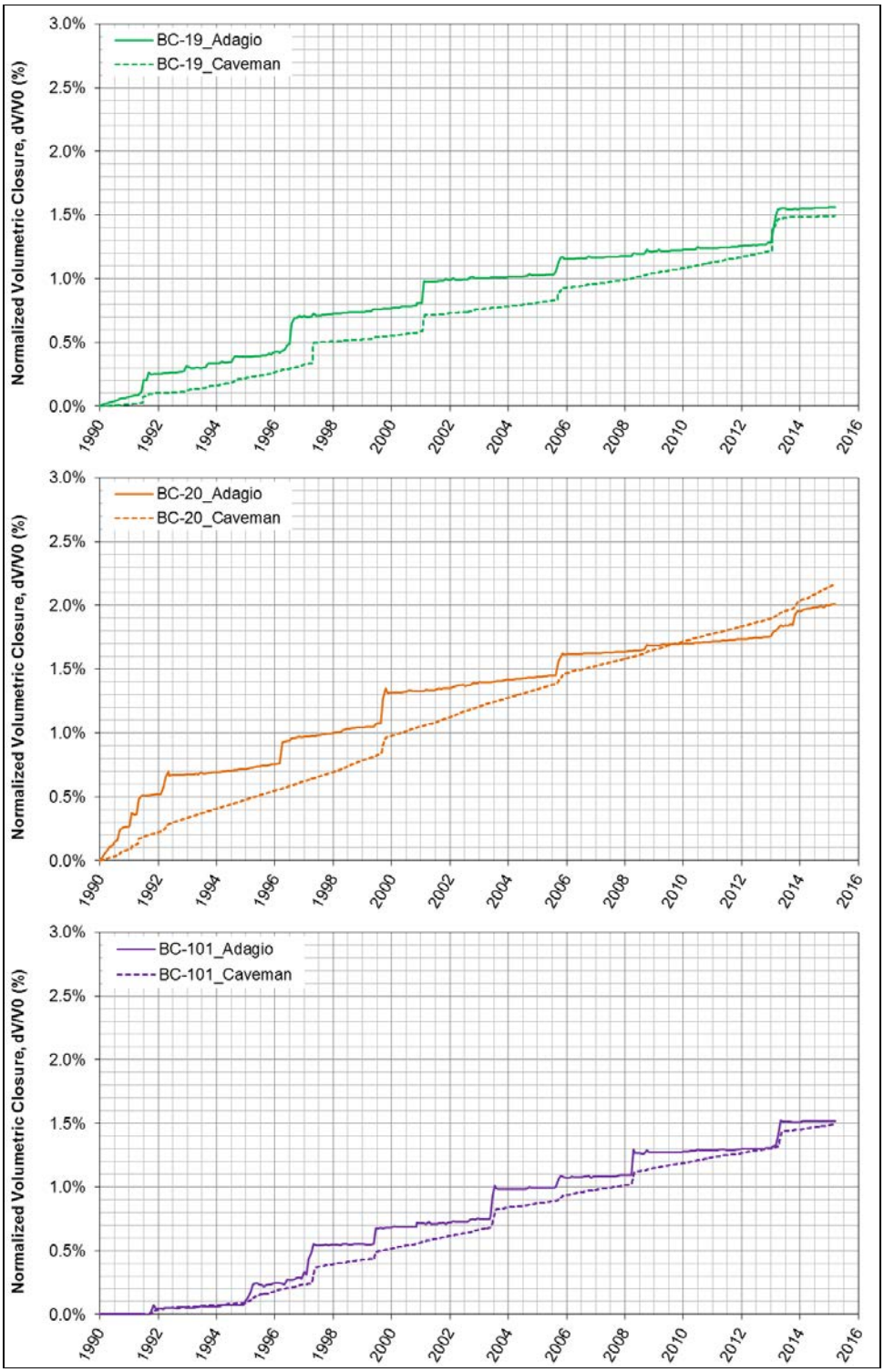

Figure 46 Volumetric closure normalized to initial cavern volumes calculated using *A2F*=10 and *K0F*=0.1 with CAVEMAN predictions for six SPR caverns

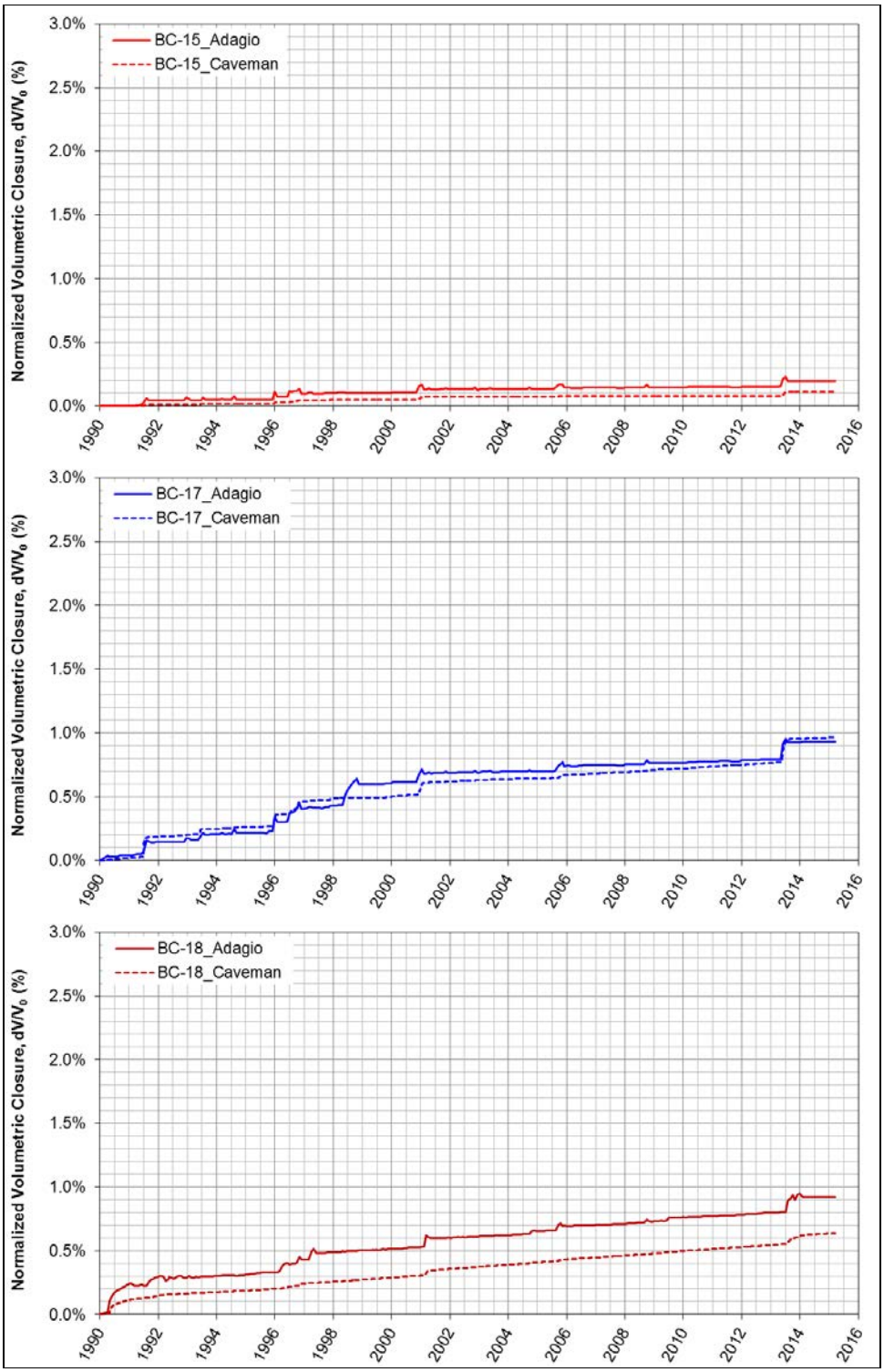
BC-15_Adagio
BC-15_Caveman
BC-17_Adagio
BC-17_Caveman
BC-18_Adagio
BC-18_Caveman
Normalized Volumetric Closure, dV/V0 (%)
3.0%
2.5%
2.0%
1.5%
1.0%
0.5%
0.0%
1990
1992
1994
1996
1998
2000
2002
2004
2006
2008
2010
2012
2014
2016

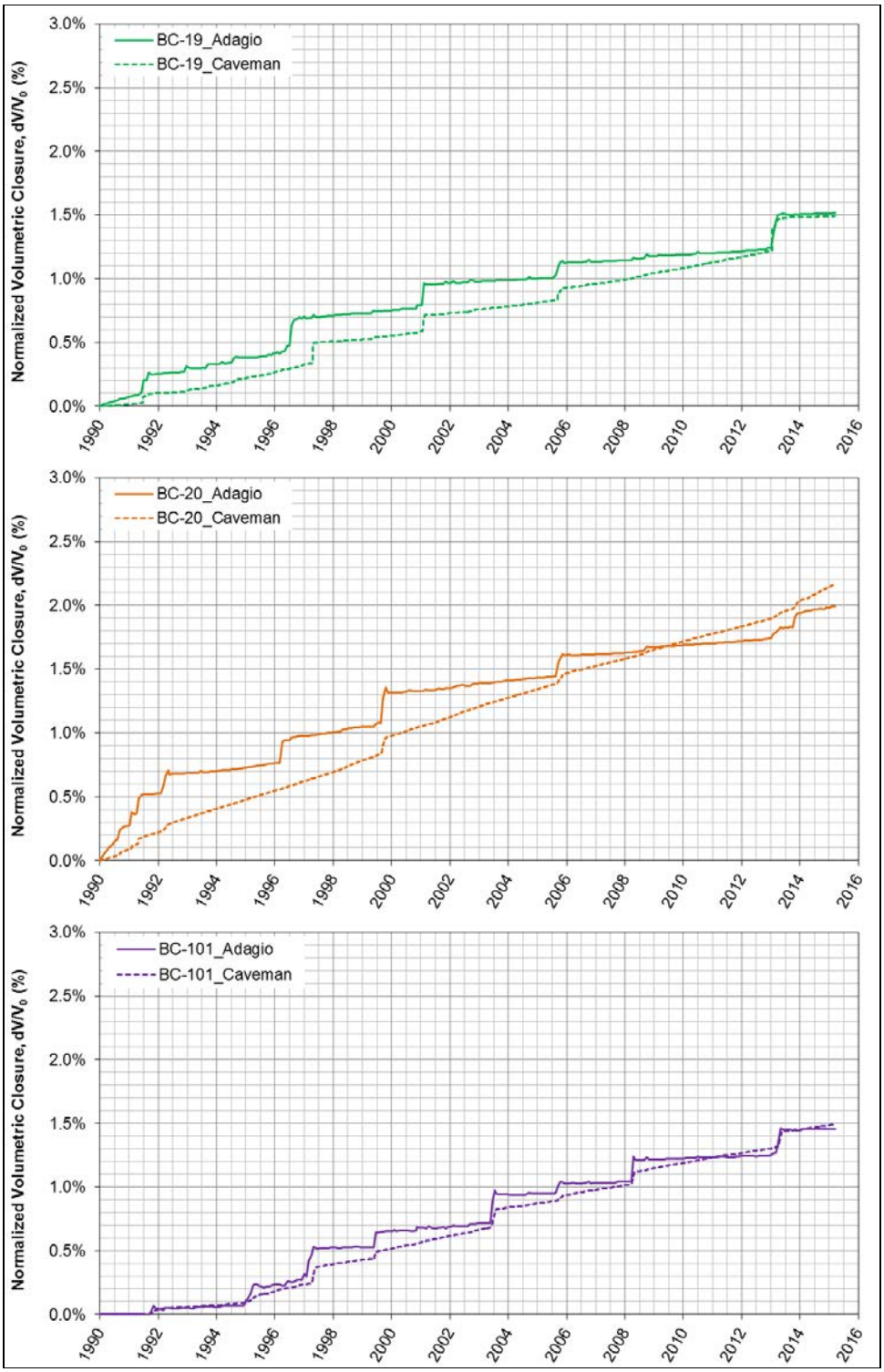

Figure 47 Volumetric closure normalized to initial cavern volumes calculated using calibrated *A2F* and *K0F* in Table 12 with CAVEMAN predictions for six SPR caverns

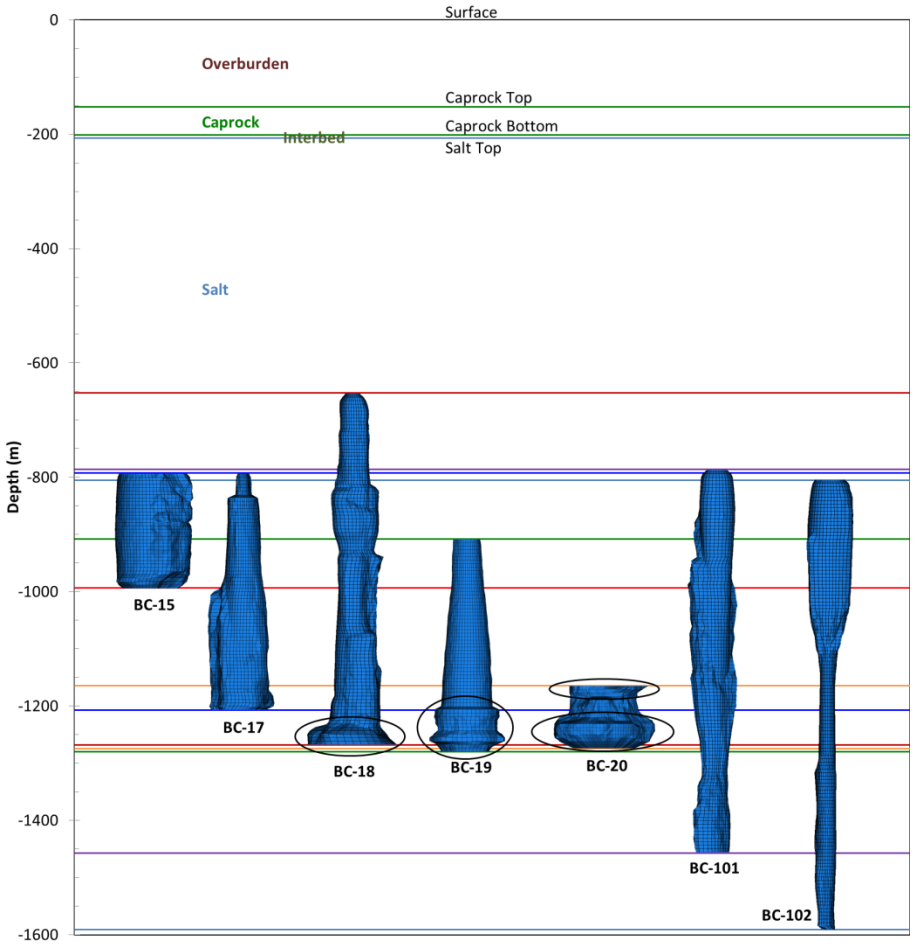

Figure 48. Side views of SPR caverns in Bayou Choctaw salt dome (vertical and horizontal scales are equal, not in true relationship to one another spatially, except for Cavern 15 and 17)

7.2. Subsidence

Figure 50 shows the surface elevation changes since 1990 at the SPR cavern wells as shown in Figure 49. The elevation changes are very irregular, sometimes showing uplift and at other times subsidence, with no clear tendency. In general, the internal pressure of a cavern is always less than lithostatic pressure, so the cavern wall moves inward over time. Ideally, surface subsidence increases with time because the cavern volumes below the surface decrease due to the salt creep closure. Figure 51 shows the measured and predicted surface subsidence since 1991 at the West Hackberry cavern wells as an example [Sobolik, 2015].

There are several possibilities but it likely due to vertical movement of the survey's datum. All of the survey's are done manually and all of the elevations given are relative to the datum they use. If the datum is subsiding it makes it look as if the site is uplifting. The other possibility is that it is actually a physical phenomenon. With the addition of GPS to some of the sites, we are beginning to see that the sites demonstrate a cyclical pattern of subsidence and uplift so the time of year the survey is taken is important. In addition, any offsite injection wells may also induce uplift. Unfortunately there is no way to calibrate the historical data since there were no other data

sources or information that verified absolute elevations of the survey datum or survey monuments [Moriarty, 2016].

To calibrate the mechanical salt parameter values, we use two field data sets such as cavern volumetric closure and subsidence. However, because of the inconsistency of the subsidence data described in Moriarty [2016], it was decided that additional calibration of the salt property values using the field subsidence data would not be productive and was not performed.

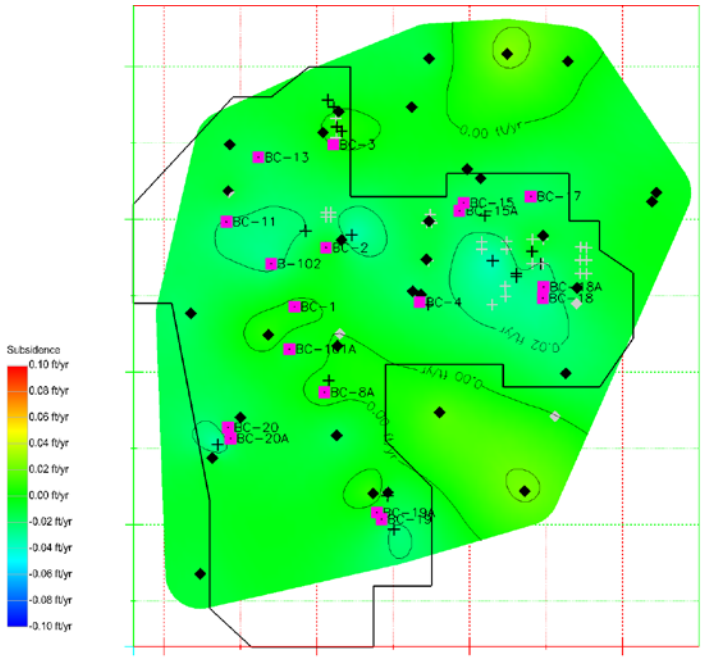

Figure 49 Contour plot of subsidence rates (ft/yr) to show the cavern well locations identified as pink squares.

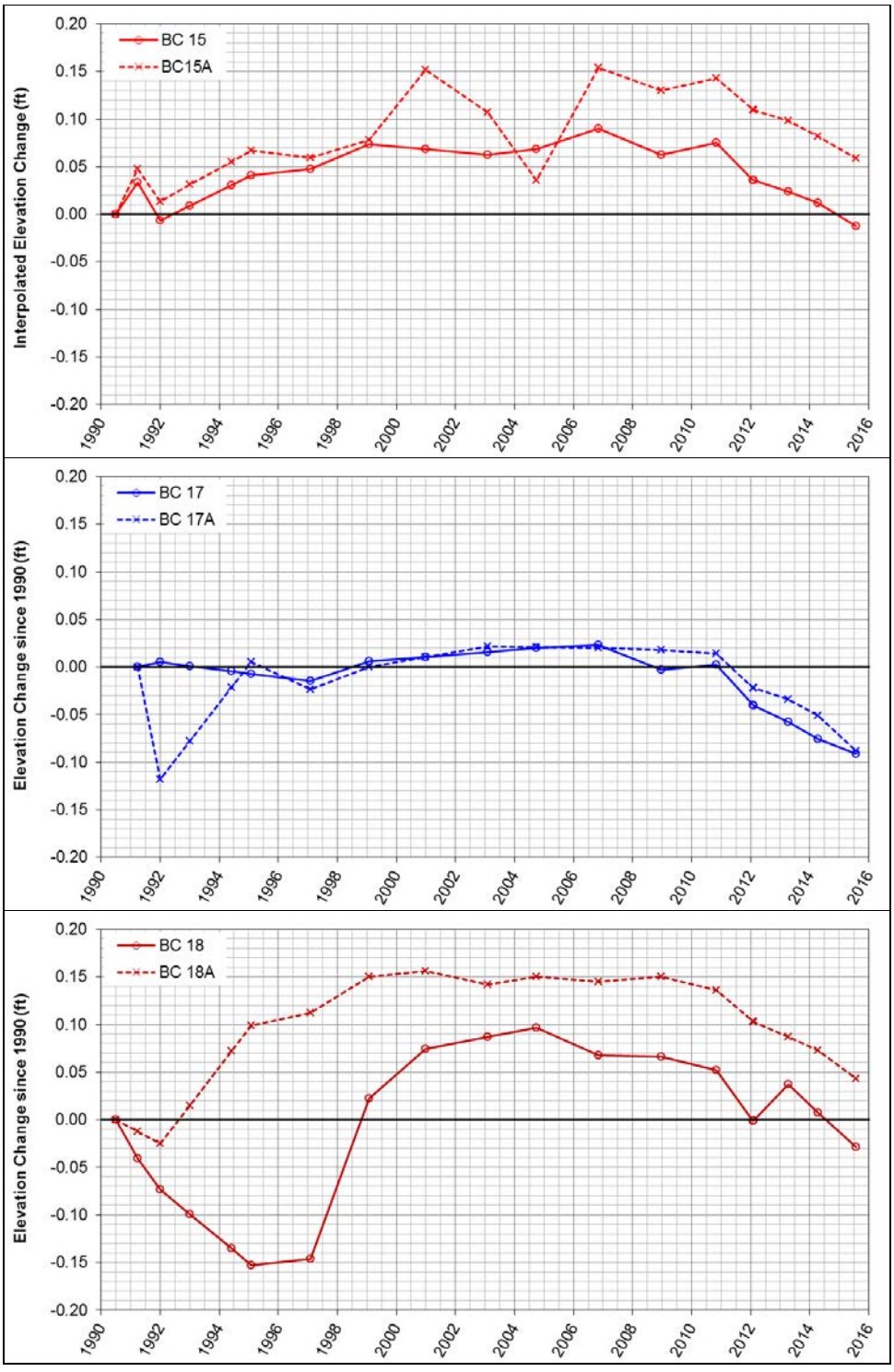
BC 15
BC15A
Interpolated Elevation Change (ft)
BC 17
BC 17A
Elevation Change since 1990 (ft)
BC 18
BC 18A
Elevation Change since 1990 (ft)
0.20
0.15
0.10
0.05
0.00
-0.05
-0.10
-0.15
-0.20
1990
1992
1994
1996
1998
2000
2002
2004
2006
2008
2010
2012
2014
2016

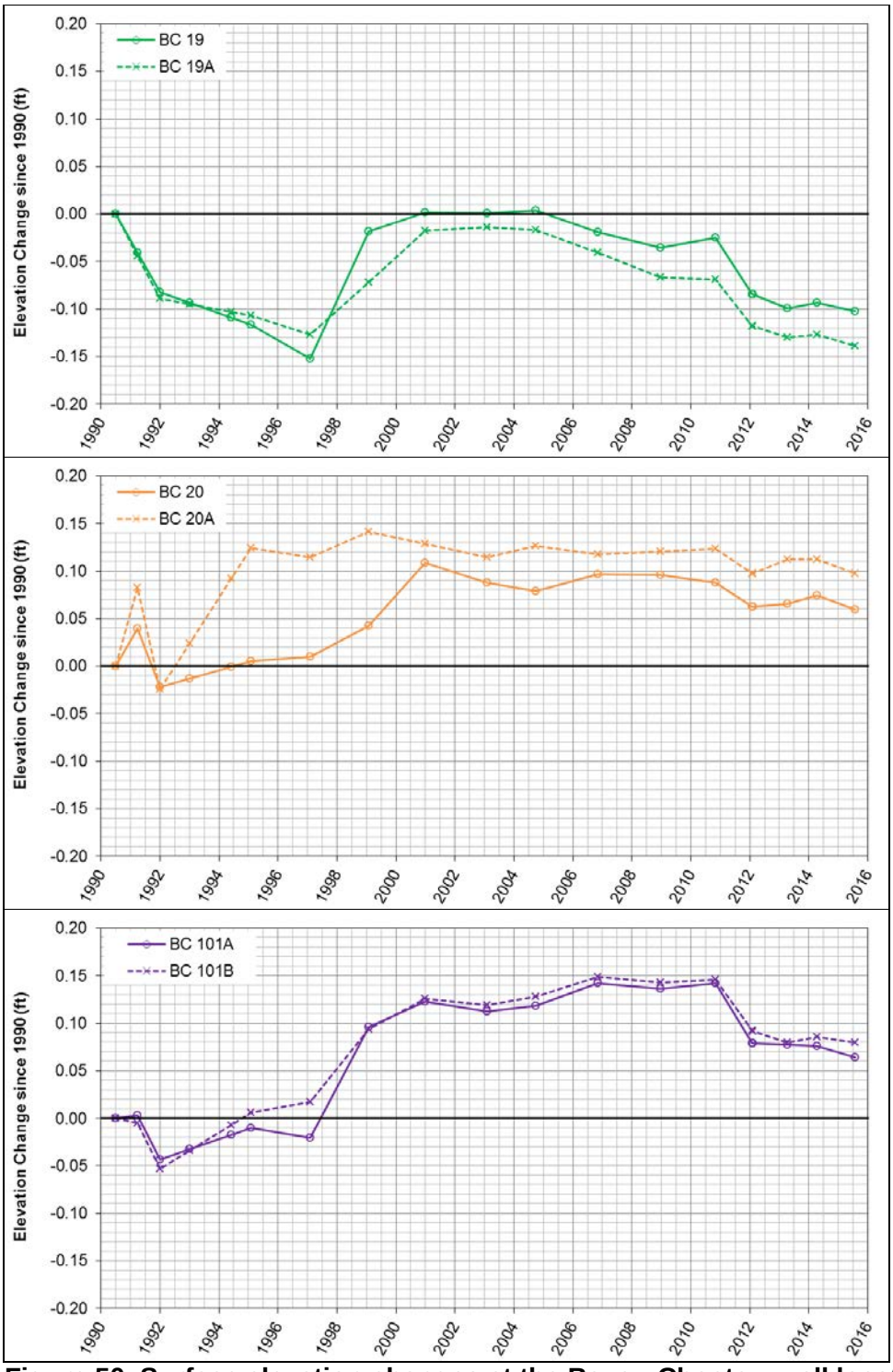

Figure 50 Surface elevation changes at the Bayou Choctaw well locations in Figure 48 since 1990

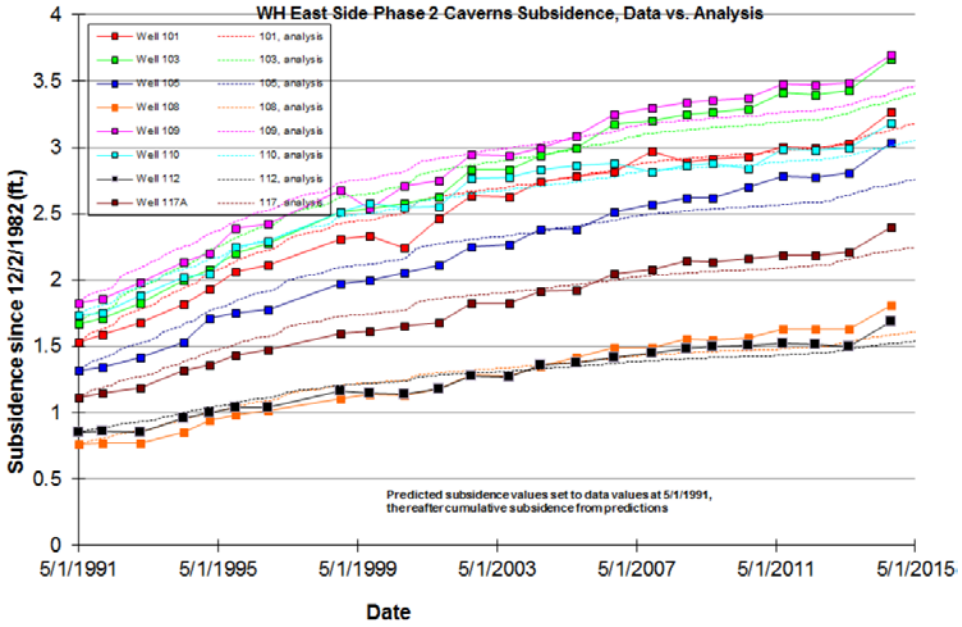

Figure 51 Subsidence since 1991 at the West Hackberry cavern wells. The solid and dotted curves indicate the measured and predicted surface subsidence, respectively [Sobolik, 2015]

Intentionally left blank

8. CONCLUSIONS

A new numerical analysis model, which consists of a realistic mesh capturing the geometries of the BC SPR site and M-D salt constitutive model using the daily data of wellhead pressure and oil-brine interface depth obtained from the field office, has been constructed. Calibration exercises have been performed to attempt to match model predictions of cavern volumetric closure with field measurements. The salt creep rate is not uniform across the salt dome and the creep test data of BC salt is limited. Therefore, model calibration is necessary to correctly simulate the geomechanical behavior of the salt dome.

The cavern volumetric closures of BC SPR caverns calculated from CAVEMAN are used for the field baseline reference. The structure factor, A_2, and transient strain limit factor, K_0, in the M-D constitutive model were used as calibration factors. The A_2 value obtained experimentally from BC salt and K_0 value of WIPP salt are used for the baseline values. To adjust the magnitude of A_2 and K_0, multiplication factors *A2F* and *K0F* are defined, respectively. The *A2F* and *K0F* values of the salt dome have been determined to be 10.0 and 0.1, respectively, through a number of back fitting analyses. The value for the salt skins surrounding each cavern has also been determined to meet the different salt creep rate at each cavern location.

The volumetric closures normalized by initial cavern volumes calculated from the new model correspond to the predictions from CAVEMAN for six SPR caverns. Therefore, the new model can reliably predict past and future geomechanical behavior of the salt dome, caverns, caprock and interbed layers. The geological concerns issuing from the BC site will be explained from this model.

A follow-up report to this work is planned for 2017. The follow-up report will provide the resolution for the following issues:

- Geomechanical concerns arise due to the close proximity of the some of the caverns to each other (e.g. BC-15 and 17) or to the edge of salt (e.g. BC-20)
- Geomechanical integrity of BC-4 which is believed to be in a quasi-stable condition
- Integrity of wellbores at the cavern roof and interbed between the caprock and salt
- Remaining number of drawdown leaches for seven SPR caverns through examining the structural integrity of the pillar between caverns with drawdowns
- The impacts of the expansion by two caverns on underground creep closure, surface subsidence, infrastructure, and well integrity

Intentionally left blank

9. REFERENCES

Arguello, J.G. & Rath, J.S. 2012. SIERRA Mechanics for Coupled MultiPhysics Modeling of Salt Repositories. CRC Press/Balkema. *SaltMech7 - 7th International Conference on the Mechanical Behavior of Salt*, Paris, France, April 2012.

Blanford, M.L., M.W. Heinstein, and S.W. Key, 2001. *JAS3D. A Multi-Strategy Iterative Code for Solid Mechanics Analysis. User's Instructions, Release 2.0*. SEACAS Library, JAS3D Manuals, Computational Solid Mechanics / Structural Dynamics, Sandia National Laboratories, Albuquerque, New Mexico.

Carmichael, R.S., 1984. *CRC Handbook of Physical Properties of Rocks*, CRC (Chemical Rubber Company) Press, Inc. Boca Raton, Fl.

Dames and Moore, 1978. *Determination of Physical Properties of Salt and Caprock, Bayou Choctaw Salt Dome, Iberville Parish, Louisiana:* in PB/KKB, Inc., 1978f, *Salt Dome Geology and Cavern Stability, Bayou Choctaw, Louisiana*, Final Report, Appendix, prepared for the U.S. Department of Energy, August.

Ehgartner, B., S. Ballard, M. Tavares, S. Yeh, T. Hinkebein, and R. Ostensen, 1995. *A Predictive Model for Pressurization of SPR Caverns*, Fall Meeting Solution Mining Research Institute, October 23-24, San Antonio, TX

Ehgartner, B.L. and Sobolik, S.R., 2002. *3-D Cavern Enlargement Analyses*, SAND2002-0526, Sandia National Laboratoires, Albuquerque, NM 87185-0706.

Hogan, R.G., 1980. *Strategic Petroleum Reserve (SPR) Geological Site Characterization Report Bayou Choctaw Salt Dome*, SAND80-7140, Sandia National Laboratories, Albuquerque, New Mexico.

Linn J.K., 1997. Memorandum to R.E. Myers, November 25, 1997 with attachment on "*SPR Ullage Study*" by B.L. Ehgartner, Sandia National Laboratories, Albuquerque, New Mexico.

Lord, A.S., B.L. Ehgartner, A.R. Sattler, C.A. Rautman, and D.J. Borns, 2009. *Geotechnical Evaluation: Bayou Choctaw Cavern Additions*, Letter Report to Wayne Elias, DOE SPR PMO dated November 15, 2009, Sandia National Laboratories, Albuquerque, New Mexico.

Moriarty, M. Dylan, 2016. Bayou Choctaw Subsidence Data, E-mail to B.Y. Park dated 10/24/2016, Sandia National Laboratories, Albuquerque, New Mexico.

Munson, D.E., 1979. *Preliminary Deformation-Mechanism Map for Salt (with Application to WIPP)*, SAND70-0079, Sandia National Laboratories, Albuquerque, New Mexico.

Munson, D.E. and P.R. Dawson, 1979. *Constitutive Model for the Low Temperature Creep of Salt (With Application to WIPP).* SAND79-1853, Sandia National Laboratories, Albuquerque, New Mexico.

Munson, D.E. and P.R. Dawson. 1982. *A Transient Creep Model for Salt during Stress Loading and Unloading.* SAND82-0962, Sandia National Laboratories, Albuquerque, New Mexico.

Munson, D.E. and P.R. Dawson, 1984. Salt Constitutive Modeling using Mechanism Maps. *1st International Conference on the Mechanical Behavior of Salt, Trans Tech Publications,* 717-737, Clausthal, Germany.

Munson, D.E., A.F. Fossum, and P.E. Senseny. 1989. *Advances in Resolution of Discrepancies between Predicted and Measured in Situ WIPP Room Closures.* SAND88-2948, Sandia National Laboratories, Albuquerque, New Mexico.

Munson, D.E., 1998. *Analysis of Multistage and Other Creep Data for Domal Salts*, SAND98-2276, Sandia National Laboratories, Albuquerque, New Mexico.

Neal, J.T., T.R Magorian, K.O. Byrne, and S. Denzler, 1993. *Strategic Petroleum Reserve (SPR) Additional Geologic Site Characterization Studies Bayou Choctaw Salt Dome, Louisiana,* SAND92-2284, Sandia National Laboratories, Albuquerque, New Mexico 87185, Livermore, California 94550.

Park, B.Y., B.L. Ehgartner, and M.Y. Lee, 2006. *Three Dimensional Simulation for Bayou Choctaw Strategic Petroleum Reserve (SPR),* SAND2006-7589, Sandia National Laboratories, Albuquerque, New Mexico.

Park, B.Y. and B.L. Ehgartner, 2008. *Expansion Analyses of Strategic Petroleum Reserve (SPR) in Bayou Choctaw Salt Dome,* SAND2008-6408, Sandia National Laboratories, Albuquerque, New Mexico.

Park, B.Y. and B.L. Ehgartner, 2010. *Expansion Analyses of Strategic Petroleum Reserve in Bayou Choctaw – Revised Locations*, SAND2010-3350, Sandia National Laboratories, Albuquerque, New Mexico.

Park. B.Y., B.L. Ehgartner, 2012. Expansion Analyses of Strategic Petroleum Reserve in Bayou Choctaw – Revised Locations, SAND-2011-6061C, *7th Conference on the Mechanical Behavior of Salt held in Paris, France, April 16-19, 2012.*

Park, B.Y., 2013. *A Validation Test for Adagio through Replication of Big Hill and Bayou Choctaw JAS3D Models*, SAND2013-4549, Sandia National Laboratories, Albuquerque, New Mexico.

Park, B.Y. 2014. Interbed Modeling to Predict Wellbore Damage for Big Hill Strategic Petroleum Reserve. *Journal of Rock Mech Rock Eng (2014) 47:1551-1561.* DOI 10.1007/s00603-014-0572-2

Park, B.Y. and B.L. Roberts, 2015. *Construction of Hexahedral Elements Mesh Capturing Realistic Geometries of Bayou Choctaw SPR site*, SAND2015-7458, Sandia National Laboratories, Albuquerque, New Mexico.

PB/KBB, 1978. SPRP - *SPR Conceptual Design* – Supplement to Salt Dome Geology and Cavern Stability Analysis Bayou Choctaw, Louisiana. Parsons Brinckerhoff and Kavernen Bau-Und Betriebs.

Preece, D.S. and J.T. Foley, 1984. *Long-Term Performance Predictions for Strategic Petroleum Reserve (SPR) Caverns*, SAND83-2343, Sandia National Laboratories, Albuquerque, New Mexico.

Rautman, C.A., K.M. Looff, and J.B. Duffield, 2008. *Letter Report Describing the First Complete-Dome Reinterpretation of the Salt Margin at the Bayou Choctaw SPR Site Using Three-Dimensional Seismic Data*, Letter from C.A. Rautman to Wayne Elias, DOE SPR PMO, FE-4432 dated March 21, 2008. Sandia National Laboratories, Albuquerque, New Mexico.

Rautman, C.A., K.M. Looff, and J.B. Duffield, 2009. *A Three-Dimensional Geometric Model of the Bayou Choctaw Salt Dome, Southern Louisiana, Using 3-D Seismic Data*, OUO SAND2009-1037, Sandia National Laboratories, Albuquerque, New Mexico.

Roberts, B.L. 2015. *BC dome seismic image*, E-mail from B.L. Roberts to B.Y. Park dated 2/5/2015. Sandia National Laboratories, Albuquerque, New Mexico.

Sandia, 2015. *CUBIT 15.0 User Documentation*, https://cubit.sandia.gov/public/15.0, Sandia National Laboratories, Albuquerque, New Mexico.

SIERRA Solid Mechanics Team, 2010. *Adagio 4.18 User's Guide*. SAND2010-6313, Sandia National Laboratories, Albuquerque, New Mexico.

SIERRA Solid Mechanics Team, 2011. *Sierra/Solid Mechanics 4.22 User's Guide*. SAND2011-7597, Sandia National Laboratories, Albuquerque, New Mexico.

Sobolik, S.R. 2015. *Analysis of Cavern and Well Stability at the West Hackberry SPR Site Using a Full-Dome Model*, SAND2015-7401, and Sandia National Laboratories, Albuquerque, New Mexico.

The Aerospace Corporation, 1980. *Preliminary Draft – Bayou Choctaw Cavern Foru subsidence Comparative Risk Assessment – Strategic Petroleum Reserve*, October 30, 1980, Los Angeles, California, 90009.

Wawersik W.R., and D.H. Zeuch 1984. *Creep and Creep Modeling of Three Domal Salts - A Comprehensive Update*, SAND84-0568, Sandia National Laboratories, Albuquerque, New Mexico.

Intentionally left blank

APPENDIX I: PRESSURE HEAD CALCULATION FOR BC-1

Elevation of surface: $ZSF := 0.ft$

Elevation of overburden bottom: $ZOB := -500ft$

Elevation of caprock bottom: $ZCR := -660ft$

Elevation of interbed bottom: $ZIB := -680ft$

Thickness of overburden: $t\_OB := ZSF - ZOB$ $t\_OB = 500 \cdot ft$

Thickness of caprock: $t\_CR := ZOB - ZCR$ $t\_CR = 160 \cdot ft$

Thickness of interbed: $t\_IB := ZCR - ZIB$ $t\_IB = 20 \cdot ft$

Overburden:

$RGOB := 1874 \cdot g \cdot \frac{kg}{m^3}$ $RGOB = 116.99 \cdot \frac{psf}{ft}$ $RGOB = 0.8124 \cdot \frac{psi}{ft}$

Caprock:

$RGCR := 2319 \cdot g \cdot \frac{kg}{m^3}$ $RGCR = 144.77 \cdot \frac{psf}{ft}$ $RGCR = 1.0054 \cdot \frac{psi}{ft}$

Salt dome:

$RGSD := 2300 \cdot g \cdot \frac{kg}{m^3}$ $RGSD = 143.58 \cdot \frac{psf}{ft}$ $RGSD = 0.9971 \cdot \frac{psi}{ft}$

Oil:

$RGOIL := 8369.62 \cdot \frac{Pa}{m}$ $RGOIL = 53.28 \cdot \frac{psf}{ft}$ $RGOIL = 0.3700 \cdot \frac{psi}{ft}$

Water:

$RGH2O := 1000g \cdot \frac{kg}{m^3}$ $RGH2O = 62.43 \cdot \frac{psf}{ft}$ $RGH2O = 0.4335 \cdot \frac{psi}{ft}$

Brine:

$RGBRI := 1200 \cdot g \cdot \frac{kg}{m^3}$ $RGBRI = 74.91 \cdot \frac{psf}{ft}$ $RGBRI = 0.5202 \cdot \frac{psi}{ft}$

Deadload on the salt top:

$DEADLOAD := RGOB \cdot t\_OB + RGCR \cdot t\_CR + RGOB \cdot t\_IB$ $DEADLOAD = 83998 \cdot psf$

==========

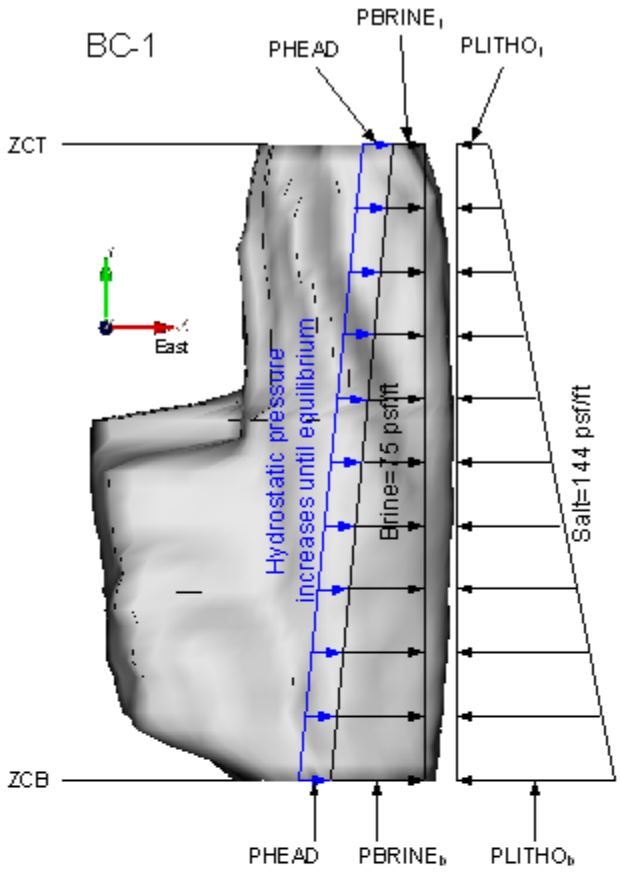

Elevation of cavern top: $ZCT := -1040ft$

Elevation of cavern bottom: $ZCB := -1780ft$

Height of cavern: $h\_c := ZCT - ZCB$ $h\_c = 740 \cdot ft$

Lithostatic pressure at cavern top:

$$PLITHO_t := DEADLOAD + RGSD \cdot (ZIB - ZCT)$$

$PLITHO_t = 135688 \cdot psf$ $PLITHO_t = 942 \cdot psi$

Lithostatic pressure at cavern bottom:

$$PLITHO_b := DEADLOAD + RGSD \cdot (ZIB - ZCB)$$

$PLITHO_b = 241941 \cdot psf$ $PLITHO_b = 1680 \cdot psi$

Lithostatic pressure distribution area:

$$ALITHO := \frac{(PLITHO_t + PLITHO_b)\cdot h\_c}{2} \qquad ALITHO = 139722815\cdot psf\cdot ft$$

Brinestatic pressure at cavern top:

$$PBRINE_t := RGBRI\cdot(-ZCT) \qquad PBRINE_t = 77910\cdot psf$$

$$PBRINE_t = 541\cdot psi$$

Brinestatic pressure at cavern bottom:

$$PBRINE_b := RGBRI\cdot(-ZCB) \qquad PBRINE_b = 133346\cdot psf$$

$$PBRINE_b = 926\cdot psi$$

Brinestatic pressure distribution area:

$$ABRINE := \frac{(PBRINE_t + PBRINE_b)\cdot h\_c}{2} \qquad ABRINE = 78164801\cdot psf\cdot ft$$

Area difference between lithostatic and brinestatic distribution areas:

$$ADIFF := ALITHO - ABRINE \qquad ADIFF = 61558014\cdot psf\cdot ft$$

Well head pressure at equilibrium state:

$$PHEAD := \frac{ADIFF}{h\_c} \qquad PHEAD = 83187\cdot psf$$

$$PHEAD = 578\cdot psi$$

At equilibrium after plugging:

$$PBRINE_t + PHEAD = 1119\cdot psi$$

$$PBRINE_b + PHEAD = 1504\cdot psi$$

Intentionally Blank

DISTRIBUTION

External Distribution

Electronic copies to:

Wayne Elias (wayne.elias@hq.doe.gov)
for distribution to DOE SPR Program Office, Washington, D.C.
U.S. Department of Energy
Office of Fossil Energy
Forrestal Building
1000 Independence Ave., SW
Washington, DC 20585

Diane Willard (diane.willard@spr.doe.gov)
for distribution to DOE and FFPO SPR Project Management Office, New Orleans, LA.
U.S. Department of Energy
Strategic Petroleum Reserve Project Management Office
900 Commerce Road East
New Orleans, LA 70123

Sandia Distribution

Print copy				
0	MS0706	L. Cunningham	6912	(electronic copy)
1	MS0706	Anna C. Snider Lord	6912	(print and electronic copy)
0	MS0750	G. Bettin	6912	(electronic copy)
1	MS0751	B. L. Roberts	6912	(print and electronic copy)
5	MS0751	B. Y. Park	6912	(print and electronic copies)
1	MS0706	D. L. Lord	6912	(print and electronic copy)
0	MS0750	D. M. Moriarty	6912	(electronic copy)
0	MS0750	K. Chojnicki	6912	(electronic copy)
0	MS0750	P. D. Weber	6912	(electronic copy)
1	MS0751	S. R. Sobolik	6912	(print and electronic copy)
5	MS0750	C. L. Kirby	6913	(print and electronic copies)
1	MS0751	C. G. Herrick	6914	(print and electronic copy)
0	MS0751	M. Y. Lee	6914	(electronic copy)
1	MS1395	H. D. Park	6931	(print and electronic copy)
0	MS0735	E. K. Webb	6910	(electronic copy)
0	MS0840	B. Reedlunn	1554	(electronic copy)
0	MS0779	E. Matteo	6222	(electronic copy)
0	MS0899	Technical Library	9536	(electronic copy)


Sandia National Laboratories